BRINGING PARTICLE SCALE PROPERTIES INTO DESCRIPTIONS OF POWDER BEHAVIOR VIA THE ENHANCED CENTRIFUGE METHOD

by

Caralyn A. Stevenson (Coultas-Mckenney)

A Dissertation

Submitted to the Faculty of Purdue University

In Partial Fulfillment of the Requirements for the degree of

Doctor of Philosophy

Davidson School of Chemical Engineering

West Lafayette, Indiana

December 2021

THE PURDUE UNIVERSITY GRADUATE SCHOOL
STATEMENT OF COMMITTEE APPROVAL

Dr. Stephen P. Beaudoin, Chair
Davidson School of Chemical Engineering

Dr. Zoltan K. Nagy
Davidson School of Chemical Engineering

Dr. Gintaras V. Reklaitis
Davidson School of Chemical Engineering

Dr. Carl R. Wassgren
School of Mechanical Engineering

Approved by:
Dr. John A. Morgan

Dedicated to my husband, Mike, and our PhD pup

ACKNOWLEDGMENTS

I would first like to thank my research advisor, Steve Beaudoin, for without his unwavering support of me as a person and a researcher, I would not have succeeded at Purdue. His continuous faith in me and guidance pushed me to excel through the obstacles I faced in my academic and research career. His support and allyship for women in engineering allowed me the ability to dedicate myself not only to my research endeavors but also to the Women in Engineering Program and the ChE Graduate Women's Group for which I will always be grateful.

I would also like to convey my appreciation to my committee members: Dr. Carl Wassgren, Dr. Zoltan Nagy, and Dr. Gintaras Reklaitis for the guidance and knowledge they kindly provided while serving on my committee. Additionally, I would like to thank our AbbVie sponsors: Dr. Vogt, Dr, Ketterhagen, and Dr. Capece, and our mechanical engineering collaborators: Dr. Wassgren and Prathamesh Sankhe for the many discussions we had to further develop this work.

I also want to thank Sandia National Laboratories and Dr. Jessica Rimsza for selecting me for the Sandia Academic Alliance Initiative for Research & Career Opportunities for Women in Microsystems, Nanotechnology & Materials program. I sincerely appreciate the support and mentorship Dr. Rimsza provided me and thoroughly enjoyed our research discussions.

Thank you to the members of the Beaudoin group for always being a group of colleagues I always felt supported by! I specifically want to thank Andrew Parker for his ever reassuring words of advice and support and for also always kindly talking through scientific concepts I didn't quite understand. My appreciation also goes to Leo Miroshnik who emphasized the importance of always taking of yourself (and your dog) and was kind to me in some of the most challenging times of grad school. I also want to say my thanks to Sydney Schierey for our numerous conversations about everything and taking care of the AFM experiments when I was away!

I want to say my appreciation goes out to all the undergraduate research assistants who ran numerous amounts of centrifuge experiments. Oftentimes, you all were my motivation to get into the lab and one of the reasons I enjoyed research. I truly enjoyed mentoring you all and watching you grow as researchers.

My appreciation also goes to my mentors, peers, and friends in the Women in Engineering Program. One of the best decisions I made in grad school was going to a GWEN seminar for the free mug. The mentorship and support provided to me by Dr. Suzanne Birkhimer, and the GWEN

2019-2020 and 2020-2021 leadership teams, gave me the courage and tools I needed to be confident in myself as a woman in engineering. I also show my appreciation to the ChE Graduate Women's Group, the mentors (Dr. Claire Liu and Dr. Laryssa Cesar to name a few) I made through GWG, and the fellow graduate students I enjoyed conversations with over Bagel Breakfasts. Thank you to Arunima, Akriti, Montgomery and Anusha for keeping the legacy of GWG going!

After stressing over this dissertation thing, (I mean it is just paper), I dedicate a piece of my doctorate to the friends whose friendship only became stronger after undergrad. Alyssa, Abigail, Katey, Jackie, LynnMarie and Rebecca you are my role models and exemplify what is means to be a kind, thoughtful, and brilliant scientist and engineer. I also want to say the same sentiment applies to the friends I made in grad school. Arunima, Akriti, and Aditi without you I would not have survived grad school. I will always admire your dedication and grit.

I want to thank my parents for their support of me through my graduate studies. If it were not for their support and care, I would not be where I am today. To my sister Cami, our daily conversations, keep me motivated and always ground me. Your confidence, grit and determination continuously remind of the mentor I need to be. I also want to show my appreciation to my brothers, brother in-laws, sister-in-law, and husband's parents for their continuous support of my endeavors.

Finally, thank you to my best friend and husband, Mike. You always had faith in me even when I was convinced I was not cut out to be a Ph.D. You validated my feelings and unfailingly supported me through some of the most challenging situations I have faced. You and Holly Bear are my sunshine.

TABLE OF CONTENTS

LIST OF TABLES

LIST OF FIGURES

ABSTRACT

Many industrial processes involve powders in some form when making products, and the behavior of the powders processed is impacted by the adhesion of the individual particles which comprise it. This adhesion behavior, in turn, is critically influenced by the complementarity between the topography of a surface and the shape and roughness of the particles that adhere to that surface. Problems such as poor flowability, dust hazards, and equipment wear arise due to uncontrolled particle adhesion and can lead to production challenges. Computational models have been developed to predict the behavior of highly idealized powders (i.e., powders comprised of simple geometries such as spheres) under various processes but are limited in their ability to model and optimize the manufacturing and handling of powders comprised of many complex particles. This work focuses on further developing an experimental and modeling framework, called the Enhanced Centrifuge Method (ECM), that maps particle-scale and surface properties onto experimentally-validated 'effective' adhesion distributions that describe the adhesion between particles in powders. These distributions represent an engineering approach that allows powders comprised of particles of complex shape and roughness, which are challenging to model, to be described as if they were perfect, smooth spheres, which are comparatively simple to model. The complexity associated with the shape and size distributions of the individual particles is captured by the 'effective' adhesion parameters. These 'effective' adhesion parameter distributions provide a quantitative guide as to how the specific particle properties are interacting with the surface topography which directly impacts the overall powder adhesion. The initial framework of the ECM is constructed around characterizing the van der Waals adhesion of silica and polystyrene powders. The impact of the surface topography and the particle properties of each of the powders is captured in 'effective' Hamaker constant distributions. These distributions provide a quantitative guide for specifically how the particles interact with the surface topography based on the respective scales of the particle and surface features. The ECM framework is further adapted here to investigate the effects of topographical changes of stainless steel due to polishing on the adhesion properties of three different pharmaceutical powders to the stainless steel. In this adaptation of the ECM framework, the force of adhesion was described by modifying the Johnson, Kendall, and Roberts (JKR) model describing elastic-like particle contact to a flat plate. Within the modified JKR

adhesion description, the work of adhesion is tuned to be an 'effective' work of adhesion parameter. These size-dependent 'effective' work of adhesion distributions provide a quantifiable measure of the change in the powder and surface adhesion that reflects the size, shape, and topographical features on the powder and surface with which the powder interacts. To investigate environmental effects on the adhesion properties, the ECM framework is also extended to characterize the effect humidity has on altering surface and particle interactions of the three pharmaceutical powders to stainless steel. In addition to the work with the pharmaceutical powders, the investigation of the effect of humidity on the powder's adhesion includes a study of the influence of water on the interactions between silica particles and a silica substrate. In all cases, the 'effective' adhesion force distributions developed through the ECM provide the ability to quickly determine quantitatively how environmental and process conditions alter particle and surface properties, and overall powder behavior.

1. INTRODUCTION

A multitude of industries - with examples being food, pharmaceutical and defense - process and handle powder at some point or another when making their products[1–7]. Examples of industrial processes that involve powders include milling, blending, spreading, and compaction[5,8–10]. The behavior of the powders under these industrial processes is impacted by the adhesion of the individual particles which comprise a powder[11]. The adhesion force is the force necessary to separate two surfaces in contact and arises due to van der Waals (vdW), capillary, and electrostatic forces present on between the surfaces[12–14].

Problems such as caking, poor flowability, dust hazards, segregation, equipment wear, and "picking and sticking" arise due to uncontrolled particle adhesion[11,15,16] and can lead to a stop in production and a loss of profit. To prevent such problems and optimize powder processes, the effect of the particles' characteristics along with the properties of the equipment surfaces towards the adhesion behavior of the powder needs to be well understood. Contact separation distance, chemical composition, particle size, particle shape and surface roughness all affect the interaction between the two materials[17–19]. It is specifically important to characterize surface roughness and particle shape because these properties vary the contact area between a particle and the interacting surface which ultimately affects the degree of adhesion[20–22]. Therefore, mathematical and computational models have been developed to understand and quantify these effects on the adhesion system[23–29].

A limitation of these computational methods lies in their inability to accurately describe the adhesion across a large number of unique particles. Oftentimes, computational models use highly idealized powders (*i.e.*, powders comprised of simple geometries such as spheres) to predict powder behavior under various processes thereby limiting the ability to model and optimize the manufacturing and handling of powders comprised of many complex particles[9,30,31]. Recently, the enhanced centrifuge method (ECM) was developed to describe the vdW adhesion of a population of particles, each with their own surface topography and shape, against a surface[32]. The ECM captures the effects of particle shape, particle size, particle surface topography, and substrate surface roughness on the adhesion system through 'effective' Hamaker constant distributions[32].

The objective of the presented research was to further investigate and decouple the effect of the particle properties and surface properties on different adhesion systems using the ECM. To begin to decouple the effect of the particles' properties from the surface properties on the vdW adhesion, the adhesion of a powder comprised of polystyrene particles was measured against silica with systematically altered surface topography. By studying the powder against silica with increasing amounts of surface topography, the effect of changing the surface topography on the adhesion is quantified through the 'effective' Hamaker constants. Root mean square (RMS) roughness is a commonly used parameter to quantify the effect of the surface roughness on the adhesion [33–35]; however, the 'effective' Hamaker constant distributions illuminated instead the adhesion behavior is impacted by the interaction between the specific surface topography features and the particles based on their relative sizes and shapes in comparison to each other. A secondary computational investigation further explored the effect of the surface and particle properties on the vdW force by superimposing sinusoidal roughness on particles and creating substrates with indented surfaces *in silico*. This investigation further revealed that the interaction between the surface topography features (the indentations) and the particle properties based on their comparative scales directly impacts the adhesion. This computational study also further validated that the 'effective' Hamaker constants quantify the effect of the particle properties on the vdW adhesion.

The ECM was then adapted to investigate the effect of the surface and particle properties on a powder's adhesion when the powder is comprised of elastic-like particles. Specifically, the ECM was modified to tune the Johnson Kendall Roberts (JKR) adhesion model which describes the adhesion between an elastic sphere and flat plate. Through this adaptation, the work of adhesion within the JKR model is tuned into an 'effective' work of adhesion parameter to capture the effect of the individual particle properties and surface topography on the adhesion. The adhesion between stainless steel that was polished in three different manners and three pharmaceutical powders of interest: lactose monohydrate, ABT 089 and Hypromellose was measured. The ECM was then utilized to output the 'effective' work of adhesion distributions which describe the effect the polishing had on the stainless steel topography and the resultant particle interactions with the surface. These distributions, like the 'effective' Hamaker distributions outputted in the vdW adhesion investigations, further revealed the impact of the relation of the particle scale features to the surface topography on the overall adhesion.

While performing these studies, the ambient condition of relative humidity proved to have an impact on the adhesion if not adequately understood and controlled. To further investigate how relative humidity impacts the particle and surface property interactions, two studies were performed. The first investigated the pharmaceutical powders' adhesion to stainless steel in two humidity ranges (10-25% and 30-40%). The 'effective' work of adhesion distributions showed the particle properties interact similarly with the stainless steel in similar manners, but to different degrees of impact depending on the humidity range. The second study investigated the change in the interaction between a powder comprised of silica particles and a silica surface across five different humidity ranges (10-25%, 30-40%, 40-50%, 50-60%, and 60-70%). In the case of this secondary humidity study, the parameter outputted by the ECM was generalized to an 'effective' force of adhesion parameter as the varying humidity conditions altered the controlling adhesion force. The 'effective' force of adhesion distributions illuminated how water condensed and layered on a surface due to the specific humidity range. Through this investigation, it was found that layering of the water directly impacted how the particle properties interacted with the surface topography.

These studies demonstrated the ECM is a technique adaptable to study powder adhesion across varying powder and environmental conditions. Furthermore, this work illustrated the value of the ECM framework and the outputted 'effective' force distributions is the ability to quickly determine in qualitative manner how environmental and process conditions alter particle and surface interactions, and overall powder behavior.

2. LITERATURE REVIEW

2.1 Particle adhesion

vdW forces, capillary forces, and electrostatic forces are all surface interactions which prompt adhesion[12–14]. Ultimately, the vdW force arises due to spontaneous electrodynamic fluctuations and subsequent induced dipole interactions[36]. Capillary forces ensue due to the condensation of water around surface contact sites[33] and electrostatic forces arise due to the interaction of particles on charged surfaces[36]. In situations of high condensed moisture, the capillary force dominates over the electrostatic and the vdW force[14,37,38].

A number of experimental techniques have been developed to characterize these adhesion forces including atomic force microscopy (AFM), electric field detachment, the centrifuge technique, the aerodynamic technique and the mechanical surface energy tester [39–41]. A simple yet relatively robust way to measure the average adhesion force of a group of particles is through the centrifuge method[32,40]. The centrifuge method involves depositing a small amount of powder onto a substrate and mounting the substrate into a specially designed centrifuge tube such that the substrate's surface is parallel to the axis of rotation of the centrifuge with the particles facing outward. The centrifuge is then rotated at a specified rotational speed. A particle detaches from the surface when the inertial force imparted by the motion of the centrifuge has overcome the adhesion force of the particle. By measuring the particles that remain on the surface as a function of the rotational speed of the centrifuge, the average adhesion force of the powder can be obtained.

The study of vdW forces is of particular interest because they are always present in a system[12,13]. The Lifshitz approach is a rigorous model used to determine the vdW force; however, this approach is difficult to validate as a complex knowledge of the opto-electric properties of each material is needed[42]. A more approximate method for determining the vdW force was developed by Hamaker in which the adhesion is calculated by pairwise additivity of the molecular interactions over the two interacting media[43]. The Derjaguin approximation is a simple model which describes the vdW interaction between a perfectly spherical rigid particle and a flat substrate surface[17]. The vdW force, F_{vdw} derived from the Derjaguin approximation is described by:

$$F_{vdW}(D) = \frac{AR}{6D^2} \quad 2.1$$

where A is the Hamaker constant, R is the sphere's radius, and D is the separation between the sphere and the flat plate. The vdW interaction between a particle and a substrate is quantified through the Hamaker constant.

For particles elastic in nature, the Johnson, Kendall, and Roberts (JKR) [44], the Derjaguin, Muller and Toporov (DMT)[45] and the Maguis-Pollock [46] are model approximations used to describe the elastic deformation towards the particle adhesion. The JKR model specifically is used to characterize the deformation for soft elastic-like particles with large radii and high surface energies [45], while the DMT characterizes the deformation for stiffer particles with small radii. The pull off force, $F_{PO,}$ for each of these models is characterized by Eq. 2.2 below:

$$F_{PO} = \alpha\pi R\Gamma \quad 2.2$$

where α is 3/2 for the JKR model and 2 for the DMT model, R is the radius of the sphere and Γ is the work of adhesion. The Marguis-Pollock model incorporates plastic deformation into the contact mechanics of the elastic sphere to a surface[47]. Conditions such as high humidity may cause a particle to become more plastic in nature due to hydration swelling [48].

Higher humidity conditions also lead to the formation of condensation on surfaces which then can lead to capillary adhesion. Generally, the capillary adhesion has been observed to be the dominant force at humidity conditions above ~50% [38,49,50]. Capillary adhesion arises due to the formation of liquid meniscii between particles and surfaces[17]. The capillary adhesion between a spherical particle and a flat substrate is represented by:

$$F_{cp} = \Delta P \times S \quad 2.3$$

where ΔP is the Laplace pressure and S is the wetted area of the substrate in contact with the meniscus[17]. The Laplace pressure is represented by the following equation:

$$\Delta P = \gamma_L \left(\frac{1}{r_1} + \frac{1}{r_2}\right) \quad 2.4$$

where γ_L is the surface tension, and r_1 and r_2 are the principal radii of curvature of the liquid bridge. It is important to note that as r_1 becomes >> than r_2, the $\frac{1}{r_2}$ term can be neglected and ΔP becomes:

$$\Delta P = \gamma_L \left(\frac{1}{r_1}\right) \tag{2.5}$$

The wetted area is represented by the following:

$$S = 2\pi\gamma R_P r_1 (cos\theta_1 + cos\theta_2) \tag{2.6}$$

with R_P being the particle radius, and θ_1 and θ_2 being the contact angles of (1) the liquid with the particle and (2) with the surface.

The expanded equations for the wetted surface and Laplace pressure together give a capillary adhesion force expression of:

$$F_{cp} = 2\pi\gamma R_P (cos\theta_1 + cos\theta_2) \tag{2.7}$$

The wetted surface area and the capillary adhesion force will be impacted by the particle properties (size, shape, topography) and the surface topography of the interacting surface [51]. These properties not only affect capillary adhesion, but also affect the vdW and elastic particle adhesion models discussed earlier in this chapter.

2.2 Methods used to characterize particle and surface properties effects towards adhesion

In addition to the chemical composition of the particle and the surface, the physical properties of the particle and the substrate are known to affect the adhesion of the particle to the substrate surface including particle geometry, size, topography, and substrate surface roughness[17–19]. Ultimately, the surface roughness on both the substrate and the particle, along with particle shape and size, affect the adhesion by varying the contact distance between a particle and a substrate[20–22].

Due to the effect of the surface roughness towards adhesion, it is important to quantitatively and qualitatively characterize the surface roughness on a substrate and particle. Profiling is used to quantitively assess surface roughness, while microscopy techniques provide more of a

qualitative characterization of a surface[52]. Scanning electron microscopy (SEM) and field emission scanning electron microscopy (FESEM) provide qualitative descriptions of the substrate and particle surfaces along with a description of the particle's shape as they show the contrast on a surface due to the surface's height features[29,53]. Profiling instruments provide the following quantitative information: the roughness average, R_a, and root mean square (rms) roughness, R_q. The RMS roughness, R_q, is described by Eq. 2.8, where n is the number of points tracked along a surface and y_i is the difference between the corresponding height value and the mean height value of the data set[54].

$$R_q = \sqrt{\frac{1}{n}\sum_{i=1}^{n} y_i^2} \qquad 2.8$$

Ultimately, the R_a and R_q are both descriptions of the average height and depth of the roughness peaks on a surface, but the R_q characterizes the standard deviation of the points tracked on a surface from the center line to help describe the variability of the peaks in a surface profile[54]. It is important to note that while two surfaces may have the same R_q, they could have different shape profiles (*i.e.*, a surface comprised of triangle peaks compared to a surface comprised of hemispherical peaks). Atomic force microscopy and profilometry are experimental techniques used to scan a surface of interest and output this quantitative information[29,53]. Although information about the surface roughness can be gained by these techniques, it is often very time consuming to obtain; consequently, models have been created to describe surface roughness and predict how particle adhesion is affected by surface roughness effects.

One technique to simulate surface roughness is to add hemispherical asperities on to a surface and particle[23–27]. Generally, hemispheres are used to simulate surface roughness compared to more complex geometries because it is easier to mathematically describe the adhesion of a sphere[25]. The Rumpf-Rabinovich model tuned a single hemispherical asperity to capture the effects of the surface features towards the vdW adhesion[22,55]. Similar asperity approaches were taken by Perni and Prokopovich to predict the effect of surface roughness on elastic particle adhesion[56,57]. Eichenlaub *et. al* compared three surface roughness description models: a hemisphere model, a Fast Fourier Transform (FFT) algorithm of a surface scan decomposed into nanoscale cylinders, and a fractal method used to predict particle adhesion[26]. Ultimately, this

study found the FFT model to be more accurate in describing particle adhesion [26]. A particle adhesion model developed by Jaiswal *et al.* used the same FFT algorithm to describe surface roughness and the surface descriptions of the particle and substrate were discretized into nanoscale cylinders[29]. The average adhesion force between the particle and surface was measured by the summation of the adhesion forces across the nanoscale cylinders. The particle adhesion model then computed the adhesion force between the nanoscale cylinders and summed all these individual adhesion forces into one overall force that describes the average adhesion of a particle to a surface[29]. Considering capillary adhesion, Ata *et. al.* defined two geographical configurations (relation of surface peak to meniscus size) that captured the effect of the surface roughness towards liquid bridge formation[51]. Similar to the vdW application, Rabinovich *et. al.* created an effective asperity parameter to capture the effect of surface roughness on capillary adhesion[58]. Ultimately, all these methods provide an estimate of how an individual particle should adhere to a surface; however, they are computationally exhaustive to use to describe a large number of particles.

In actuality, a powder is comprised of thousands of particles-each with their own shape, size, and surface roughness; consequently, it can be difficult to model such particle variations across a powder. Discrete element method (DEM) modelling describes the movement and contact mechanics of a group of particles[5]. The most common particle shape used in DEM simulations is a sphere because the contact mechanics of a sphere is relatively simple to model[28,59].. However, a powder may not actually be comprised of spherical particles; consequently, DEM models have moved towards describing complex particle shapes and surface topographies by computationally adhering spheres together (referred to as the glued sphere method)[5,28,60,61]. By creating these particle shapes from the same mathematical description used for spherical particles, the simple contact mechanics of spheres can be used for these non-spherical particles. Although non-spherical shapes can be created through the glued-spheres method, a study showed the mechanical behavior of a particle is influenced by the number of particles used to create the non-spherical particle shape[60]. Consequently, the particle mechanics of a glued-sphere particle may not represent the mechanics of the actual particle. An additional downfall to the glued sphere method is the computational time needed to determine the contact behavior increases for sphere clusters (*i.e.*, glued-sphere particles)[5,60]. Superquadrics is a method similar to the glued sphere method in that the geometrical description of the particle is simple, but the superquadrics method allows the ability to create particle shapes with more angularity than the particle shapes created

through the glued sphere method[5]. Computer-aided design (CAD) packages have also been developed to create complex particle shapes[30,59]. Graphical processing units (GPUs) are then used to determine the contact points between the particles shaped through CAD in a relatively efficient manner[30,59]. It is easier for the GPU to process the contact points between particles because of the basic algebra used to describe the contact between surfaces[30]. Ultimately, this method is similar to the glued sphere method in that it breaks down a complex shape into small, simple components.

Although, the glued-sphere technique and other methods exist to simulate different particle shapes and surface roughness variability, DEM models still face the challenge of modelling more than a handful of particle shapes at a time. Currently, only about five to ten different particle shapes can be incorporated into a DEM model[8,28]; this means that only a small fraction of the particles in a powder are represented in a DEM simulation. Another challenge faced is accounting for the entire size distribution of a powder[62], as most DEM investigations only simulate a unimodal or bimodal size distribution. It is also important to note DEM simulations utilize large particle parcels mm in size (agglomerates comprising the individual particles) to describe the powders which can lead to misrepresentation of the actual small scale particle mechanics if parameters are not tuned properly[62].

2.3 Enhanced centrifuge method

To begin to address the community's need to describe the effect of the individual particle properties, such as shape and surface roughness, towards the overall behavior of a powder, Thomas and Beaudoin developed a technique called the enhanced centrifuge method (ECM)[32]. The ECM describes the vdW adhesion of a population of realistic particles, each with their own surface topography and shape, against a substrate surface through 'effective' Hamaker constant distributions[32]. These distributions represent an engineering approach that allows powders comprised of particles of complex shape and roughness, which are challenging to model, to be described as if they were perfect, smooth spheres, which are comparatively simple to model. The complexity associated with the shape and size distributions of the individual particles is captured by the 'effective' Hamaker constants. As it is, these 'effective' Hamaker constants quantify both the effect of the particles' properties and the effect of the surface properties towards the particle-

surface interactions. The objective of this research is to advance the ECM to characterize these effects on different adhesion forces beyond the vdW force.

3. THE EFFECTS OF SURFACE AND PARTICLE PROPERTIES ON VAN DER WAALS (VDW) ADHESION QUANTIFIED BY THE ENHANCED CENTRIFUGE METHOD

Reprinted with permission from Powder Technology. 2021, 392. DOI: 10.1016/j.powtec.2021.07.028 Copyright 2021 Elsevier B.V.

3.1 Introduction

Powder technology plays a significant role across a number of industries. Example industries include the food and pharmaceutical processing industries, in which a great many ingredients are processed in powder form [1–5]. Security and defense applications also put emphasis on powder technology, specifically understanding explosive, propellant and pyrotechnic powder adhesion during processing or detection. Examples of industrial processes that involve powders include milling, blending, spreading, and compaction [5,8–10]. The behavior of the powders in these processes is impacted by the adhesion of the individual particles which comprise the powder [11]. Behaviors such as caking, poor flowability, dust hazards, segregation, equipment wear, and "picking and sticking" arise due to uncontrolled particle adhesion and cohesion [11,15,16] and can lead to manufacturing problems. The adhesion force is the force necessary to separate a particle in contact with a dissimilar surface while cohesion is the force necessary to separate two particles of the same composition [12]. To prevent such problems and optimize powder processes, the effects of the particle and equipment surface characteristic on the adhesion behavior of the powder needs to be well understood. The adhesion force in non-reactive, non-deformable powders is attributed to van der Waals (vdW), capillary, and electrostatic forces present between adherent surfaces [12–14]. Contact separation distance, chemical composition, particle size, particle shape and surface roughness all affect the interaction between two adherent objects [17–19]. It is especially important to characterize surface roughness and particle shape because these properties cause variations in the contact area between a particle and interacting surface which ultimately affects the degree of adhesion [20–22]. Therefore, mathematical and computational models have been developed to understand and quantify these effects on the adhesion systems [23–29,55,63,64].

A common limitation of these methods lies in their inability to accurately describe the adhesion of populations of particles. Often, computational models use highly idealized powders

(*i.e.*, powders comprised of simple geometries such as spheres) to predict powder behavior under various process conditions. This limits the ability to optimize the manufacturing and handling of powders comprised of complex (real) particles [9,30,31]. Recently, the enhanced centrifuge method (ECM) was developed to address this need by describing the adhesion between surfaces and powders comprised of particles with varying surface topography and shape [32]. This method involves tuning the Hamaker constant, A_{132}. This constant is ordinarily a parameter that captures the ability of dipoles in adherent materials to interact with the fields produced by dipoles in opposing adherent materials. It is a function only of the composition of the interacting surfaces and the intervening medium, and it is useful to quantify the vdW adhesion between two materials (represented by subscript 1 and 2 in A_{132}) in a medium (subscript 3 in A_{132}). When this parameter is tuned to capture the effects of particle shape, particle size, particle topography, and surface roughness on the adhesion system, it is no longer a material-dependent constant, but now is expressed as distributions of 'effective' Hamaker constants represented by A'_{132}. This tuned distribution captures the effects of the shape, size, topography, and composition of the objects in the adherent system [32].

The purpose of this work is to demonstrate that 'effective' Hamaker constants can be used to quantify the effects of surface and particle topographical properties on the resulting particle-surface adhesion and to identify limiting topographies that cause powder adhesion to surfaces to be controlled by either the particles or the surfaces. These 'effective' Hamaker constants are valuable to practitioners who process powders as the distributions can be used to describe expected powder behavior as a function of particle and surface properties.

To illustrate how these distributions can be used to quantify the effect of surface and particle properties on the powder adhesion, the adhesion of polystyrene powders was measured against silica that was systematically polished to have increasing amounts of roughness. Root mean square (RMS) roughness has been a commonly-used parameter to easily quantify surface roughness [33–35]. However, studies have shown RMS roughness is an inaccurate descriptor of how the surface roughness will affect the adhesion; the adhesion behavior is a result of the interaction between the topography on the surface and the particles based on their relative sizes and shapes [63,65,66]. This was confirmed by a computational investigation of particle adhesion using a previously validated adhesion simulator [67], which confirmed that the relationship

between the height of the surface roughness peaks, the distance between roughness peaks, and the particle size are all important to the observed powder adhesion.

3.2 Materials and methods

3.2.1 Materials

Fluorescently marked polystyrene spheres (Fluoresbrite® YG Microspheres 25 µm) were provided by Polysciences, Inc. (U.S.A.). These non-deformable rigid polystyrene particles have a general shape of a sphere and a particle material density of 1.05 g/cm^3. High Purity Silica Single Crystal purchased from Silica Source was the surface of choice because it is initially highly uniform and because it can easily be polished to systematically change its surface roughness. The silica was cut into 0.5 x 0.5 x 0.07 cm pieces and glued onto stainless steel (type 316, McMaster-Carr Supply Company, 9745K15) backings to ensure the silica did not shatter under the inertial force introduced by the centrifuge. The stainless steel backings were cut to 1 x 1 x 0.07cm in order to fit into specially-designed centrifuge tubes. The centrifuge tubes are 11 cm in length and have a diameter of 2.5 cm. The tubes are solid except for a 2 cm x 2 cm opening on the side that contains a holder for the plates. The holder allows the silica plates to be orientated such that the silica surfaces are parallel to the center of rotation of the centrifuge. The schematic of these tubes is presented in Fig. 3.1.

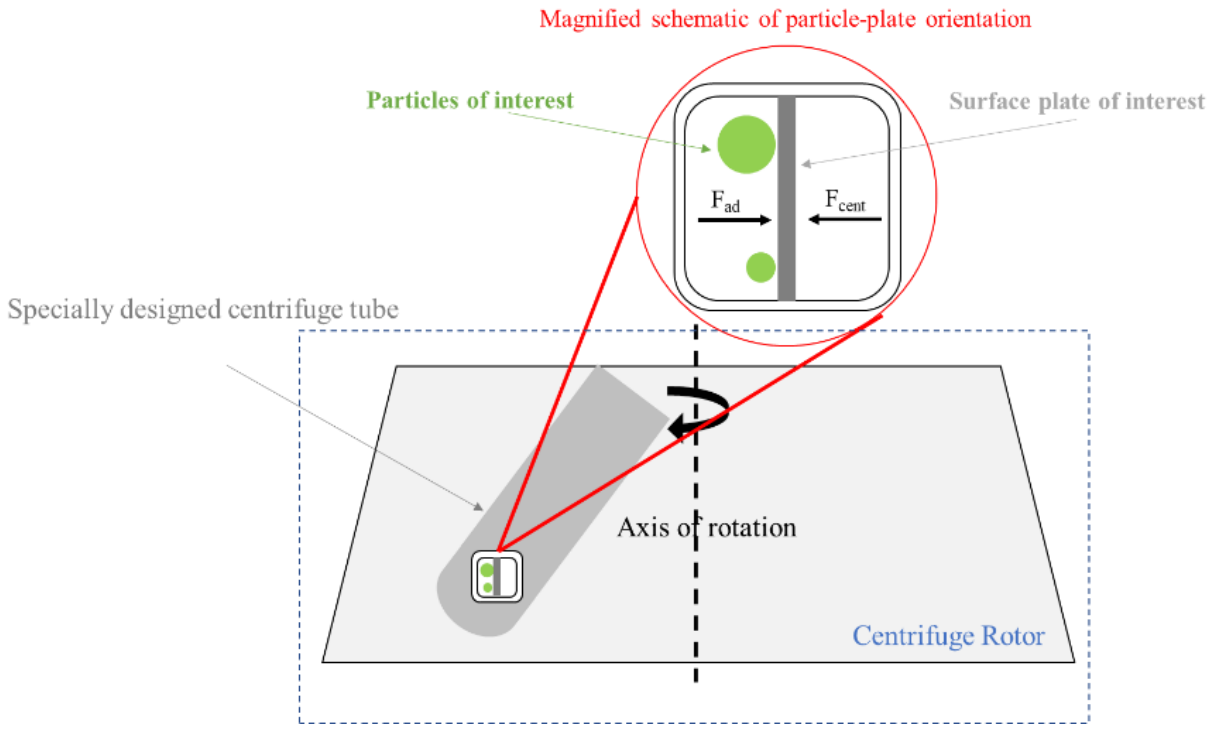

Figure 3.1 Illustration of a powder-laden surface mounted in a specially designed centrifuge tube. The powdered surface is oriented parallel to the axis of rotation of the centrifuge with the particles facing radially outward. When a particle detaches from the surface, the inertial force, F_{cent}, has overcome the particle's adhesion force, F_{ad}.

3.2.2 Experimental methods

Silica polishing and cleaning procedure

A Buehler Minimet 1000 polisher was used to systematically alter the surface roughness of the silica. Silica squares (2.5 cm x 2.5 cm) were mounted to the polishing arm with mounting wax. The polishing cloth used was MasterMet cloth (Buehler). The plates were polished each with a different MetaDi Supreme Diamond Suspension paste. Table 3.1 shows the average diamond particle diameter, d_{50}, in each paste. Each silica piece was polished for five minutes at 30 revolutions per minute (RPM) under a 13 N load. After polishing, each silica piece was cut into four pieces, each approximately 0.5 x 0.5 x 0.07cm. The pieces were then soaked in a warm acetone bath for at least ten minutes to dissolve any residual mounting wax. They were then rinsed with methanol and dried with compressed nitrogen, after which each silica piece was glued to its stainless steel backing with Scotch Advanced Formula Super Glue and allowed to dry overnight.

Table 3.1. Dimensions of pastes used to roughen silica plates in this work.

Silica Surface	Polishing Paste, d_{50} (µm)
A	No Polishing
B	6
C	30
D	Sandpaper - Grit 60

Surface topographical evaluation by profilometry

A Dektak XT profilometer was used to measure the roughness of the silica pieces after polishing and cleaning. After each polished silica surface was cut into four pieces, four regions of interest were identified on each of the pieces and a topographical scan was taken on each region (4 regions per piece, 4 pieces per surface to yield 16 scans per surface). Each topographical scan length was 100µm.

Amplitude spectra surface scans

A representative roughness scan was selected from the 16 profilometry scans for each surface. In order to study the roughness features that existed on each of the surfaces beyond an RMS analysis, the roughness scans were transformed into numerical descriptions via a Fast Fourier Transform (FFT). The amplitude spectrum as a function of wavelength was then constructed from the FFT via MATLAB. The amplitude spectra were constructed to provide insight on the height (amplitude) of the peaks and the distance between peaks that may exist on a surface (wavelength).

Centrifuge method

To perform the centrifuge method, the following steps were executed. First, a #3 paint brush was dipped into the polystyrene powder and tapped just above the silica so that the particles fell on the silica without agglomerating. The particles were deposited in the presence of a STATICMASTER Ionizer (500 µCi) chip which ionized the air to neutralize the charge on all surfaces to reduce electrostatic forces and prevent agglomeration. To reduce the effect of capillary forces, the

particles were deposited onto the plates in a relative humidity environment of less than 20% by performing the deposition in a dry nitrogen ambient in a glove bag. The humidity was measured using a hygrometer.

A Nikon SMZ18 Stereoscope was used to capture optical images of the polystyrene particles adhering to the silica. The images were taken at 5X magnification to easily differentiate the particles from any defects on the silica surface. To perform the particle removal, the surface was mounted in the specially designed centrifuge tubes described above and illustrated by Fig. 3.1. Based upon the orientation of the surface and particles in the tube, it can be inferred that when a particle detaches from the surface, the inertial force generated by the centrifuge has overcome the adhesion force. The inertial force, F_{cent} (N) is described in Eq. 3.1, where R (m) is the radius of the particle, ρ_p (kg/m^3) is the particle density, ω (s^{-1}) is the angular velocity of the rotor and r_c (m) is the distance of the particle-laden surface from the center of rotation:

$$F_{cent} = \frac{4}{3}\pi R^3 \rho_p \omega^2 r_c \tag{3.1}$$

A Sorval Lynx 6000 centrifuge was set to the following rotational speeds: 1500, 3000, 4500, 6000, 7500, 9000, 10500 and 12000 RPM for one-minute intervals to perform the particle removal. After rotation at each speed, the Nikon SMZ18 Stereoscope was used to take optical images of the particles remaining on the surfaces and ImageJ (NIH) was used to process these images to determine the number of particles remaining as a function of the rotational speed. The entire surface and the initial size distribution of the deposited polystyrene particles were captured by analysis of an image taken before the plates were placed in the centrifuge at the start of an experiment (*i.e.*, when 100% of the particles were on the surface).

3.2.3 Simulation methods

Determination of A'_{132} distribution

After performing the centrifuge method, the ECM was executed. The ECM was developed to determine the adhesion force of all the particles of a powder against a surface as a function of their size [32]. The ECM is an engineering approach that allows powders comprised of real particles, which are challenging to model, to be described as if they are comprised of perfect, smooth spheres, which are comparatively easy to model. In this case, the complexity associated with the

actual particles and their interactions with a complex surface is captured by an empirical A'_{132} in a vdW force model, although other force models could be applied if desired [55,63]. In brief, the procedure for determining these A'_{132} used to capture the effect of surface roughness and particle shape and topographical properties on the adhesion through the ECM is described through the following steps (an in-depth description is given elsewhere [32]):

1. The size distribution of the experimental powder as deposited on a plate at the start of an experiment is measured via ImageJ.
2. A simulated powder comprised of 1000 spherical particles is generated *in silico* such that the size distribution matches that of the experimental powder. This distribution is referred to as the *ideal particle size distribution*.
3. The vdW adhesion force is computed between the ideal spheres from step 2 and a flat surface *in silico* using Eq. 3.2:

$$F_{vdW}(D) = \frac{A'_{132}R}{6D^2} \text{ or } \frac{F_{vdW}(D)}{R} = \frac{A'_{132}}{6D^2} = constant \qquad 3.2$$

   where A'_{132} is the 'effective' Hamaker constant, R is the radius of the sphere, and D is the separation between the sphere and the flat plate at contact [67]. The Hamaker constant is initially set to an artificially low value of 5 zJ for all particles. This value is readily adjusted to map the adhesion behavior of the ideal particles to the adhesion behavior of the experimental powder. A standard separation distance at contact, D, accepted by the community is 0.4 nm [68]. The Derjaguin approximation for the vdW force [36] (Eq. 3.2) was used in lieu of a more complex model, such as the Rabinovich model [55], in order to keep the mathematical framework of the model as simple as possible. While other models capture the effects of topography and shape through parameters such as asperity radii [63,66,69–72], the ECM captures the effects of surface roughness and shape through the A'_{132}.
4. The adhesion force represented by Eq. 3.2 is related to the inertial force represented by Eq. 3.1 to determine the angular velocity necessary to dislodge the spherical particles from the smooth surface

$$\omega = \sqrt{\frac{3F_{cent}}{4\pi R^3 \rho_P r_c}} \tag{3.3}$$

and the angular velocity is converted into RPM through Eq. 3.4:

$$RPM_{removal} = \frac{60\omega}{2\pi} \tag{3.4}$$

5. The 'experimental powder adhesion curve' is created by plotting the observed percent of polystyrene powder remaining adhered to the silica as a function of the rotational speed of the centrifuge when using the centrifuge method discussed in section 3.2.2 (inertial force from the centrifuge causes particles to detach from the surface, and optical and image analysis is used to track the number of particles of each size that remain as a function of inertial force).

6. The 'ideal powder adhesion curve' is created using Eqs. 3.1-3.4 with the ideal particle size distribution and an assumed value of A'_{132}, and then plotting the percent of particles remaining adhered after each rotational speed increment of the centrifuge. At this point, the 'ideal' powder adhesion curve is predicted using an assumed value of A'_{132} of 5 zJ and the 'experimental' powder adhesion curve is measured experimentally via the centrifuge technique. The 'ideal' and 'experimental' adhesion curves will not match because the ideal adhesion case has not been tuned to account for the particles' surface roughness and shape variation, nor for the roughness on the silica.

7. To map the ideal powder behavior to the experimental powder adhesion, the ideal particle size distribution is sorted from largest to smallest and the particles are placed in bins by size, such that the percent of particles in each bin matches the percent of particles observed to be removed at each RPM increment implemented experimentally. For example, if 30% of the experimental powder was removed between 0 and 2000 RPM, bin 1 would contain the largest 30% of the ideal size distribution. Note: an assumption/limitation of this method is that the particles fall off from largest to smallest as the inertial force increases.
8. The average particle size for each bin, also called the mean bin particle diameter (D_{mean}), of the discretized ideal size distribution is determined and the A'_{132} is adjusted for each bin

such that a particle with the mean bin particle diameter is removed at the observed experimental rotational speed. In this way, the adhesion of the ideal D_{mean} is adjusted by tuning the $A_{132}^{'}$ parameter so that the adhesion of the ideal powder matches that of the experimental powder

The distribution of $A_{132}^{\prime}$ values as a function of D_{mean} approximately quantifies the effects of the roughness of the surface and the effects of the shape, roughness, and size variation of the particles on the adhesion between the powder and the surface.

Three-Dimensional (3D) surface generation

MATLAB was used to generate a model rough surface in the form of a 3D sinusoidal mesh grid with 512 points per line. The roughness features generated resembled an egg crate where the same sinusoid description was used in the $\hat{\imath}$ and $\hat{\jmath}$ directions. To create different levels of RMS roughness, the amplitude of the sinusoid was adjusted. To change the distance between the roughness peaks, the wavelength of the sinusoid was adjusted.

Particle adhesion simulator

An existing model-based simulator (the *Particle Adhesion Simulator*) was used to describe the adhesion force between realistic particles and surfaces [29,67]. This simulator takes user input descriptions of the particle size and shape, and the particle and surface topography, discretizes the two interacting surfaces into nanoscale cylinders, brings the two surfaces into close contact (0.4 nm separation) and calculates the adhesion forces between opposing cylinders in the two objects[29]. One overall adhesion force representing the particle and surface interaction, while accounting for the surface roughness and shape properties of the two materials, is determined by summing the individual adhesion forces representing the interactions between the nanoscale cylinders across the discretized surfaces. This process is repeated 1200 times to generate a distribution of estimated adhesion forces to provide a representative average adhesion force to describe the interaction between the two materials taking into account the surface roughness and shape effects on the adhesion[29].

Simulation of centrifuge method

The *Particle Adhesion Simulator* was used to simulate a centrifuge experiment involving polystyrene particles with diameters ranging from 1 to 50 μm adhering to a perfectly flat silica surface generated *in silico*. For each particle size, the average simulated adhesion force was converted into an average RPM of removal based on Eqs. 1-4 above. Using the particle size distribution measured experimentally and this simulated average RPM removal data, a 'simulated particle adhesion curve', which describes the fraction of particles remaining at each centrifuge RPM, was constructed.

3.3 Results and discussion

3.3.1 Silica surface roughness results

As described in the methods section, four silica surfaces were polished to different degrees of roughness, each was divided into four pieces, and four profilometer scans were obtained for each piece for a total of 16 scans for each surface (each different degree of roughness). The root mean square (RMS) roughness, R_q, of each scan was calculated according to

$$R_q = \sqrt{\frac{1}{n}\sum_{i=1}^{n} y_i^2} \qquad 3.5$$

where n is the number of points tracked along a surface and y_i is the difference between the height value of each point and the mean height value of the data set (the trace)[54]. An average RMS roughness was calculated by taking the average of the RMS values from each of the 16 scans of each of the 4 polished silica surfaces, and this value was used to describe each surface as a whole. Table 3.2 contains the average RMS roughness across each polished silica surface and the standard deviation in the RMS roughness values.

Table 3.2. Roughness characteristics of 4 surfaces used in powder adhesion study.

Silica Substrate	Average RMS Roughness (nm)	Standard Deviation (nm)
A	3	1
B	7	2
C	192	150
D	437	180

3.3.2 Centrifuge method results

The relative humidity was controlled during particle deposition and during the centrifuge experiments. However, the relative humidity was not rigorously controlled when the plates were removed from the centrifuge, evaluated in the microscope, and returned to the centrifuge. During these times, the plates with mounted particles experienced adsorption of moisture and capillary forces may have developed. This condensation likely was not fully reversible so that these experimental studies may have been influenced by a combination of vdW and capillary forces, although for these first generation experiments it was assumed that the adhesion was due to vdW forces only. Even with this limitation, the A'_{132} distributions determined from these experiments still quantify the effects of the topography of the surface and the topography and shape of the particles on the overall adhesion.

The distributions in Fig. 3.2 represent the observed percent of particles that remained after each RPM increment. Each data set represents the average of four experiments. Fig. 3.2 shows that the adhesion between the powder and the surfaces does not vary smoothly with increasing RMS roughness on the surfaces. Based on the vdW adhesion for smooth spheres against flat surfaces in Eq. 3.2, the particle-surface adhesion should increase linearly with increasing particle radius. Eq. 3.1 shows that the removal force increases linearly with rotational speed and with the particle radius cubed (through the sphere volume which influences the mass of each sphere). This means that, all other things being equal, the largest particles will come off at the lowest rotational speeds. So, at rotational speeds below 7500 RPM, the larger particles in the powder were assumed to be removed, with the smaller ones removed at greater speeds. At speeds below 7500 RPM, surfaces A and B (with 3 and 7 nm RMS roughness,) retained larger percentages of particles at all speeds

than either surfaces C (RMS roughness = 192 nm) or D (RMS roughness = 437 nm). Also, for all speeds in this range, the percentage remaining consistently was the lowest for the roughest surface. These results suggest that the largest particles in the powder are influenced differently by different levels of roughness on the silica. For the most rough surfaces (C and D), the adhesion between the large particles and the surfaces clearly drops as the RMS roughness increases. This is consistent with the idea that the large-scale topographical variations on the extremely rough surfaces directly modulate the number of contacts with the large particles over the length scale of the large particle diameters. For the extremely smooth surfaces, though, the adhesion of the largest particles is influenced by the topography of the surfaces in a more complex manner. First, when the surfaces shift from being extremely rough to being extremely smooth, the retention of the large particles increases. It is likely that the reduced overall level of roughness results in a greater area of close contact available between the particles and the surface, resulting in stronger vdW forces. However, the surface with 7 nm of RMS roughness retains the same or more particles than the surface with 3 nm of RMS roughness over all of the large particle sizes. This implies that some set of features on surface B (7 nm RMS roughness) interacts more strongly with the features on the large spheres than do any of the features on surface A (3 nm RMS roughness), leading to larger adhesion than in the absence of these features. Based on the relatively small RMS roughness of surface B, these features which so strongly influence the adhesion must be very small, as they have a minimal effect on the RMS roughness.

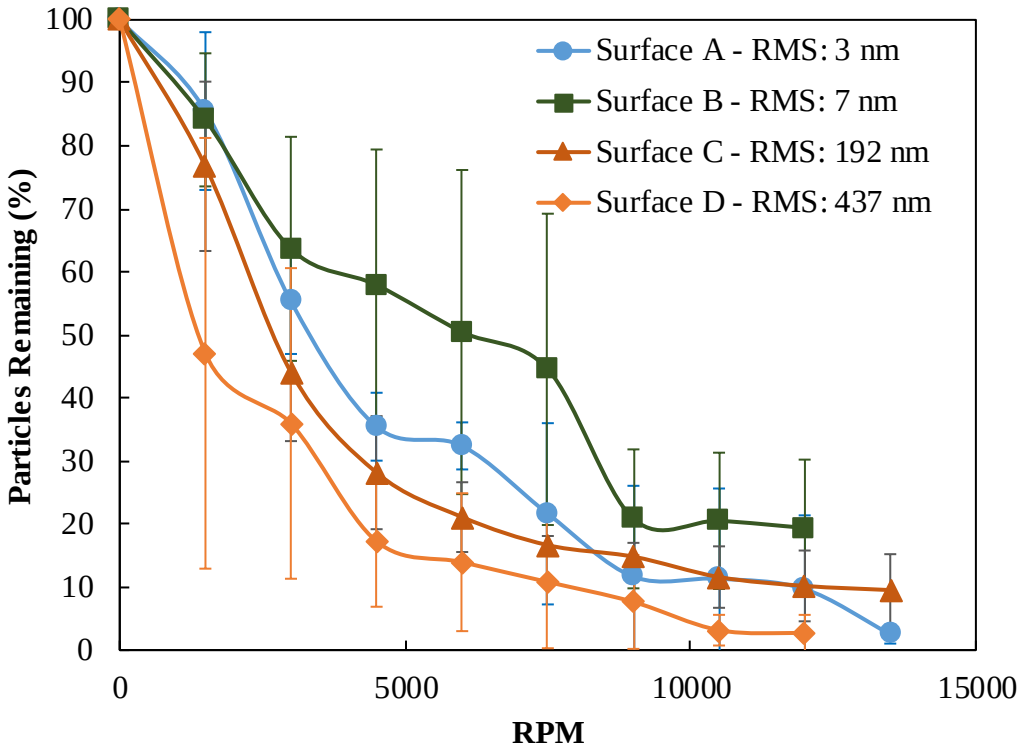

Figure 3.2 Observed percent of polystyrene spheres remaining on rough silica surfaces after rotation in centrifuge at various rotational speeds. Error bars represent the standard deviation of the percent adhering to each surface across all replicates for that surface.

When the rotational speed varies from 9000 to 12000 RPM, the smaller particles in the distribution are removed. For every rotational speed in this range, surface B (7 nm RMS roughness) retained the largest fraction of particles. However, the retention on surfaces A and C (3 and 192 nm RMS roughness) was virtually indistinguishable over this range. As a very smooth surface becomes rougher with polishing, it is expected that the rough peaks on the surface prevent close contact between the particle and the surface, reducing the adhesion. However, when certain roughness features are present on the surface, it is possible for a particle to "nest" in the feature, as illustrated in Fig. 3.3A. This nesting phenomenon results in an increase in area of close approach between the particle and surface, causing the adhesion to be higher compared to what may be observed in the presence of a smoother surface. Alternatively, although a surface may have a lower level of RMS roughness, the roughness peaks may be distributed such that the particle rests on top of the peaks instead of nesting between them, as illustrated in Fig. 3.3B. In this case, the adhesion will be lower because the particle is less intimately contacting the surface.

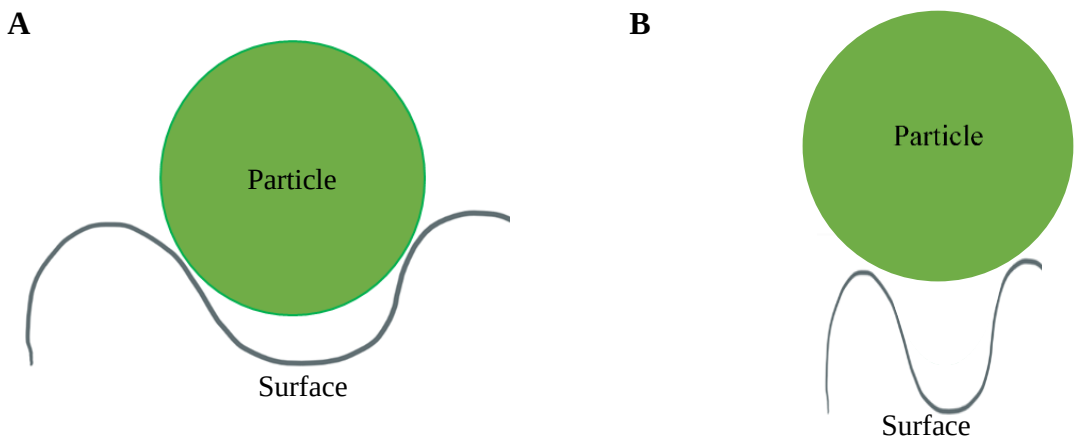

Figure 3.3 Illustration of a spherical particle nesting within (A) or on top of (B) surface roughness peaks for roughness peaks of similar height.

To determine if this nesting behavior is a plausible phenomenon for the silica surfaces and polystyrene particles used in this study, ImageJ analysis of samples of the polystyrene powder deposited on surface A was performed to determine the size distribution of the particles present on the surface. The particle diameter distributions on surface A, across four replicates, were selected in lieu of distributions determined by laser diffraction to represent the size distribution across all surfaces used in this study. This was because the images on this surface had little to no background noise, facilitating accurate particle counting, and because errors in the observed size in each experiment (due to shadowing, for example) would be consistent with the errors in the size distribution and would have less of an effect on the overall analysis. A lognormal distribution was used to describe the observed number-based particle diameter distribution shown in Fig. 3.4, with the following lognormal parameters: $\mu = 3.368$ with 95% confidence interval and $\sigma = 0.136$.

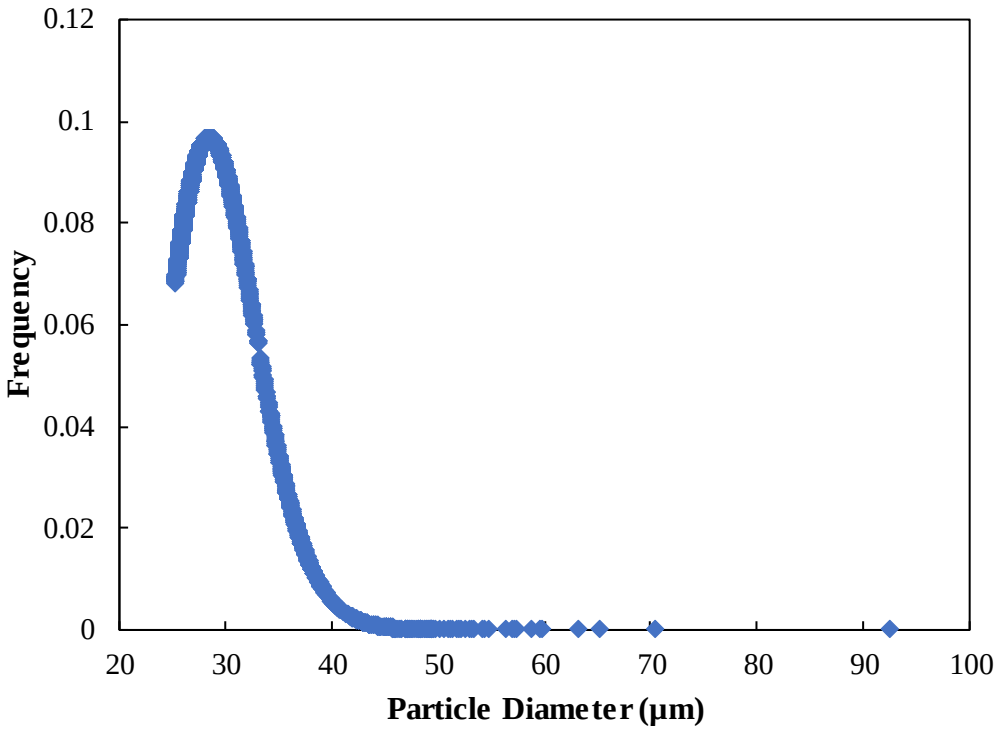

Figure 3.4 Number-based particle diameter frequency distribution determined through ImageJ analysis of polystyrene distributed on silica surface A.

To investigate the relationship between the adhesion, the particle size and the distance between surface peaks, an amplitude spectrum analysis of the topography of each surface scan was executed via the procedure discussed in section 3.2.2 (the surface scan is converted into a numerical description via FFT and the amplitude spectrum is then constructed from this FFT *in silico*). Fig. 3.5 illustrates all four surfaces contain wavelength features (*i.e.*, distance between peaks) that could allow the particle nesting illustrated by Fig. 3.5 and the size distribution presented in Fig. 3.4. For example, surface D has peaks that have amplitudes greater than 50 nm in height and wavelengths greater than 30 µm such that particles with radii ranging from 1 µm to 15 µm are able to nest in the peak features and come into more intimate contact with the surface than in the absence of such a relationship between particle size and peak distance. It is important to note that the amplitudes that correspond to the larger wavelengths (larger distance between peaks) vary amongst the surfaces studied here. The amplitude spectra representing surfaces A and B are on the same scale as each other as seen in Fig. 3.6, while the amplitudes on surfaces C and D are one or two orders of magnitude greater than those on surfaces A and B, as seen in Fig. 3.7. The

relationship between the amplitude and the wavelength of the peaks is important to consider. For example, corresponding larger peaks that are separated from each other by distances greater than the size of the particle diameters will allow for particle nesting and more intimate contact with the surface, while the same large peaks positioned at separations smaller than the particle diameters would instead cause point contact and reduce the particle adhesion.

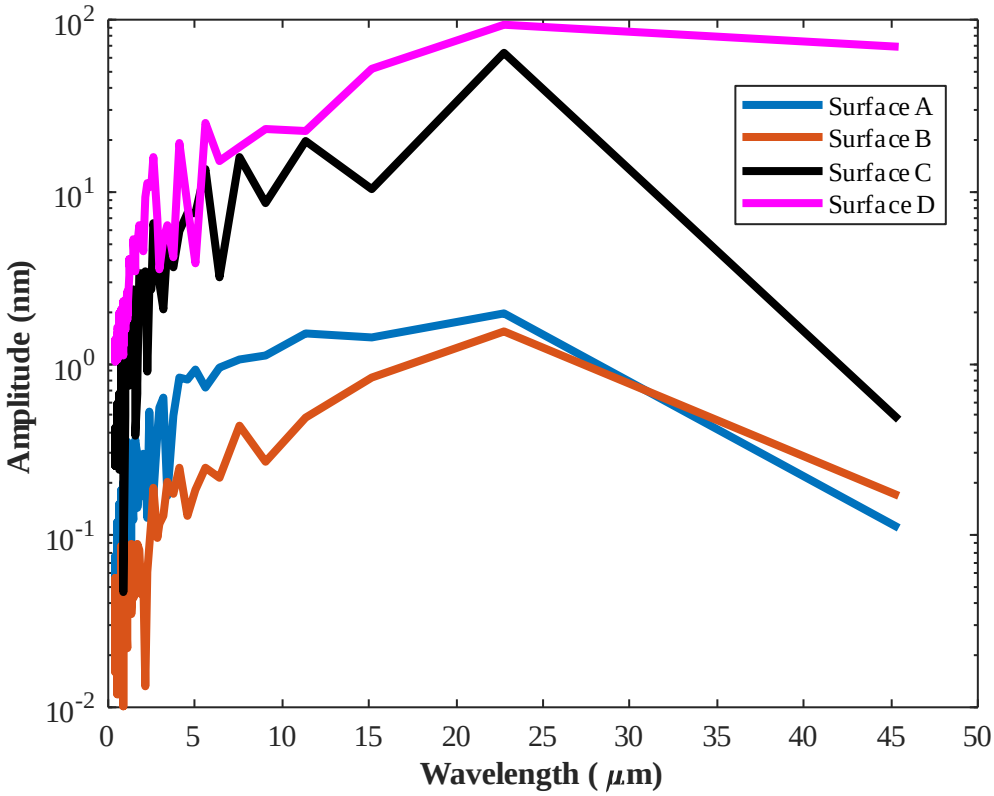

Figure 3.5 Amplitude spectra of the four silica surfaces as a function of the wavelength for surfaces A through D. Note, the y-axis is plotted on a log scale.

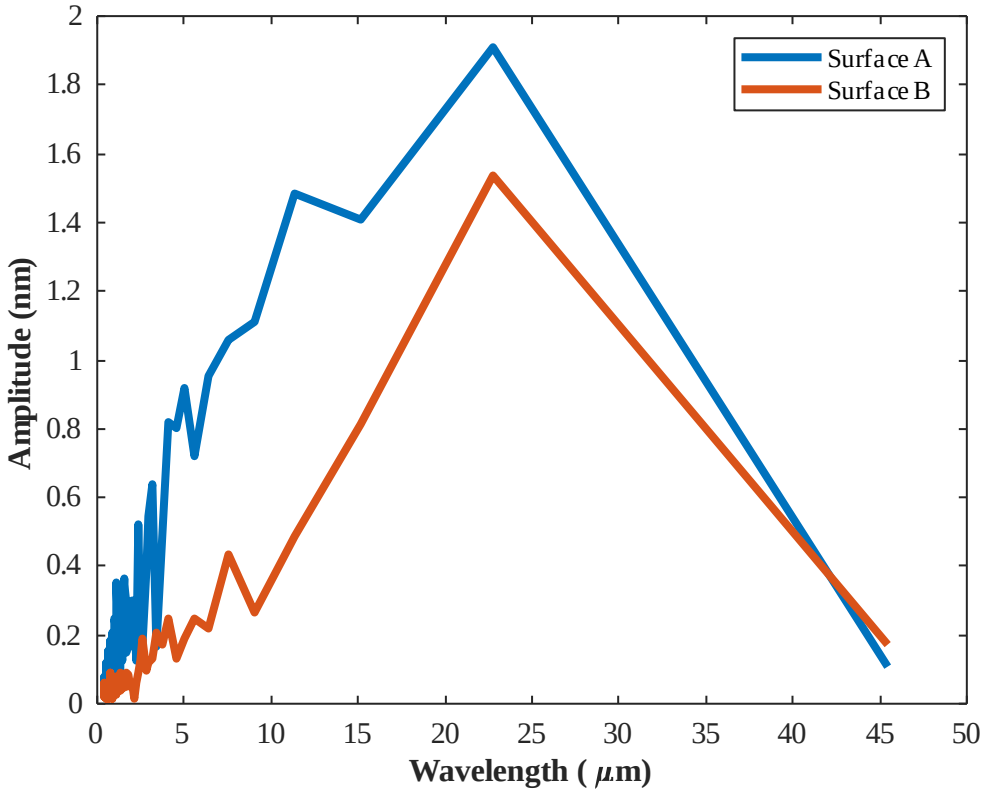

Figure 3.6 Amplitude spectra of the four silica surfaces as a function of the wavelength for surfaces A and B.

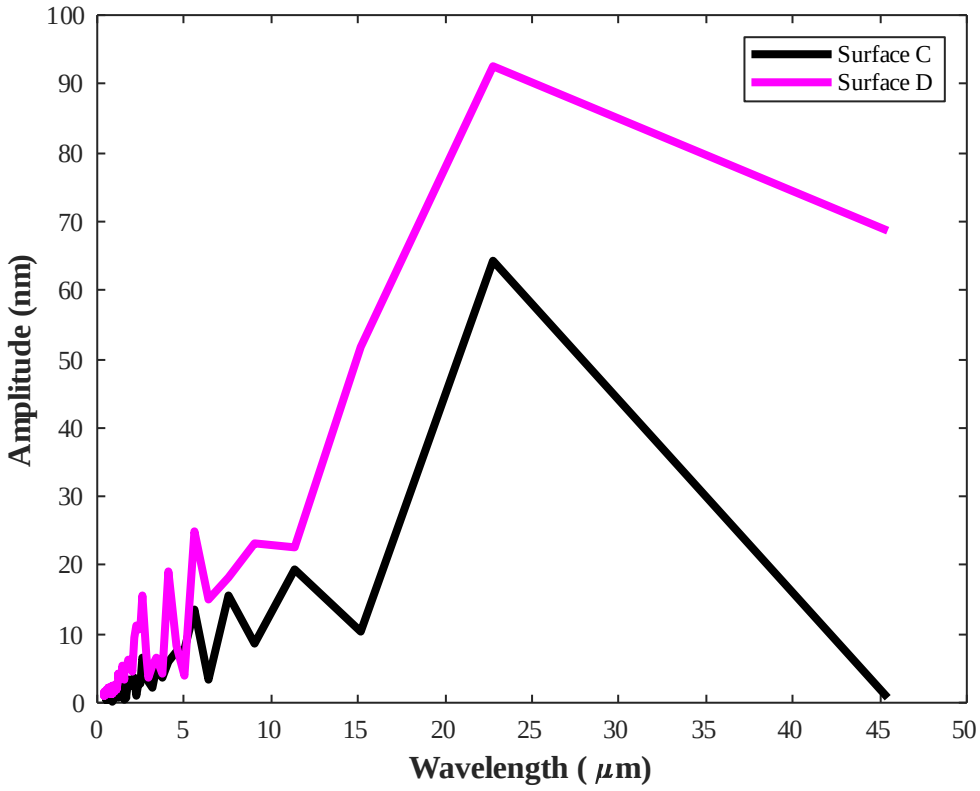

Figure 3.7 Amplitude spectra of the four silica surfaces as a function of the wavelength for surfaces C and D.

Overall, these amplitude spectra illustrate that all surfaces have features that could encourage nesting or discourage it as seen in Figures 3.5 through 3.7, depending on the scale of the particle features relative to the amplitude and wavelength of the features on the surfaces. The initial adhesion behavior illustrated in Fig. 3.2 between surfaces A and B indicates that although the amplitude spectra may overall be similar, slight differences in the scale of the amplitude can cause adhesion variation. The A'_{132} distributions are developed to capture and describe these variations in adhesion that occur due to small differences in the powder and surface properties.

3.3.3 Enhanced centrifuge method and results

The ECM was implemented to assess how the variations in observed particle adhesion resulting from the changes in surface roughness due to polishing are reflected by the A'_{132} distributions. A key component of the ECM is first determining the size distribution of the powder on the surfaces.

For this purpose, the size distribution determined via images of the polystyrene particles deposited on surface A presented in Fig. 3.4 was used.

The *Particle Adhesion Simulator*, discussed in section 3.2.3, was used to approximate the adhesion force between perfect spherical particles with diameters between 25 μm and 50 μm and a perfect flat surface. A Hamaker constant of 120 zJ, presented as an estimate for the adhesion between silica and polystyrene from previous studies, was used to represent the adhesion between the silica and the polystyrene particles to execute this procedure [17]. The adhesion forces corresponding to the particles in the size distribution were used to simulate the centrifuge method by approximating the percentage of particles remaining adhered to the flat silica as a function of RPM for the perfect powder. This *ideal powder adhesion curve* relates the *ideal particle size distribution* to the expected adhesion forces through the value of A'_{132} for each particle size.

The fitted A'_{132} distributions for the polystyrene adhesion against surfaces A-D, normalized by the estimated true Hamaker constant, $A_{'True'}$, for polystyrene spheres against a flat silica plate (120 zJ), are presented in Fig. 3.8. The vertical axis of Fig. 3.8 shows that the range of A'_{132} values representing the adhesion against each of the surfaces never goes beyond 0.5. This shows how the topography of the spheres and the surfaces prevents close approach between the particles and the surface over all particle sizes. The error bars displayed in Fig. 3.8 describe the standard deviation around the mean A'_{132} determined for each size bin (see steps 6-8 in simulation methods section) the ideal powder is discretized into based on the experimental percent remaining information.

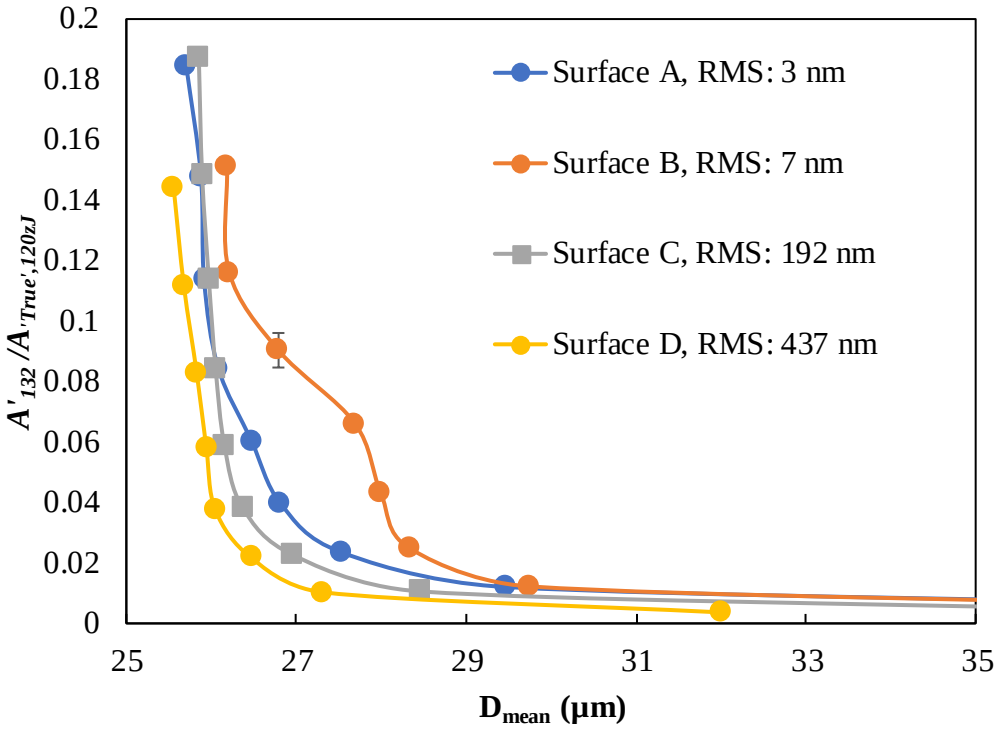

Figure 3.8 Fitted A'_{132} normalized by the ideal (true) Hamaker constant for polystyrene particles against a flat silica plate ($A_{'True'}$; 120 zJ) for polystyrene powder against surfaces A through D. The error bars represent the standard deviation around the mean normalized A'_{132} for each bin of the ideal powder size distribution (steps 6-8 used to create the A'_{132} describe binning process in the simulation methods section).

In Fig. 3.9, the A'_{132} are normalized by particle diameter. For large particle diameters (~30 µm or larger) there is little change in the normalized A'_{132} for surfaces A through D. In this regime, the particles are sufficiently large compared to the topographical features on the silica that the silica acts like an effective, highly porous flat plate and the behavior scales as one would expect for a sphere-flat plate system (Eq. 3.2). In this case, the normalized A'_{132} distributions should be independent of size, which is observed. For D_{mean} less than 30 µm, the A'_{132} distributions vary between the silica surfaces. In these cases, the 'effective' Hamaker constants describe the interplay between the surface topography and the particles' surface features.

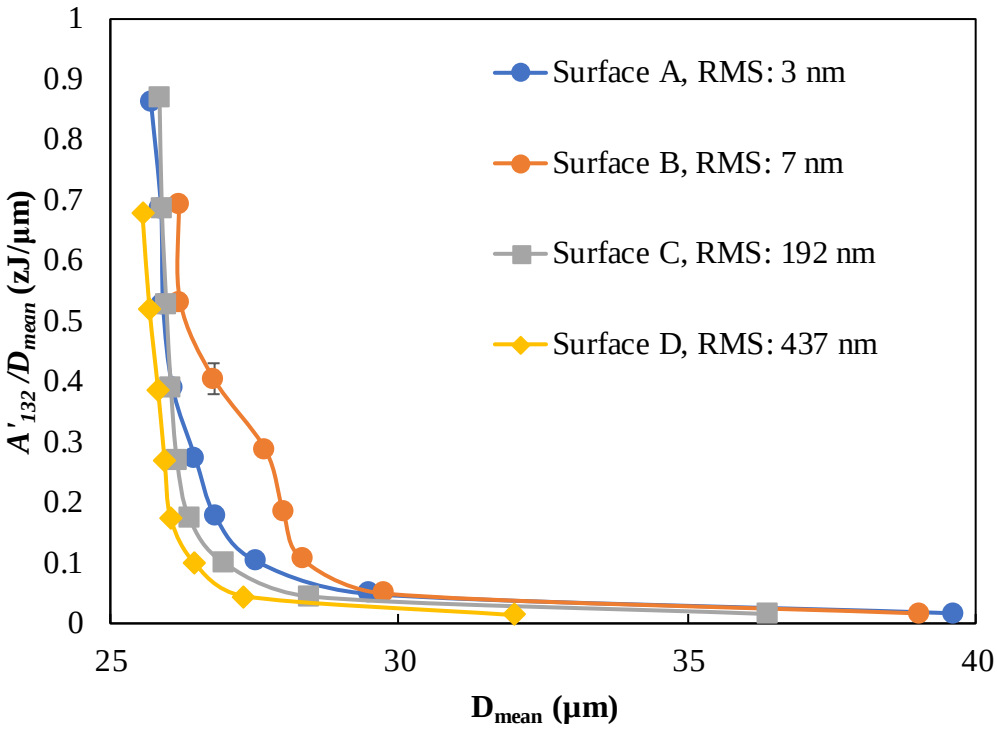

Figure 3.9 Fitted A'_{132} normalized by D_{mean} for the polystyrene particle adhesion against surfaces A through D. The error bars represent the standard deviation around the mean normalized A'_{132} for each bin of the ideal powder size distribution (steps 6-8 used to create the A'_{132} describe binning process in the simulation methods section).

The A'_{132} values corresponding to diameter sizes ranging from 27 µm to 30 µm are similar across all surfaces except surface B. In the case of surface B, the A'_{132} values are slightly higher compared to the other three surfaces. The higher adhesion suggests the relationship between these particle sizes and the roughness features, in terms of amplitude and wavelength on surface B encouraged the particles of this size range to come into more intimate contact with the surface causing higher adhesion than on the other surfaces.

Fig. 3.9 illustrates that the A'_{132} distributions representing the adhesion against surfaces A through D align well with each other at D_{mean} less than the 27 µm value. This implies that these particle sizes are interacting with the peaks across all surfaces in a similar manner. The amplitude spectra of all surfaces presented in Fig. 3.5 support this postulation as they are seen to have similar scale wavelengths (*i.e.* groves for the particles to nest within). The A'_{132} distributions representing the adhesion against surfaces C and D were similar for D_{mean} of 27 µm and higher implying these

particle sizes interacted with surface C and D and their features in a similar manner, as well. However, at D_{mean} of less than 27 μm, the A'_{132} were higher for surface C than for surface D. Upon looking back at the amplitude spectra presented in Fig. 3.6 representing the peaks on surfaces C and D, it is seen the amplitudes corresponding to the peaks on surface D are larger than the amplitudes corresponding to the peaks on surface C. The larger peak amplitudes on surface D are likely the cause to why the particles of size smaller than 30 μm are adhering less strongly to surface D compared to surface C.

3.3.4 In silico investigation of the effect of the surface roughness features on adhesion

To illustrate how particle adhesion is affected by the interplay between the particle properties and the topography of the opposing surface, a study was performed *in silico* using the *Particle Adhesion Simulator* in section 3.2.3. Specifically, the effect of particle nesting within features on surfaces was investigated, with a goal of evaluating the appropriateness of using RMS to guide particle adhesion discussions[55,65,73].

Two sinusoidal surfaces with RMS roughness of 25 nm were generated according to the procedure presented in section 3.2.3 (3D sinusoidal mesh surfaces were generated via MATLAB software). The distance between peaks (*i.e.* wavelength) on surface 1 was set to be 500 nm while the distance between peaks on surface 2 was set to be 10000 nm. The two surfaces are shown graphically in Fig. 3.10.

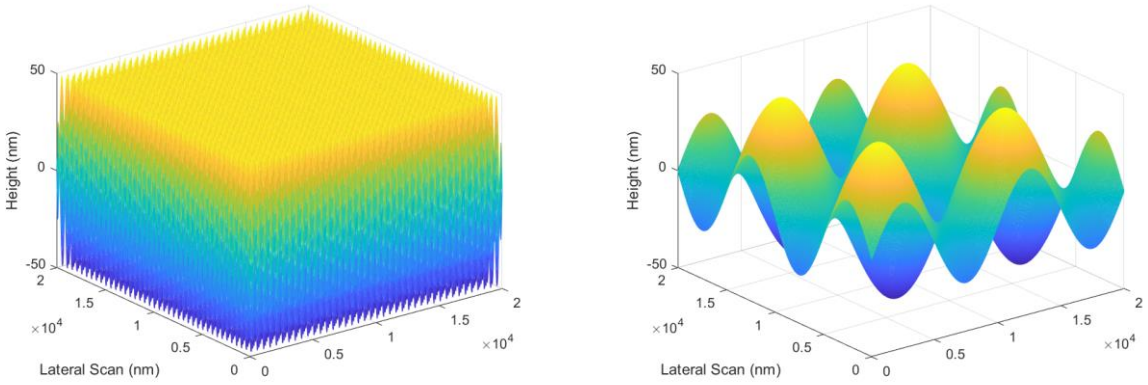

Surface 1 Surface 2

Figure 3.10 MATLAB generated topographical maps of surface roughness features on 2 surfaces. The lateral scan length was 20000 nm in the x-y direction.

Using the *Particle Adhesion Simulator*, spherical particles with diameters ranging from 0.1 to 50 μm were allowed to approach these two surfaces. An initial Hamaker constant of 120 zJ was inputted into the simulator, representing the adhesion between polystyrene and silica [17]. The particle and surface were brought into contact, computationally, 1200 times at random locations on the surface, and an average adhesion force, F_{ad}, was determined for each particle diameter, D_p.

The normalized (by D_p) calculated F_{ad} are plotted as a function of particle diameter in Fig. 3.11. The normalized F_{ad} distribution representing the particle adhesion against a flat plate is constant across all particle sizes, as expected from Eq. 3.2. The same result occurs when the particles interact with surface 2. Although surface 2 has an RMS roughness of 25 nm, the low occurrence of peaks due to the long wavelength of the roughness across the surface causes the adhesion to be essentially the same as when the particles adhere to a flat plate. The slightly higher adhesion and little to no standard deviation of the F_{ad} values seen for particle diameters less than 10 μm against this surface illustrates that these particles are able to nest within the surface peaks and more intimately contact the surface in a consistent manner than when larger particles are considered. In addition, for particle sizes above 10 μm, the standard deviation of the F_{ad} increases as a function of particle size because the diameters of these particles are larger than the wavelength 10 μm making it such that the particles sometimes partially nest within the surface (multiple points

of close contact) and sometimes rest on the apex of the peaks created by the sinusoidal surface roughness (one point of close contact).

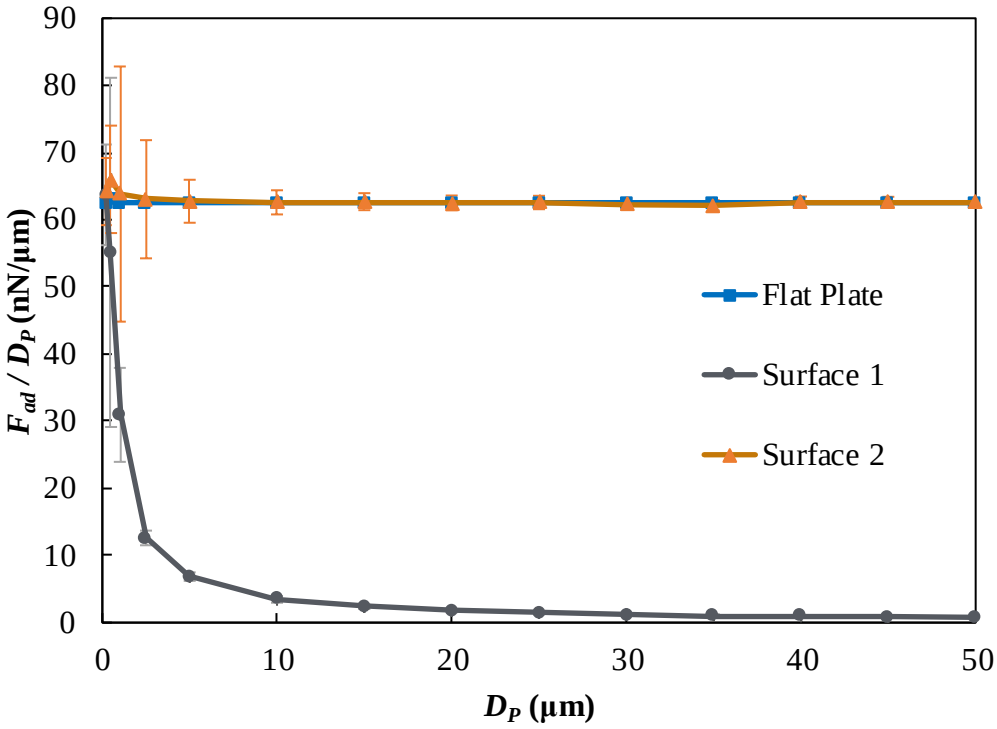

Figure 3.11 Normalized F_{ad} values for polystyrene spheres in contact with a simulated flat silica plate and the simulated rough silica surfaces 1 and 2. The RMS roughness was 25 nm on both surface 1 and surface 2. The error bars represent one standard deviation around the mean adhesion force.

Fig. 3.11 illustrates the F_{ad} values decrease dramatically with increasing particle diameter from 0.5 to 10 µm in the presence of surface 1 compared to surface 2. The dramatic decrease in both F_{ad} and its standard deviation over this range occurs for the same reason as when the particle diameters went above 10 µm on surface 2 – as the particle size increases the particles less frequently nest within the surface features until they reach a point where their diameters are larger than the wavelength between peaks and they can never nest. For particle diameters above 1 µm adhering to surface 1, the normalized F_{ad} levels off and becomes constant across increasing particle sizes because the particles are sufficiently large that they always sit atop 3 peak apexes on surface 1, independent of size.

To further illustrate the relationship between particle and surface scale features and adhesion, nanoscale sinusoidal waves (amplitude 3 nm and wavelength 0.5 μm) were added on top of the original micron-scale sinusoidal features on surface 2 to create surface 3. Fig. 3.12 provides a visual comparison of surfaces 2 and 3. Surfaces 1, 2 and surface 3 have the same RMS roughness of 25 nm.

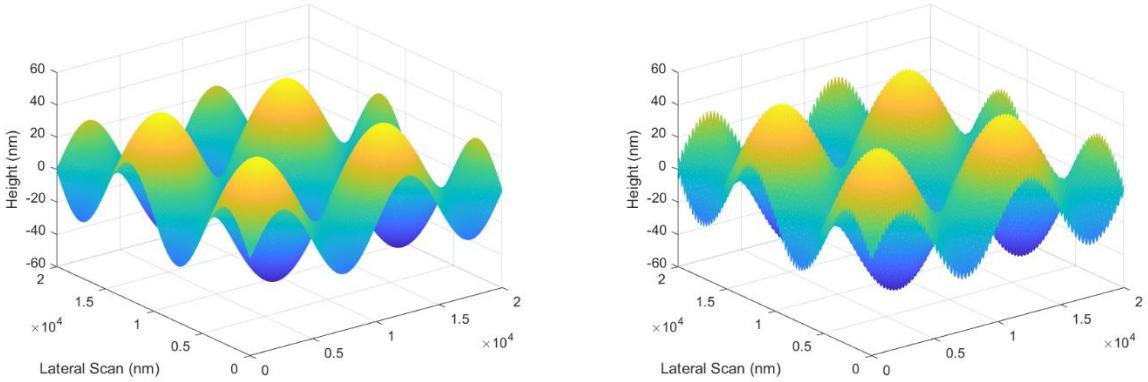

Substrate 2 Substrate 3

Figure 3.12 Visual comparison of simulated surfaces 2 and 3. Surface 3 has the same large scale sinusoidal peaks as surface 2 with added small scale (amplitude 3 nm) sinusoidal peaks on top of the large peaks.

The normalized F_{ad} distribution presented in Fig. 3.13 representing the particle adhesion against surface 3 illuminates the interplay between particle size and multiscale surface roughness. The normalized F_{ad} distributions against surface 3 and surface 2 are nearly identical at the smallest particle size. At this condition, the particles nest within the topography dictated by the global roughness on the surfaces and make point contact with one spot (surface 2), or with three or more points (surface 3) at the base of the global topography. In general, when the nanoscale roughness pushes the bulk of a particle away from a surface, the overall adhesion force should drop. However, the presence of the nanoscale roughness allows multipoint contact instead of single point contact, so that this effect is somewhat reduced. As the particles grow larger, they continue to interact with either one or three points on a surface that has nanoscale roughness. While increasing the size of the particle causes the denominator in the normalized force to grow larger, it does not produce a

corresponding increase in the number of contacts, nor in the adhesion force, so that the net effect is a reduction in the normalized force expression, as is seen for surface 3.

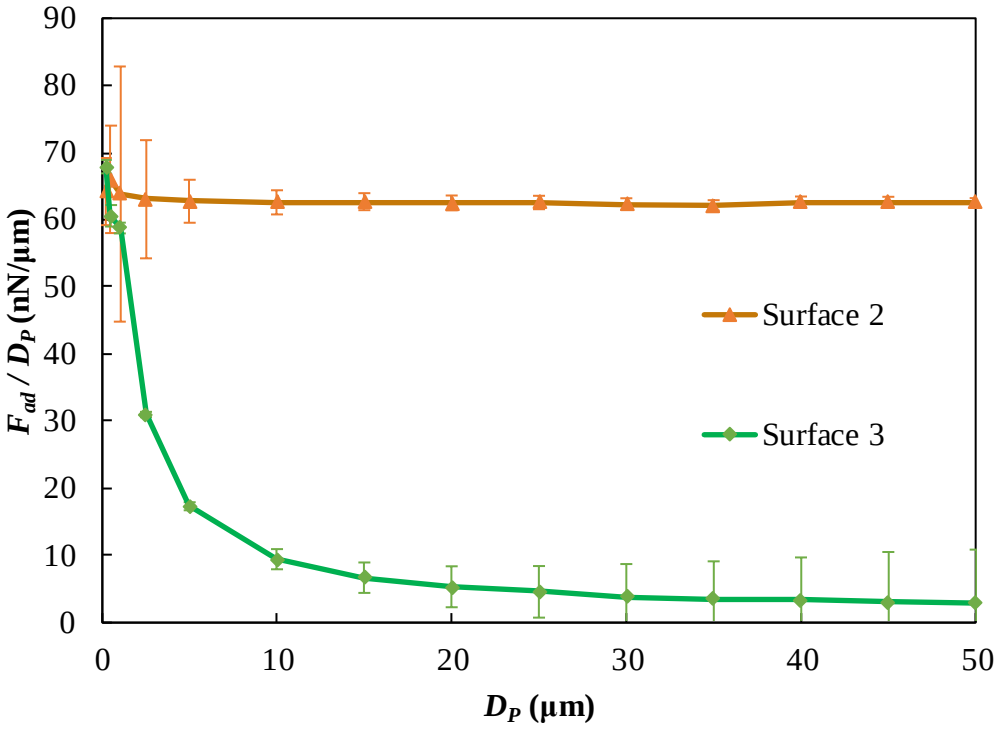

Figure 3.13 Normalized F_{ad} distributions between smooth spheres and surfaces 2 and 3.

This study executed through the *Particle Adhesion Simulator* exemplified that RMS roughness does not provide sufficient information to determine how a particle interacts with a surface. A particle will behave very differently against two surfaces with the same RMS roughness due to the scale of the roughness features in comparison to the particle size. Because the relationship between particle size and the different scales of surface roughness can be complex, the A'_{132} distributions appear increasingly useful. The A'_{132} distributions can be used as a simple and quick way to describe how a powder will interact with a surface's specific properties.

3.4 Conclusions

The adhesion of polystyrene powder to silica surfaces polished to have different levels of RMS roughness was studied using the enhanced centrifuge method (ECM). The adhesion forces against four surfaces with well-defined levels of RMS surface roughness correlated more significantly

with the scale of the surface roughness compared to the scale of the particles than with the RMS roughness. When the ECM was applied and the adhesion between the rough particles and rough surfaces was modeled as though it were a system of smooth particles on smooth surfaces that was dominated by vdW interactions, the effects of particle size and surface roughness were reflected in the resulting A'_{132} distributions. Across all four surfaces, the A'_{132} distributions decreased as particle diameter increased, asymptotically approaching a limiting value as the particle diameters became much larger than the surface roughness features. For the smaller particle sizes, the A'_{132} distributions were heavily influenced by the way each specific particle interacted with the surface's specific roughness features.

This study revealed that RMS roughness of the surface to which a particle adheres is a poor predictor of the van der Waals force of adhesion between these two. Rather, one must consider topographical features on the surface that are of the length scale of the particle diameter. Within such regions, both the nanoscale topography of the surface and of the particle, and the particle scale complementarity of the two surfaces, dictate the strength of the overall van der Waals particle adhesion. The investigation of the relationship between surface roughness features and adhesion completed by simulation validated the observations made via experiment. The adhesion behavior varied quite significantly between surfaces that had the same RMS roughness, but which had roughness features whose height and location (*i.e.* frequency of peak occurrence) varied relative to the scale of the particle size. Both the computational and experimental studies demonstrated that the relationship between the scale of surface roughness features (global and local), relative to the scale of the particle properties need to be considered when predicting how a powder will adhere to a surface and confirmed that RMS analysis is of minimal value.

3.5 Acknowledgements

This material is based upon work supported by the U.S. Department of Homeland Security, Science and Technology Directorate, Office of University Programs, under Grant Award 18STEXP00001-03-02, Formerly 2013-ST-061-ED0001. The views and conclusions contained in this document are those of the authors and should not be interpreted as necessarily representing the official policies, either expressed or implied, of the U.S. Department of Homeland Security.

4. AN ENHANCED CENTRIFUGE-BASED APPROACH TO POWDER CHARACTERIZATION: THE INTERACTION BETWEEN PARTICLE ROUGHNESS AND PARTICLE-SCALE SURFACE TOPOGRAPHY DESCRIBED BY A SIZE-DEPENDENT 'EFFECTIVE' HAMAKER CONSTANT

Reprinted with permission from Powder Technology. 2021, 391. DOI: 10.1016/j.powtec.2021.07.028 Copyright 2021 Elsevier B.V.

4.1 Introduction

A large number of commercial products involve the handling of particulate solids at some point in the manufacturing process. This is especially true for the pharmaceutical industry, where powders are commonly found in oral dosage forms [74–78]. Caking, poor flowability, dust hazards, consolidation, and segregation are examples of problems that can occur during the processing, handling, and storage of powders [79–81]. These issues are caused by the properties of the individual particles that compose a powder and their effects on the resulting particle adhesion.

In cases of simple contact, which does not involve mechanical interlocking or chemical bonding between surfaces, the adhesion force is the force needed to separate two surfaces from contact. The topography of the interacting bodies influences how the surfaces will come into contact and plays an important role in the adhesion. Specifically, nanoscale surface roughness and particle scale surface topographical variation cause variations in the contact area between a particle and the interacting surface which ultimately affect the force of adhesion [20–22]. Various models have been used to describe surface roughness using spheres [23,82], hemispheres [20,83–85], and fractals [86–89]. Other existing methods, such as the Rabinovich approach, the Rumpf model, and the modified Rabinovich and Rumpf models quantify the effect of surface roughness through tunable parameters such as asperity radii [63,66,69–72]. With proper calibration, models like these describe the effects of surface roughness on particle adhesion.

In order to characterize experimentally the effects of surface roughness on particle adhesion, it is critical to determine the magnitude of adhesion forces that occur in a system of interest. Various techniques are available to measure adhesion forces, which include: the centrifuge technique, the aerodynamic technique, the hydrodynamic technique, the impact-separation method, the ultrasonic vibration method, the electrical field detachment technique, force

microscopy, the drop test, and acoustic base excitation [40,81,90,91]. The centrifuge technique is a practical method that measures particle adhesion, is simple to perform, and describes the adhesion behavior of an ensemble of particles in terms of the average adhesion force. In this work, simulations of the centrifuge technique were completed to illustrate an enhancement of the method that will allow the determination of the adhesion force distribution and the effect of the roughness of the particulate ensemble and the opposing surface on that force distribution. Through this method, the adhesion is assumed to be controlled by van der Waals forces, and the effect of surface roughness is described by a distribution of tuned parameters called 'effective' Hamaker constants. The 'effective' Hamaker constants resulting from this enhancement of the centrifuge method provide a simple and computationally straightforward and inexpensive way to describe complex (rough) particles on topographically interesting surfaces as equivalent smooth spheres on flat surfaces while still capturing the effects of the surfaces on the adhesion.

4.2 Materials and methods

4.2.1 Materials

This work involves simulations of the adhesion and removal of particles from textured plates in a centrifuge apparatus. The plates have distinct (non-overlapping) hemispherical indentations of specified radius embedded in their surface. The simulated plates are assigned the material properties of silicon to enable future experimental validation of this work. Specifically, because silicon can be etched isotropically to fabricate hemispherical indentations, it is straightforward to create experimental systems to test these results. The simulated indentations are specified to have diameters of 10, 20, 30, 40, 50, and 60 micrometers, and all indentations on a plate are assumed to be the same size. In this configuration, six plates will be required to evaluate the behavior when the method is reduced to practice.

Colloidal silica particles (AEROPERL® 300 Pharma) were supplied by Evonik (U.S.A.). The particles are spherical and rigid, with density of 2.2 g/cm^3 and index of refraction of 1.45. The size distribution measured for this powder was the basis of the adhesion force simulations performed below.

4.2.2 Methods

Measured silica particle size distribution

In previous work [92], a particle size distribution for the silica particles, based on the volume equivalent sphere diameter, was measured using laser diffraction (Malvern Mastersizer 2000). This result is reproduced in Fig. 4.1. The median particle size, d_{50}, was 23.8 µm, while the tenth and ninetieth percentiles were 9.82 µm and 52.2 µm. A lognormal distribution was fit to the measured size distribution. The resultant distribution had the parameters $\mu = 3.197$ with a 95% confidence interval of (3.184 – 3.210) and $\sigma = 0.664$ with a 95% confidence interval of (0.654 – 0.673). The lognormal description of the measured particle size distribution was used whenever descriptions of the powder were required in the simulations below.

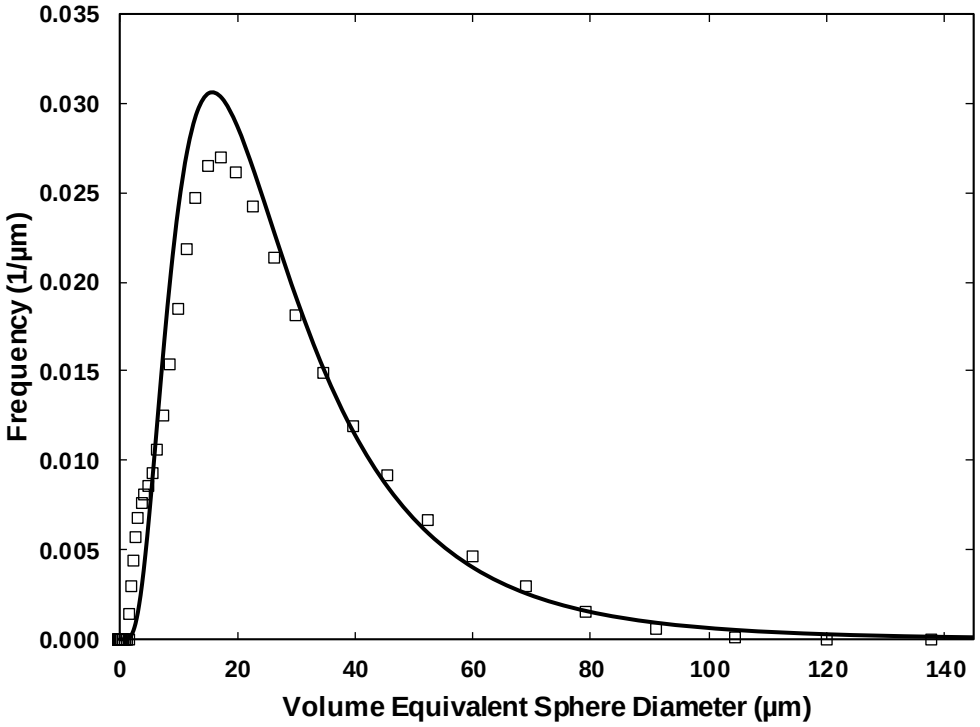

Figure 4.1 Particle size distribution of silica powder as measured by laser diffraction (□), and associated lognormal fit (line)[32].

Centrifuge technique description

The centrifuge technique is a common but valuable tool that provides the mean adhesion force of a powder measured against a surface of interest [12,13,40,93,94]. In this method the inertial force of the centrifuge is compared to the adhesion force of the particle, and particles are assumed to be removed when the inertial force equals the adhesion force. Surfaces of interest are dusted with powder and positioned in specially designed centrifuge tubes (see right hand side of Fig. 4.2) such that their orientation is parallel to the axis of rotation of the centrifuge and the particles are facing outward.

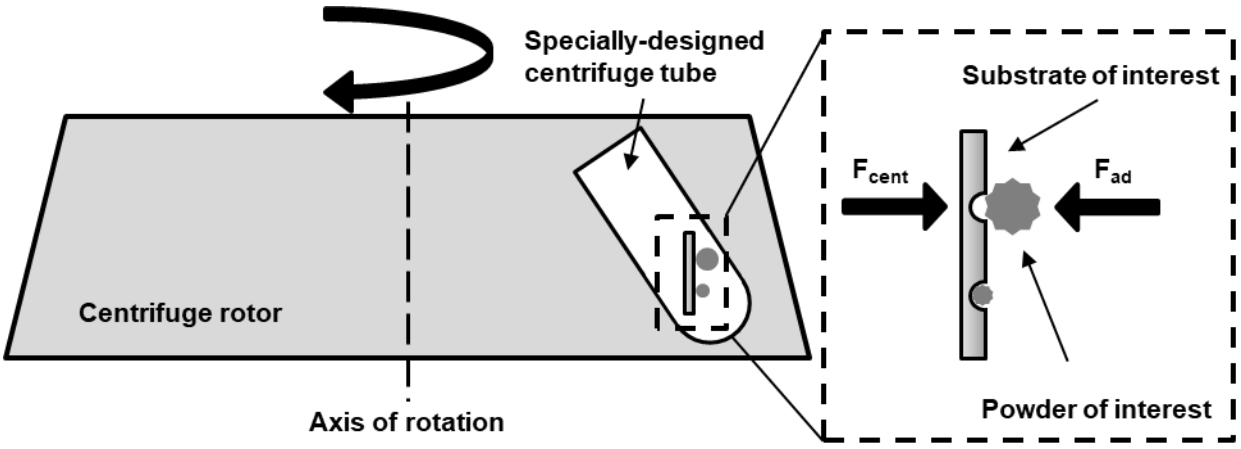

Figure 4.2 Schematic of the centrifuge technique method to measure adhesion of rough particles to hemispherically-indented surfaces.

A microscope and camera system is used to track the number of particles that remain on the surface as a function of inertial force. Historically, the characteristic adhesion force obtained using the centrifuge method is the geometric median adhesion force, defined as the force where 50% of particles remain adhered to the surface [95]. This force is assumed to represent the mean adhesion force for the system. The computational approach discussed here depicts how the centrifuge technique was simulated computationally.

Computational approach

In this work, the van der Waals adhesion between spherical particles with nanoscale surface roughness and flat surfaces with smooth hemispherical indentations was calculated. The removal force resulting when these plates are placed in a centrifuge and rotated at specified angular velocities was calculated *in silico*, and the number of particles removed at each angular velocity was determined. This information was then used to calculate the effect of the particle surface roughness on the adhesion force distribution of the particles and the expected particle removal in the centrifuge.

Surface element integration

Surface element integration (SEI) was used to determine *in silico* the adhesion forces between rough, spherical particles in smooth, hemispherical indentations [96]. This is the same method that was applied to a smooth particle adhering to an indentation [97] but now the method is extended to evaluate surface roughness effects that were not considered in that prior work. To impose surface roughness on the particle, the equation for a rippled sphere model as described by Bhattacharjee et al. was slightly modified [96]. The adhesion force, F_{ad}, was approximated by integrating over the surface area of the particle using the expression for the van der Waals force per unit area of two flat plates as a function of separation distance between the particle and indentation, $F_{vdW}(D)$:

$$F_{ad} = \int_{S_p} dF_{ad} = \int_{S_p} (\boldsymbol{n_p} \cdot \boldsymbol{k_p})(\boldsymbol{n_i} \cdot \boldsymbol{k_i}) F_{vdW}(D)\, dS_p \qquad 4.1$$

where S_p is the surface area of the particle, $\boldsymbol{k_p}$ and $\boldsymbol{k_i}$ are the unit outward vectors normal to the particle and indentation, and $\boldsymbol{n_p}$ and $\boldsymbol{n_i}$ are the unit vectors in the radial direction projecting out of each surface. The $(\boldsymbol{n_p} \cdot \boldsymbol{k_p})$ and $(\boldsymbol{n_i} \cdot \boldsymbol{k_i})$ terms take into account the curvature of the surfaces of both the particle and the indentation. By calculating the adhesion force in this manner, the curvature of the surfaces was taken into account while utilizing the established adhesion force relationship of two flat plates per unit area to calculate the adhesion forces.

The adhesion force was calculated between a single particle and a single indentation with the particle and indentation aligned center-to-center and then brought to the point of minimum

separation (which was assumed to be 4 Å). Adhesion was approximated by applying the expression for the van der Waals force per unit area between two flat plates as a function of separation distance:

$$F_{vdW}(D) = \frac{A_{132}}{6\pi D^3} \tag{4.2}$$

where A_{132} denotes the Hamaker constant of the system, and D represents the separation distance between the two surfaces. The differential surface area of the particle, dS_p, is given by:

$$dS_p = r_p^2 \sin\theta_p \, d\theta_p d\varphi \tag{4.3}$$

where r_p is the radius of the particle, θ_p is the polar angle of the particle, and φ is the azimuthal angle in spherical coordinates. These are shown schematically in Fig. 4.3. The separation distance between the particle and indentation was calculated for two orientations: i) a particle that is smaller than the indentation and ii) a particle that is larger than the indentation.

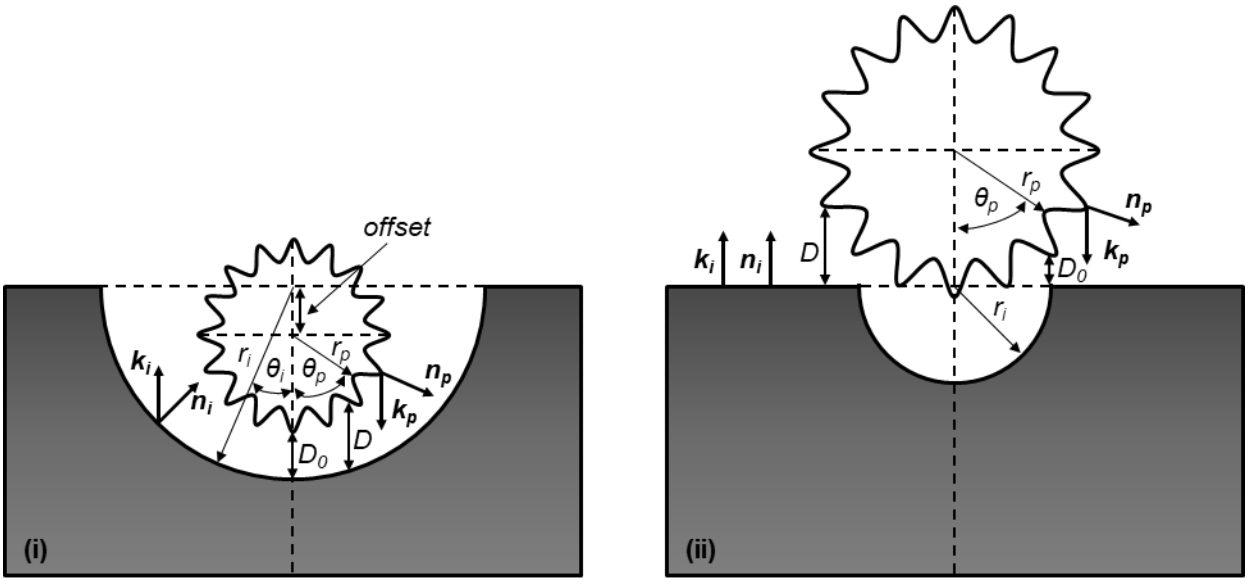

Figure 4.3 Schematic of the contact between an indentation and a rippled sphere that is smaller (i) and larger (ii) than the indentation.

The equation describing the rippled sphere surface is [96]:

$$r_p = a\left(1 - \lambda_{\theta_p}\cos\left(n_{\theta_p}\theta_p\right) - \lambda_{\varphi}\cos\left(n_{\varphi}\varphi\right)\right) \quad 4.4$$

where a is the radius of the equivalent spherical particle (the radius of the particle without roughness), λ_{θ_p} and λ_{φ} are the scaled amplitudes in reference to the surface roughness and particle scale, *offset* is the distance from the center of the indentation to the center of the particle at contact, and n_{θ_p} and n_{φ} are the frequencies of the asperities along each respective directional angle. The resulting particle is nominally spherical with sinusoidal features along the surface, as shown in Figure 4.3.

The starting point for the computation of the interaction force involved co-location of the central point of the particle and the indentation. Next, one quadrant of the particle and indentation was considered for the calculation of the *offset* for all combinations of the particle radius and roughness parameters. By using only a quadrant, a very fine mesh size could be used to describe both surfaces carefully while keeping the needed computational capacity within reason. Along with the *offset*, all variables in the surface integration must be related to the particle position because that is the surface over which the integration is performed. Thus, it was necessary to find an expression for the indentation polar angle, θ_i, in terms of the particle polar angle, θ_p, and indentation radius, r_i, as follows:

$$r_i \sin\theta_i = r_p \sin\theta_p \quad 4.5$$

$$\theta_i = \sin^{-1}\left(\frac{r_p}{r_i}\sin\theta_p\right) \quad 4.6$$

For the case of a particle smaller than the indentation, local separation distance between the particle and the indentation at the minimum separation distance, D_0, is:

$$D = D_0 + r_i\cos\left(\sin^{-1}\left(\frac{r_p}{r_i}\sin\theta_p\right)\right) - r_p\cos\theta_p - offset \quad 4.7$$

For this case, the final integral for the adhesion force was determined by substituting Eqs. 4.2, 4.3, and 4.7 into the initial surface integral (Eq. 4.1). The procedure used to determine the value of the $(\boldsymbol{n_p} \cdot \boldsymbol{k_p})$ and $(\boldsymbol{n_i} \cdot \boldsymbol{k_i})$ terms is well-documented [96]. In this case, $(\boldsymbol{n_i} \cdot \boldsymbol{k_i})$ is found to be $\cos\theta_i$. The $(\boldsymbol{n_p} \cdot \boldsymbol{k_p})$ term is much more complicated, however, because of the roughness applied to the particle. It is given by:

$$\boldsymbol{n_p} \cdot \boldsymbol{k_p} =$$

$$\frac{r_p \sin\theta_p \cos\theta_p + a\lambda_{\theta_p} n_{\theta_p} \sin\left(n_{\theta_p}\theta_p\right) \sin^2\theta_p}{\sqrt{\left(\left(r_p \sin\theta_p\right)^2 + \left(a\lambda_{\theta_p} n_{\theta_p} \sin\left(n_{\theta_p}\theta_p\right)\sin\theta_p\right)^2 + \left(a\lambda_{\varphi} n_{\varphi} \sin\left(n_{\varphi}\varphi\right)\right)^2\right)}} \quad 4.8$$

The adhesion force integral for a particle smaller than the indentation, without substituting the separation distance expression, Eq. 4.7, or the expression for $(\boldsymbol{n_p} \cdot \boldsymbol{k_p})$, Eq. 4.8, is now:

$$F_{ad} = \int_0^{2\pi} \int_0^{\pi} (\boldsymbol{n_p} \cdot \boldsymbol{k_p}) \cos\left(\sin^{-1}\left(\frac{r_p}{r_i}\sin\theta_p\right)\right) \frac{A_{132}}{6\pi D^3} r_p^2 \sin\theta_p \, d\theta_p d\varphi \quad 4.9$$

For the case where the diameter of the particle is larger than the diameter of the indentation, the separation distance was calculated in the same manner as described for a particle smaller than the indentation, except that the separation distance was only calculated for the part of the particle outside of the indentation. This is because the adhesion of the particle to the inside of the indentation is negligible by comparison. In the case where the particle is larger than the indentation the lower limit of integration for the polar angle, θ_l, occurs at the point where the particle and indentation come into contact. The value for θ_l was determined at the same time the offset distance was determined. For this case, $(\boldsymbol{n_p} \cdot \boldsymbol{k_p})$ is still given from Eq. 4.8 and $(\boldsymbol{n_i} \cdot \boldsymbol{k_i}) = 1$ because $\boldsymbol{n_i}$ and $\boldsymbol{k_i}$ are equivalent vectors. Thus, the final form of the adhesion integral for a particle larger than the indentation, without substituting in the expressions for the separation distance and $(\boldsymbol{n_p} \cdot \boldsymbol{k_p})$, appears as:

$$F_{ad} = \int_0^{2\pi} \int_{\theta_l}^{\pi} (\boldsymbol{n_p} \cdot \boldsymbol{k_p}) \frac{A_{132}}{6\pi D^3} r_p^2 \sin\theta_p \, d\theta_p d\varphi \quad 4.10$$

As a note, all calculations were performed with consideration of particles nestled within or on top of an indentation. Instances of particles resting on the area between indentations were not taken into consideration for this work.

Roughness effects on residual adhering percentage (RAP) curves

From the lognormal fitted distribution, 1,000 particles were randomly generated with diameters between 2 and 105 μm for use in the particle-indentation adhesion simulations. Sinusoidal surface roughness features were imposed on the particles in the simulated distribution. These were described by the roughness parameters λ_{θ_p}, λ_{φ}, n_{θ_p}, and n_{φ}. For each simulated particle, the values of the amplitude of the roughness were randomly selected according to:

$$1\ nm \leq \lambda_{\theta_{p,i}} = \lambda_{\varphi_{p,i}} \leq 20\ nm$$

where $\lambda_{\theta_{p,i}}$ is the amplitude of the sinusoids on particle i in the θ direction and $\lambda_{\varphi_{p,i}}$ is the amplitude of the sinusoids on particle i in the φ direction. Similarly, the frequencies of the sine waves were randomly selected according to the following constraint:

$$\frac{5}{(D_{p,i})} \leq \left(n_{\theta_{p,i}}\right) = \left(n_{\varphi_{p,i}}\right) \leq \frac{30}{(D_{p,i})}$$

where $n_{\theta_{p,i}}$ is the frequency of the sinusoids on particle i in the θ direction, $n_{\varphi_{p,i}}$ is the frequency of the sinusoids on particle i in the φ direction, and $D_{p,i}$ is the diameter of particle i. In this case, the frequencies are defined as the number of cycles per unit particle diameter. By constraining each particle to have sinusoids with the same amplitudes and the same frequencies in both angular directions, each sphere was uniformly rippled. Because the amplitudes and frequencies of the simulated roughness varied randomly from particle to particle, a wide range of roughness effects could be explored.

Once all the particles were defined, the adhesion force of each particle-indentation interaction was calculated. This process was repeated for each indentation size. The calculated

adhesion force was then related to the inertial force imparted by the motion of the centrifuge by equating the two forces:

$$F_{ad} = F_{cent} = m\omega^2 r_c \tag{4.11}$$

Because the particles are spherical, the mass was calculated by multiplying the volume and density, ρ_p, of the particle. The nominal radius of the equivalent spherical particle, a, was used to calculate the volume because the volume of the protrusions and intrusions cancel out to leave the volume of the equivalent sphere. Eq. 4.11 then yields:

$$F_{ad} = \frac{4}{3}\pi a^3 \rho_p \omega^2 r_c \tag{4.12}$$

For the simulations, both ρ_p and r_c were held constant, at 2.2 g/cm^3 and 9 cm. By setting the expressions for the adhesion and inertial forces equal to one another, the angular velocity can be calculated and then the rotational speed required to remove the particle from the indentation can be determined by:

$$\omega = \sqrt{\frac{3F_{ad}}{4\pi r_p^3 \rho_p r_c}} \tag{4.13}$$

$$RPM_{removal} = \frac{60\omega}{2\pi} \tag{4.14}$$

Knowing the required rotational speed to remove each simulated particle from an indentation provides a means to determine the Residual Adhering Percentage (RAP) of particles when a given rotational speed is simulated in the centrifuge. Specifically, after 1000 particles are placed into simulated contact with indentations on the surface, the surfaces are assumed to be placed in the centrifuge and the centrifuge is assumed to be rotated at a given speed. For the assumed rotational speed, the fraction of particles whose adhesion force is less than or equal to the applied inertial force is determined, and these particles are assumed to be removed from the surfaces. The fraction of particles remaining on the surfaces is called the Residual Adhering Percentage (RAP). Thus, the RAP for each size of indentation on a substrate (based on the simulations) can be determined as a function of rotational speed.

Describing the adhesion of rough particles in terms of equivalent smooth particles

While other models capture the effects of topography and shape on van der Waals adhesion through parameters such as tunable asperity radii [63,66,69–72], in this work the behavior is described in terms of equivalent smooth particles with the same radii as the rough particles and described by a corresponding 'effective' Hamaker constant distribution. The effect of the particle surface roughness is mapped onto the 'effective' Hamaker constants through the following steps:

1) For each indentation size, the simulated RAP curves for the smooth and rough particles are plotted as the required speed for removal (ordinate) as a function of particle size (for discrete particle sizes, abscissa) resultant from Eqs. 13 – 15. Note that an arbitrary (estimated) Hamaker constant is used to create the curve for the smooth particles.
2) The rotational speeds at which the rough particles are removed from the indentation are compared to the rotational speeds required to remove smooth particles of the same diameter.
3) To reconcile the difference between the observed adhesion of the rough particles and the predicted adhesion of smooth particles of the same size, the Hamaker constants used to predict the adhesion force of the 'effective' smooth particles are modified so that the smooth particles are removed at the same RPM as the rough ones. This process is repeated for all particle sizes.

By completing this Hamaker constant adjustment process, a new Hamaker constant distribution (the 'effective' Hamaker constant distribution) is identified which allows a population of 'effective', smooth particles to be used to represent the observed adhesion and removal behavior of the rough particles.

4.3 Results and discussion

4.3.1 Describing rough particle adhesion using smooth particles and 'effective' Hamaker constants

In order to ascertain the effect of surface roughness on the RAP curve, the simulated centrifuge technique was used to compare the adhesion of smooth particles to particles that had surface roughness imposed onto their surfaces *in silico*. Fig. 4.4 shows the RAP curves of the smooth and

rough particles against a surface with a 40 µm indentation using an 'effective' Hamaker estimate of 65 zJ.

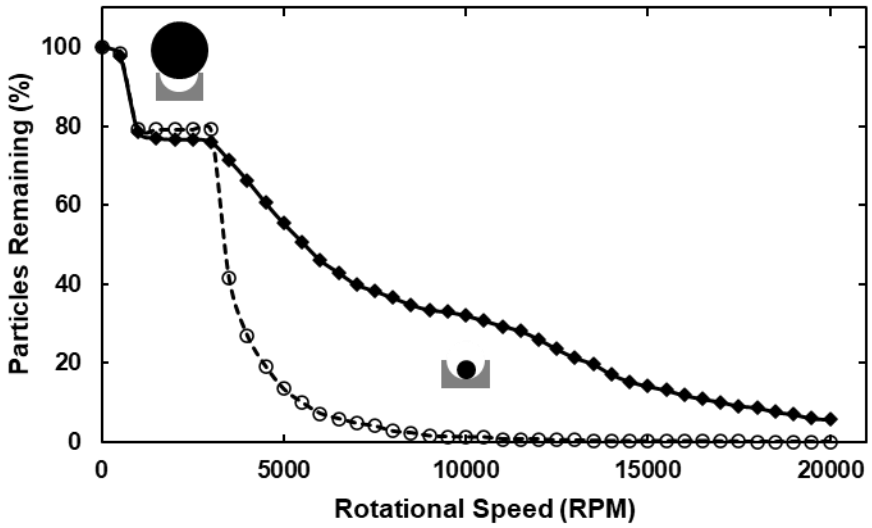

Figure 4.4 Simulated RAP curves of (♦) rough particles and (○) smooth particles on a 40 µm diameter indentation with inset schematics showing the regions where particles sit above and inside the indent.

The RAP curve for the rough particles shares the same plateau characteristic as the RAP curve for the smooth particles seen in Fig. 4.4 between the RPM increment range of 1500 to 3000; this plateau behavior is the result of the particles' sizes dictating the adhesion in a similar manner in both the rough and smooth particle adhesion cases. Specifically, at the plateau, the particles ride above the indentations and make contact only at a ring of points around the edge of the particle. At this condition, they have very low adhesion force against the surface, independent of the roughness. As previously discussed [97], the fraction of particles remaining adhered at the plateau for indentations of different size can be used to determine the cumulative size distribution of the particles. From Figure 4.4, it is clear that the rough particles behave the same as the smooth ones, and thus particle size distributions can still be obtained from the behavior on indented surfaces when roughness is present on the particles. The RAP curves to the right of the plateau (rotational speeds > 3000 RPM) differ between the smooth and rough particles because particle size is no longer the dominating feature of the adhesion. Instead, the adhesion at rotational speeds greater than 3000 RPM reflects the effect of the particle scale roughness on the adhesion. The adhesion of

the rough particles is greater than the smooth particles at rotational speeds greater than 3000 RPM because the roughness makes the rough particles are to be effectively larger than the smooth ones, bringing more area into close contact with the surface which causes a greater adhesion force. All particles in this range are small enough that they fall into the indentations on the surface.

The benefit of the enhanced centrifuge technique is the ability to describe the effect of the particle roughness on the adhesion in the region beyond 3000 RPM in terms of the behavior of 'effective' smooth spheres. These smooth spheres, which are simple to describe computationally, describe the roughness effects using 'effective' Hamaker constants. A comparison between the rotational speeds needed to detach the smooth particles and rough particles as a function of size is plotted in Fig. 4.5. The parabolic section of the curve on the left side of the graph reflects particles adhering inside the indentation, while the plateau on the right results from particles larger than the indentation, which are removed at much lower rotational speeds. As one moves right to left from a particle size of 40 μm to approximately 20 μm, one sees a reduction in required centrifuge RPM to remove the particles from the indented surface. This portion of the graph describes the transition from particles intimately nesting within the indentation (40 μm particles nesting perfectly in a 40 μm indentation) to a point where the particle rests within the indentation but has much less intimate contact with the indentation (20 μm particles nesting in a 40 μm indentation). As one continues to move left from 20 μm to 1 μm, there is a corresponding increase in the RPM required for particle removal. This is because particles of this size are much less massive than larger particles and therefore gain less momentum from the motion of the centrifuge than larger particles. The difference between the required RPM for removal of the powder comprised of smooth particles and the powder comprised of rough particles for sizes less than 40 μm is due to the effect of the particle roughness on the adhesion. Specifically, the rough particles have less mass in close proximity to the indentation surface than the smooth ones of the same diameter. This reduced mass leads to a reduction in the adhesion force, allowing much larger rough particles to be removed at the same rotational speed than in the smooth case.

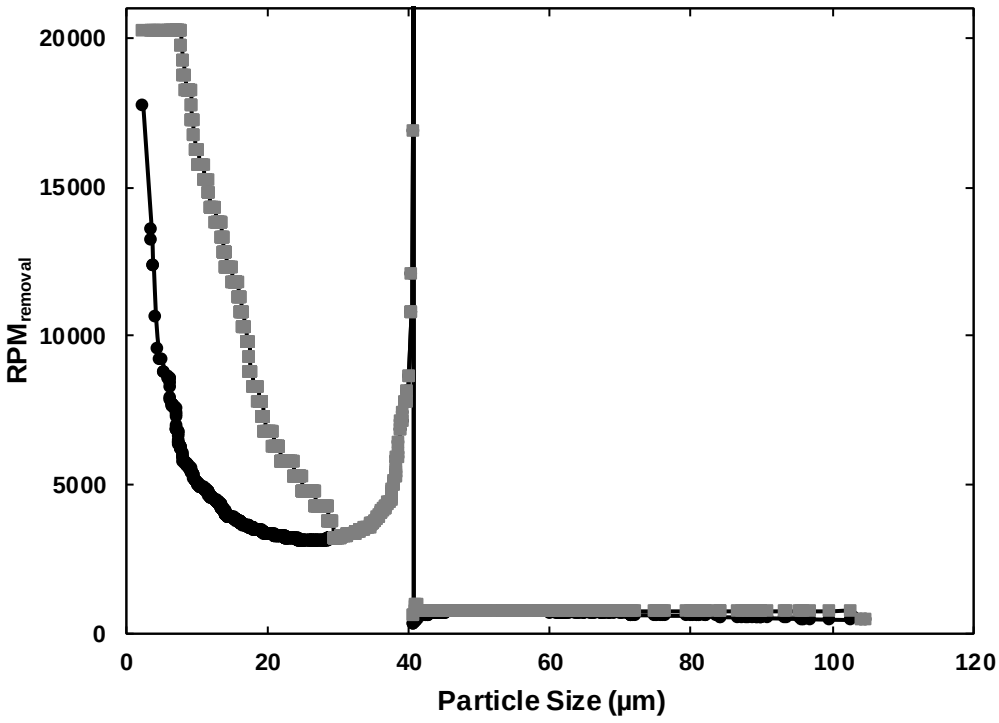

Figure 4.5 Required centrifugal speed (RPM) needed to dislodge a particle from a 40 µm diameter indentation for a powder comprised of ideal, smooth particles (●) and a powder comprised of rough particles (■).

To map the smooth particle adhesion behavior seen in Fig. 4.5 to the rough particle behavior in that figure, the Hamaker constants of the smooth particles were adjusted for all the particle sizes where the adhesion between the two cases differed. These adjusted Hamaker constants are the 'effective' Hamaker constants that were discussed above. Fig. 4.6 shows how the resultant RAP curve for the equivalent smooth particles based on the adjusted Hamaker constants maps very well onto the RAP curve for the rough particles, in the case of a surface with indentations of 40 µm. This shows how the 'effective' Hamaker constants capture the effect of particle surface roughness towards the adhesion.

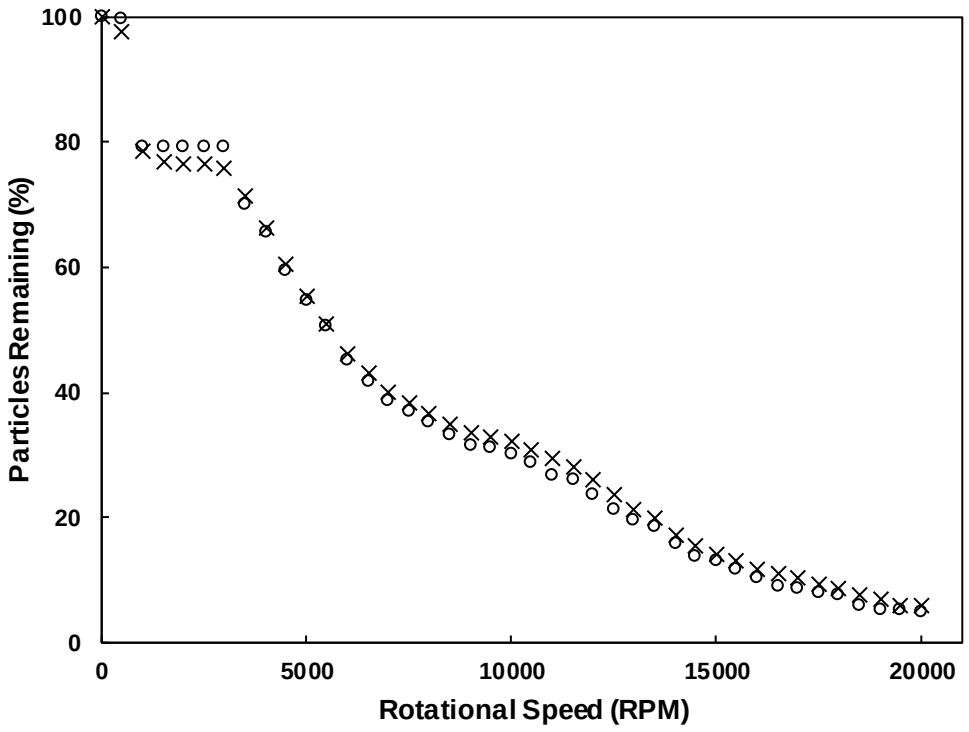

Fig.4.6 Simulated RAP curves of (x) rough particles and (○) equivalent smooth particles on a 40 μm diameter indentation. The adhesion force for each smooth particles was determined on the basis of a size-dependent Hamaker constant.

4.3.2 Applying 'effective' Hamaker constant distribution to other adhesion systems

The distribution of Hamaker constants required to capture the effects of the particle roughness on the adhesion of equivalent spherical particles is linked to the size of the particles. To illustrate this dependency, each size-dependent 'effective' Hamaker constant determined from the 40 μm indentation study was normalized to the particle size and then plotted as a function of particle size, as seen in Fig. 4.7. As can be seen in this figure, the Hamaker constant distribution is lognormal. For particle sizes greater than 40 μm, the particles do not fit within the indentation, there is point contact, and the rough and smooth particles will adhere similarly (*i.e.* have similar 'effective' Hamaker constants). As the particles get smaller than 40 μm, they begin fitting in the indentations, and the rougher ones adhere more strongly than the smooth ones, because they are effectively larger than the smooth ones; this stronger adhesion results in an increase in the 'effective' Hamaker constants. Once the particles become small enough that the roughness no longer interacts as significantly with the sidewalls of the indentations, the adhesion between the

rough and smooth particles becomes more and more similar, resulting in a decrease in the 'effective' Hamaker constants. These specific interactions explain the lognormal distribution observed in Fig. 4.7.

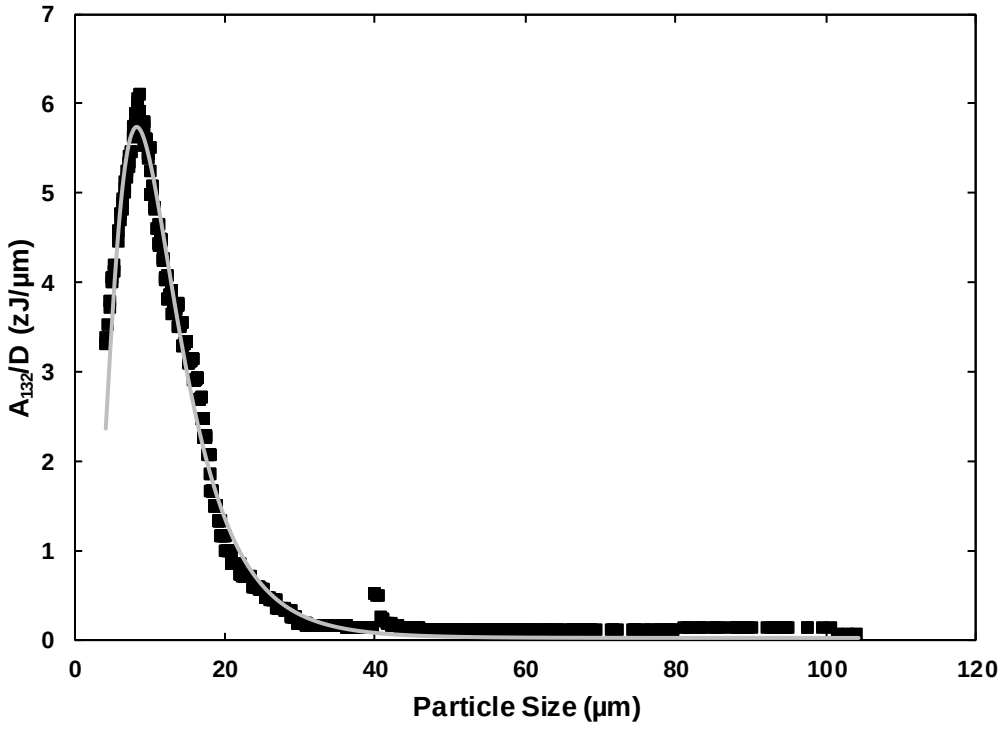

Figure 4.7 The (■) 'effective' Hamaker constant data normalized by particle size for indentation size of 40 μm plotted along with the (gray line) lognormal fit.

A lognormal function of particle diameter, d_p, was used as the functional form to express the size-dependent 'effective' Hamaker constant:

$$\frac{A_{132}}{d_p}(d_p) = \frac{\alpha}{d_p \sigma \sqrt{2\pi}} e^{\frac{-(\ln d_p - \mu)^2}{2\sigma^2}} + \beta \qquad 4.15$$

Fitting parameters α and β were applied to the typical lognormal equation with its parameters μ, the mean, and σ, the standard deviation. The resultant fit had an R-squared value of 0.99 with parameters: $\alpha = 70.3\, zJ$, $\beta = 0.02435\ \frac{zJ}{\mu m}$, $\mu = 2.378$, and $\sigma = 0.5208$. After multiplying by the particle size across Eq. 4.15, the 'effective' Hamaker constant is now a function of the particle size described as:

$$A_{132}(d_p) = \frac{\alpha}{\sigma\sqrt{2\pi}} e^{\frac{-(\ln d_p - \mu)^2}{2\sigma^2}} + \beta d_p \qquad 4.16$$

In order to determine how well this approach allows the use of ideal particles to fit the RAP curves for rough particles against different indented surfaces, the procedure above for the 40 µm particles was repeated for indentations from 20 - 50 µm. Fig. 4.8 illustrates the 'effective' Hamaker constants generated from Eq. 4.16 capture the effect of the particle properties on the adhesion. As can be seen, the roughness RAP curves across all indentations align with the 'effective' smooth RAP curves. The agreement between the roughness RAP curves and the 'effective' smooth RAP curves demonstrates that the equation for the size-dependent 'effective' Hamaker constants for smooth particles can adequately represent the effects caused by rough particles.

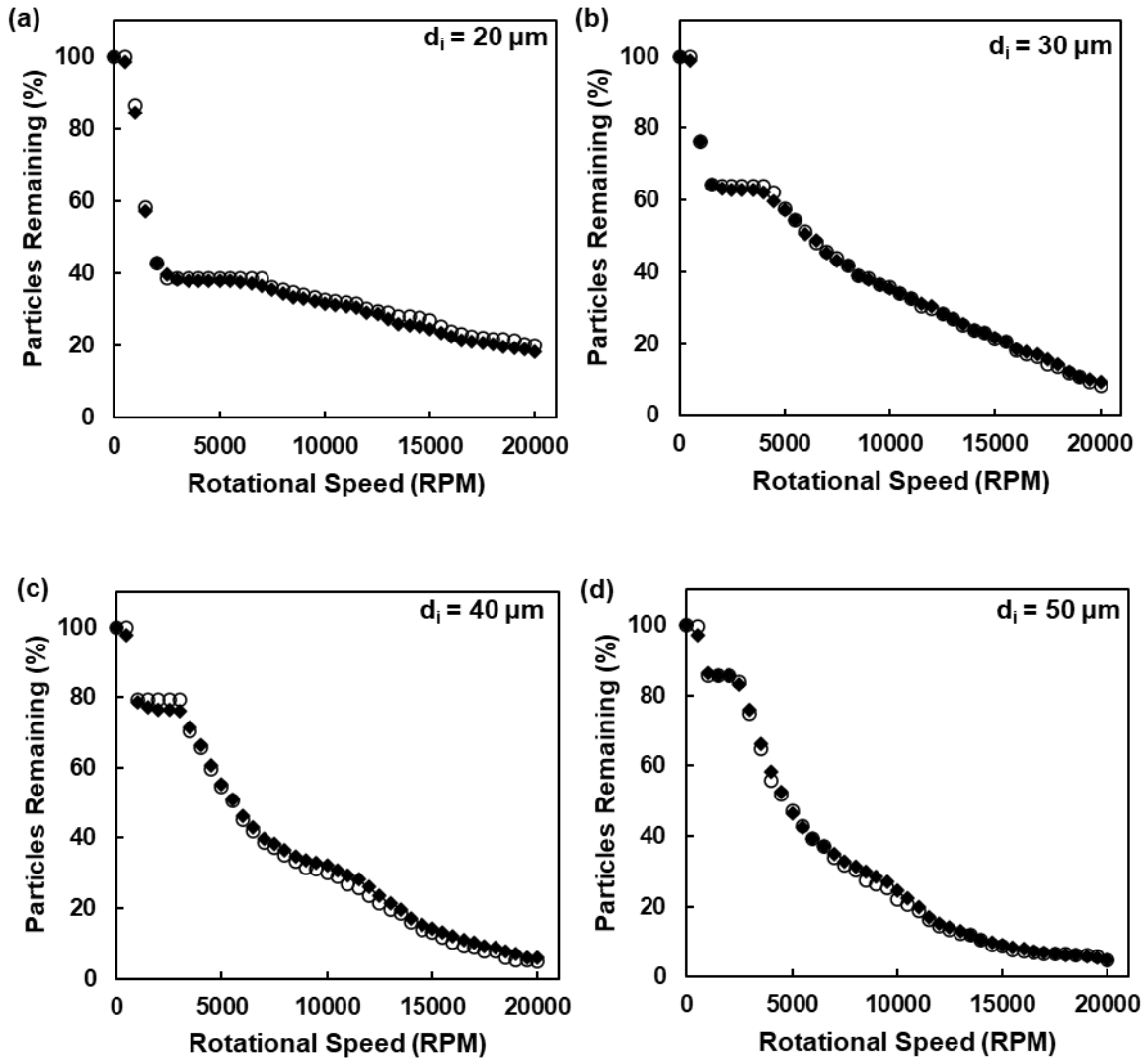

Figure 4.8 Simulated RAP curves of (♦) rough particles and (○) 'effective' smooth particles (adhesion described by calculated size-dependent 'effective' Hamaker constants) from plates with indentation diameters, di, of (a) 20 µm, (b) 30 µm, (c) 40 µm, and (d) 50 µm.

4.4 Conclusion

The enhancement of the centrifuge technique through the application of specially-designed substrates was investigated via simulation of the adhesion between a realistic powder and the substrates. Sinusoidal roughness was applied to a collection of spherical particles with the same size distribution as a real powder. A smooth plate with smooth, hemispherical indentations of 40 µm was then simulated, and the removal of the rough particles from the plate using the centrifuge

method was simulated. When the van der Waals adhesion was measured between the rough particles adhered to the surface with hemispherical indentations, 2 regimes of behavior were observed. When the particles were larger than the indentations, the rough particles adhered equally strongly as smooth particles of the same diameter. When the particles were smaller than the indentations, the rough particles adhered more strongly than smooth particles of the same nominal diameter. For the case of the large particles that were inside indentations, the rough particles adhered more strongly than the smooth ones because the rough particles had more regions of close contact with the indentation walls than in the smooth case. An 'effective' Hamaker constant distribution was used to describe the adhesion of the rough particles in terms of the behavior of smooth particles of the same diameter. In this case, the roughness effects were captured in the 'effective' Hamaker constants, and excellent agreement was obtained between the adhesion behavior for rough particles on or in the indentations and 'effective' smooth particles on or in the same indentations. This demonstrates that the van der Waals adhesion of rough particles to an ideally textured surface can be well-represented by considering the behavior of smooth particles of the same size with 'effective' Hamaker constants that capture the roughness effects. This can be useful for powder characterization and for modeling powder behavior to provide important information to engineers as they develop powder formulations and select processing conditions.

4.5 Acknowledgements

The authors acknowledge the support provided by the US National Science Foundation through the Engineering Research Center for Structured Organic Particulate Systems under grant EEC-0540855.

5. THE EFFECT OF THE VARIATION OF STAINLESS STEEL SURFACE AND PHARMACEUTICAL PARTICLE PROPERTIES ON POWDER ADHESION QUANTIFIED THROUGH THE ENHANCED CENTRIFUGE METHOD

5.1 Introduction

Understanding powder adhesion is of importance to the pharmaceutical industry as adhesion directly affects pharmaceutical powder storage and processing[3,98–101]. Compaction, tableting, blending, and spreading are just a few processes used by the pharmaceutical industry impacted by a powder's adhesion[9,98,102–105]. Poor understanding of a powder's adhesion can lead to issues such as jamming, and picking and sticking[15,106,107]. Powder adhesion may be driven by van der Waals (vdW), capillary, and electrostatic forces; and the conditions the powder is stored and handled in determine which of the three forces dominate the adhesion.

The individual particle properties, the surface topography of the interfacing equipment, and environmental factors, such as humidity, all affect the forces contributing to a powder's adhesion[66,108–111]. The contact area between a particle and surface is directly impacted by surface topography, particle shape and size, and depending on the relative humidity, the formation of condensation on a surface[18,51,55,111]. Particle deformation may occur depending on material characteristics and other contributing factors, such as swelling due to moisture uptake. This alters the contact area between the surface and particle, changing the adhesion force[20,103,112,113].

The interplay between the surface topography and the deformation of a particle directly impacts the contact area between the particle and surface[20,57,114]. A number of methods exist to quantify these effects towards particle adhesion[47,56,57,115]. However, existing adhesion models are lacking in their ability to quickly and effectively capture the individual particle and surface effects across entire powder size distribution. To address the need to quickly capture these effects in a computationally non-exhaustive way, the enhanced centrifuge method (ECM) was developed to describe the effect of the properties of the individual particles and the adherent surface on the adhesion through tunable 'effective' adhesion parameters[32,116]. In these prior studies, the ECM was used to quantify the effects of the particles' properties and surface topography towards the vdW adhesion through 'effective' Hamaker constants[32,116].

The ECM is further adapted in this work to capture the particle and surface effects on the adhesion between stainless steel and three pharmaceutical powders: lactose monohydrate, hypromellose (HPMC) and ABT 089. Specifically, assuming the particles deform only elastically, the work of adhesion parameter within the Johnson, Kendall and Roberts (JKR) model describing the adhesion between a surface and an elastic deformable particle was turned into a parameter called the 'effective' work of adhesion, Γ'_{132}, to capture the individual particle and surface effects towards the measured adhesion.

The Γ'_{132} distributions outputted by the ECM are evaluated at two relative humidity (RH) ranges: 10-25% and 30-40%. The high RH range was selected because the common ambient condition in a pharmaceutical powder processing facility is ~35%. The low humidity range provides a liming condition where condensed moisture should not play a significant role in the adhesion. The Γ'_{132} distributions provide a quantitative guide for how the particle and surface properties effect the adhesion in the presence and absence of moisture-driven deformation.

A secondary study is presented in this work which demonstrates that these 'effective' work of adhesion parameters provide a quantitative description of how the particle and surface topography affects the work of adhesion. The adhesion of each of the pharmaceutical powders was measured against stainless steel that was polished to three different levels of roughness, and the 'effective' work of adhesion distributions were evaluated.

5.2 Materials and methods

5.2.1 Materials

Three pharmaceutical powders of interest, lactose monohydrate (Kerry), hypromellose (Sigma, H9262), and ABT-089 (AbbVie), were provided by AbbVie Inc.

Stainless steel (type 316, McMaster-Carr Supply Company, 9745K15) was the surface of interest because it is commonly used in pharmaceutical powder processing equipment. Additionally, the stainless steel surface can be polished to systematically alter its surface topography. The stainless steel plates were cut to 1 x 1 x 0.07cm in order to fit into specially-designed centrifuge tubes. The centrifuge tubes are 11 cm in length and have a diameter of 2.5 cm. The tubes were machined to have 2 x 2cm opening on the side that contains a holder for the plates.

The holder positions the stainless steel plates such that they are parallel to the center of rotation of the centrifuge. A schematic of these tubes is presented in Fig. 5.1.

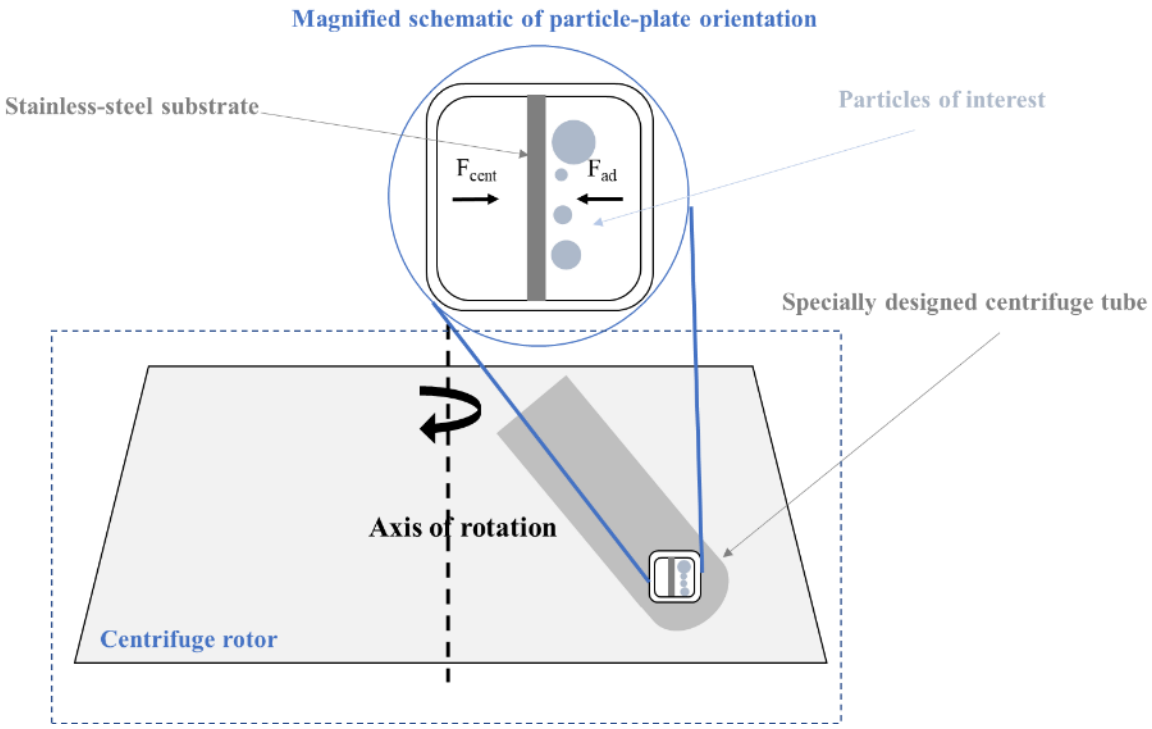

Figure 5.1 Illustration of a powder-laden stainless steel substrate mounted in a specially designed centrifuge tube. The powdered surface is oriented parallel to the axis of rotation of the centrifuge with the particles facing radially outward. When a particle detaches from the surface, the inertial force, F_{cent} imparted by the centrifuge has overcome the adhesion force, F_{ad}.

5.2.2 Experimental methods

Stainless steel polishing and cleaning procedure

A Buehler Minimet 1000 polisher was used to systematically alter the surface roughness of the stainless steel. Each stainless steel plate (1 x 1 x 0.07cm) was mounted to the polishing arm with mounting wax.

To create the 'smooth' stainless steel plates, each plate was polished with a Diamond Grinding Disc (grit of $d_{50} \sim 45$ μm) with MetaDi Supreme Diamond Suspension paste ($d_{50} \sim 45$ μm) and MetaDi fluid as a lubricant for four minutes at 25 revolutions per minute (RPM) under a 20 N

load. Next, the plate was polished on a MasterMet cloth (Buehler) with a combination of MetaDi Supreme Diamond Suspension paste (d_{50} ~ 30 μm) and MetaDi fluid for 2 minutes at 25 RPM under a 20 N load. The third step involved using MetaDi Supreme Diamond Suspension paste (d_{50} ~ 9 μm) and MetaDi fluid for four minutes under the same speed and load conditions. The last two steps involved polishing the plate for 4 minutes using first the MetaDi Supreme Diamond Suspension paste (d_{50} ~ 3 μm) with MetaDi fluid, and then MetaDi Supreme Diamond Suspension paste (d_{50} ~ 1 μm) with the MetaDi fluid.

To create the 'rough' stainless steel plates, each plate was polished with a Diamond Grinding Disc (DGD) (d_{50} ~ 45 μm) with MetaDi Supreme Diamond Suspension paste (d_{50} ~ 45μm) and MetaDi fluid as a lubricant for four minutes at 25 revolutions per minute (RPM) under a 20 N load. The second step involved polishing with a DGD (d_{50} ~ 9 μm) with MetaDi Supreme Diamond Suspension paste (d_{50} ~ 45μm) and MetaDi fluid as a lubricant for four minutes at 25 revolutions per minute (RPM) under a 20 N load.

After polishing, all plates (smooth and rough) were soaked in a warm acetone bath for at least ten minutes to dissolve any residual mounting wax. They were then rinsed with methanol and dried with compressed nitrogen.

Atomic force microscopy surface topography imaging

A Bruker Multi-Mode 8 atomic force microscope was used to measure the surface topography of the stainless steel after polishing and cleaning. For each stainless steel plate, five topographical scans were made to compile a number of representative scans of the surface topography. Each topographical scan covered a 5 x 5μm square region.

Humidity control

To ensure RH did not vary across experiments, a humidity control zone was constructed around the experiment workspace. This zone was constructed by creating a 2 x 4 x 3m enclosure made out of plastic tarp and PVC pipe. The RH within this enclosure was controlled to a specific RH range through the use of humidifiers and dehumidifiers.

Centrifuge method

To perform the centrifuge method, the following steps were executed. First, a #3 paint brush was dipped into the pharmaceutical powder of interest and tapped just above the stainless steel so that the particles fell on the stainless steel without agglomerating. The particles were deposited in the presence of a STATICMASTER Ionizer (500 µCi) chip which ionized the air to neutralize the charge on all surfaces to reduce electrostatic forces and prevent agglomeration.

A Nikon SMZ18 Stereoscope was used to capture optical images of the particles deposited on the stainless steel. The images were taken at 5X magnification to easily differentiate the particles from any defects on the steel surface. Each powdered surface was mounted in the specially designed centrifuge tubes described above and illustrated by Fig. 5.1. Based upon the orientation of the surface and particles in the tube, it can be inferred that when a particle detaches from the surface, the inertial force of the centrifuge has overcome the adhesion force. The inertial force, F_{cent} (N) is described in Eq. 5.1, where R (m) is the radius of the particle, ρ_p (kg/m^3) is the particle density, ω (s^{-1}) is the angular velocity of the rotor and r_c (m) is the distance of the particle-laden surface from the center of rotation:

$$F_{cent} = \frac{4}{3}\pi R^3 \rho_p \omega^2 r_c \qquad 5.1$$

A Sorval Lynx 6000 centrifuge was set to the following rotational speeds: 500, 750, and then increments of 1000 RPM for two-minute intervals to perform the particle removal.

After rotation at each speed, the Nikon SMZ18 Stereoscope was used to take optical images of the particles remaining on the surfaces and ImageJ (NIH) was used to process these images to determine the number of particles remaining as a function of the rotational speed. The entire surface and the initial size distribution of the deposited pharmaceutical particles were captured by analysis of an image taken before the plates were placed in the centrifuge at the start of an experiment (*i.e.*, when 100% of the particles were on the surface). After each measurement, the plates were returned to the centrifuge, the RPM was increased, and the process repeated until all particles were removed from the plates.

5.2.3 Simulation methods

Determination of Γ'_{132} distribution

After performing the centrifuge method, the ECM was executed. The ECM was developed to determine the adhesion force of all the particles of a powder against a surface as a function of their size [32]. The ECM is an engineering approach that allows powders comprised of real particles, which are challenging to model, to be described as if they are comprised of perfect, smooth spheres, which are comparatively easy to model. Previous studies have validated that the complexity associated with the actual particles and their interactions with a complex surface is captured by the empirical force parameters outputted by the ECM approach [32,116]. Due to the deformable nature of the pharmaceutical particles used in this work, the ECM was modified to the JKR adhesion force model describing elastic-like particle adhesion[44] such that the effect of the stainless steel surface and pharmaceutical particle properties towards the adhesion is captured through 'effective' work of adhesion parameters, Γ'_{132}. A model, such as the Maguis-Pollock adhesion force model[46], which incorporates plastic deformation was not used as the particles were assumed to be only elastic in nature for this initial adaption to the ECM framework used to describe deformable powders.

The procedure for determining the Γ'_{132} is described through the following steps (an in-depth description is given elsewhere[32,116]):

1. The size distribution of the pharmaceutical powder as deposited on a plate at the start of an experiment is measured via ImageJ. A powder of ideal spheres is generated *in silico* with the same size distribution as the deposited powder.
2. The JKR adhesion force is computed between the ideal spheres from step 1 and a flat surface *in silico* using Eq. 5.2:

$$F_{JKR} = \frac{3}{2}\pi R\Gamma'_{132} \text{ or } \frac{F_{JKR}}{R} = \frac{3}{2}\pi\Gamma'_{132} = constant \qquad 5.2$$

where Γ'_{132} is the 'effective' work of adhesion, and R is the radius of the sphere[44]. The surface energy value is arbitrarily set to a low value of 0.001 J/m^2. This value is readily adjusted to map the adhesion behavior of the ideal particles to the adhesion behavior of the experimental powder. The JKR force model was used to describe the particle adhesion due

to the observed elastic-like (deformable) nature of the pharmaceutical powders used. This specific approximation of the adhesion between elastic spheres and a flat plate was selected, instead of a model that incorporates roughness asperities into the mathematical description[20,57,117], in order to keep the math simple and the computational load as low as possible. With this approach, the effects of the surface roughness and particle properties are captured quickly and easily through the tunable parameter Γ'_{132}.

3. The adhesion force represented by Eq. 5.2 is related to the inertial force represented in 5.1 to determine the angular velocity necessary to dislodge the spherical particles from the smooth surface

$$\omega = \sqrt{\frac{3F_{cent}}{4\pi R^3 \rho_P r_c}} \tag{5.3}$$

and the angular velocity is converted into RPM through Eq. 5.4:

$$RPM_{removal} = \frac{60\omega}{2\pi} \tag{5.4}$$

4. The 'experimental powder adhesion curve' is created by plotting the observed percent of pharmaceutical particles remaining adhered to the plate as a function of the rotational speed of the centrifuge when using the centrifuge method discussed in section 5.2.2.
5. The 'ideal powder adhesion curve' is created using Eqs. 5.1-5.4 with the ideal particle size distribution and an assumed value of Γ'_{132}, and then plotting the percent of particles remaining adhered after each rotational speed increment of the centrifuge. At this point, the 'ideal' powder adhesion curve is predicted using an assumed value of 0.001 J/m^2 for Γ'_{132} and the 'experimental' powder adhesion curve is measured experimentally via the centrifuge technique. The 'ideal' and 'experimental' work of adhesion curves will not match initially because the ideal work of adhesion has not been tuned to account for the particles' surface roughness and shape variation, nor for the roughness on the steel.
6. To map the ideal powder behavior to the experimental powder adhesion, the ideal particle size distribution is sorted from largest to smallest and the particles are placed in bins by size, such that the percent of particles in each bin matches the percent of particles observed

to be removed at each RPM increment implemented experimentally. For example, if 20% of the experimental powder was removed between 0 and 500 RPM, bin 1 would contain the largest 20% of the ideal size distribution. Note: an assumption/limitation of this method is that the particles fall off from largest to smallest as the inertial force increases.

7. The average particle size for each bin, also called the mean bin particle diameter (D_{mean}), of the discretized ideal size distribution is determined and the Γ'_{132} is adjusted for each bin such that a particle with the mean bin particle diameter is removed at the observed experimental rotational speed. In this way, the adhesion of the ideal D_{mean} is adjusted by tuning the Γ'_{132} parameter so that the adhesion of the ideal powder matches that of the experimental powder

The distribution of Γ'_{132} values as a function of D_{mean} approximately quantifies the effects of the roughness of the surface and the effects of the shape, roughness, and size variation of the particles on the adhesion between the powder and the surface.

5.3 Results and discussion

5.3.1 Powder adhesion under different humidity conditions

The adhesion of the lactose, HPMC and ABT-089 was measured against stainless steel in two different RH ranges, 10-25% and 30-40%, through the centrifuge method described above. The adhesion was measured in these RH ranges to capture how the powder adhesion changes as a function of the RH at which the powder is stored and processed. Fig. 5.2 illustrates the average percent of particles remaining on the stainless steel at each RPM increment studied for the three powders in the two RH ranges. The error bars included in Fig. 5.2 describe the standard deviation in particles remaining across four replicates. This characterizes the variability in the adhesion caused by the variation in the particle and surface topography properties across both the powder and the surface. According to Fig. 5.2 (A) and (B), the lactose and the ABT 089 in general have very similar adhesion behaviors in that the particles remaining in the 30-40% RH range are higher across nearly all rotational speeds compared to the particles remaining in the 10-25% RH range. For the lowest rotational speeds, however, the ABT 109 adhesion was higher in the lower RH range implying the moisture condensation acted to screen the vdW adhesion instead of encouraging it through particle deformation at this condition. The HPMC behavior in Fig. 5.2 (C)

shows a higher number of particles remaining across all rotational speeds in the 10-25% RH range compared to the 30-40% condition. In addition, most of the particles have been removed by the 4000 RPM increment in the 30-40% RH case. To describe the adhesion in the two RH ranges across the entire size distribution of each powder, the ECM described in section 5.2.3 was used to determine the 'effective' surface energy distributions.

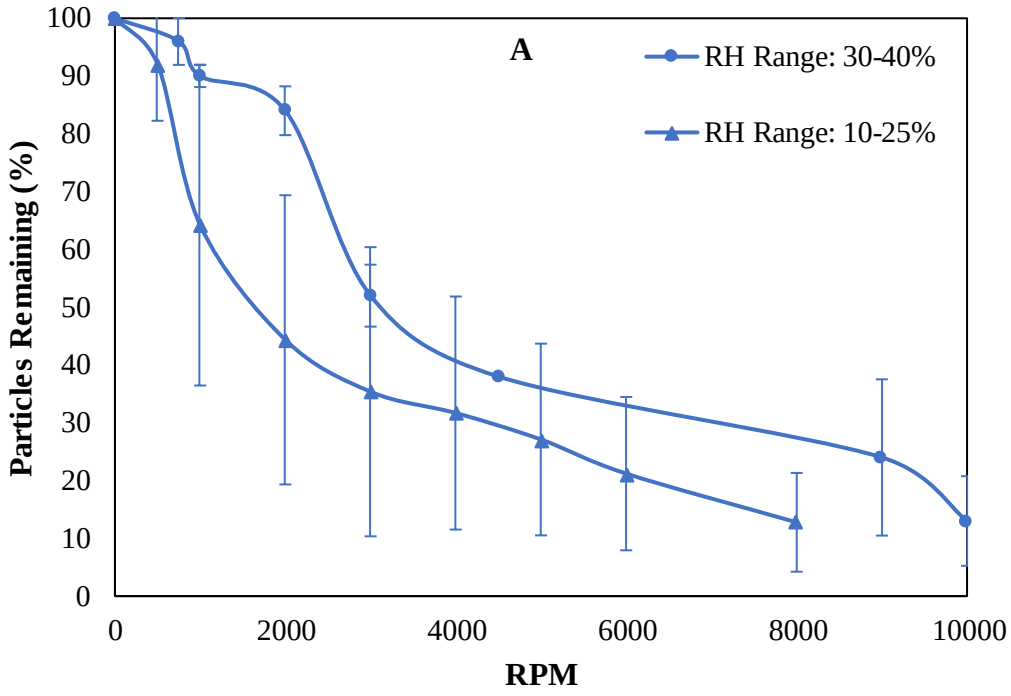

Figure 5.2 The average (of 4 replicates) percent of particles remaining as a function of applied inertial force (RPM) for (A) lactose, (B) ABT 089, and (C) HPMC adhesion adhering to stainless steel in two RH ranges: 10-25% (triangle) and 30-40% (circle). The error bars represent the standard deviation in particles remaining across the 4 replicates

Figure 5.2 continued

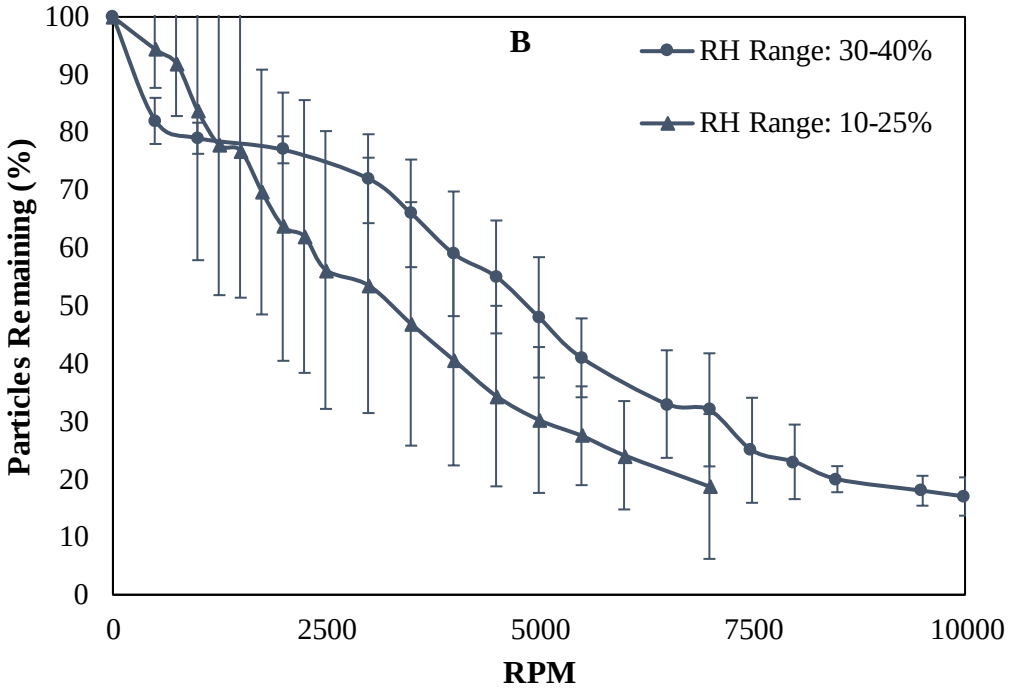

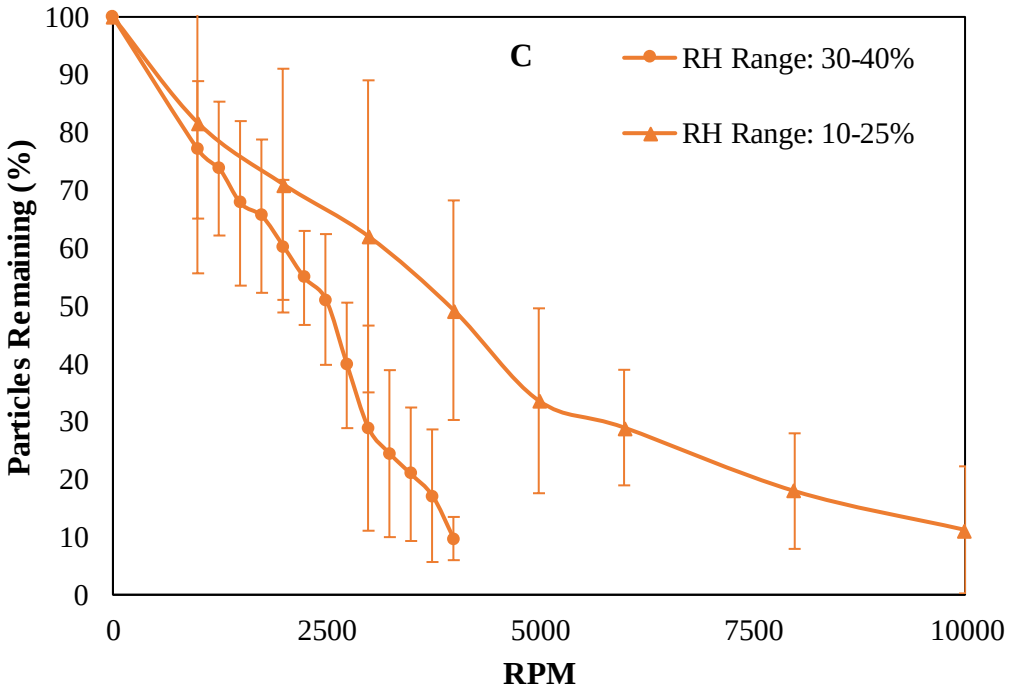

Two key pieces of information required to execute the ECM to determine the 'effective' work of adhesion distributions are the particle remaining curves such as in Fig. 5.2 and the size distributions of each of the deposited powders displayed in Fig. 5.3. The size distribution of the particles was determined through the Nikon stereoscope and ImageJ particle analysis as described in the methods section. Fig. 5.3 illustrates a representative size distribution for the lactose, ABT 089 and HPMC. Particle size directly affects the contact area a particle has with a surface which in tum impacts the adhesion.

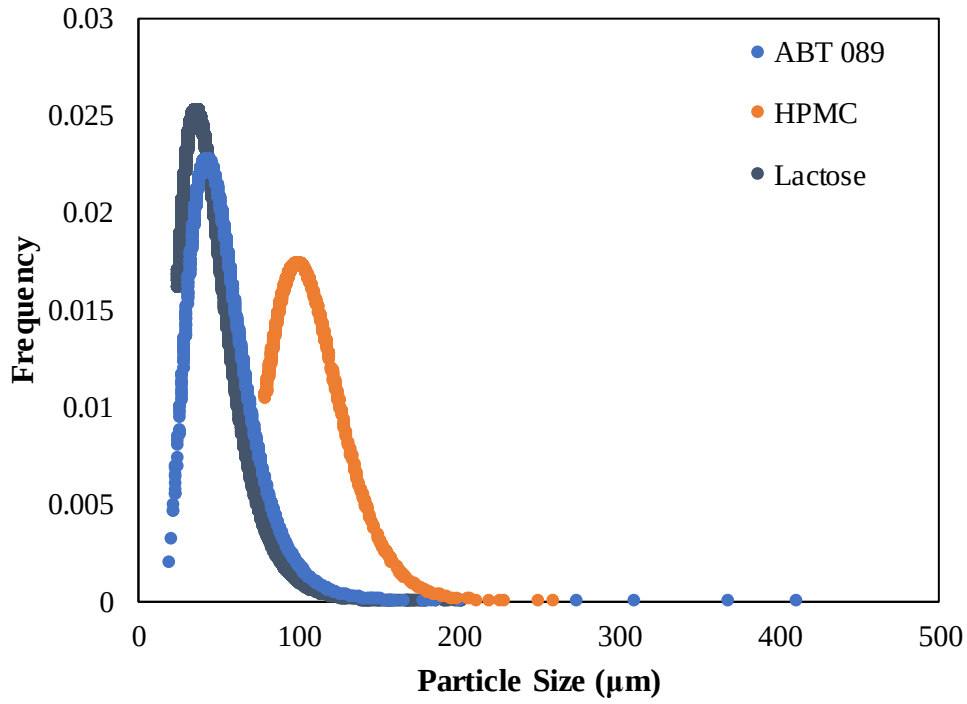

Figure 5.3 Number-based particle diameter frequency distribution determined through ImageJ analysis of ABT 089 (blue), HPMC (orange) and lactose (grey).

Fig. 5.4 illustrates the 'effective' work of adhesion distributions normalized by particle diameter outputted from the ECM for (A) lactose, (B) ABT 089, and (C) HPMC adhered to stainless steel in the two RH ranges. In Fig. 5.4(A), for particle sizes above 60 µm, the adhesion of the lactose is identical in the two RH ranges. At this condition, the particles are very large compared to the scale of the surface topography features. For particles smaller than 40 µm, the Γ'_{132} values are larger for the higher humidity range of 30-40%. The effects water of uptake,

subsequent volume increase and deformation are more significant for the smaller particles because this change brings the majority of the particle bulk into contact with the surface. Qualitatively, the trend lines describing the Γ'_{132} in each RH range have the same overall shape. The similar qualitative trend illuminates that the same properties control the adhesion with the effect enhanced by the condensation that occurs at the higher RH. Due to the hydrophilic nature of lactose monohydrate[112], it is hypothesized it absorbs the water that condenses in the higher RH, becomes more deformable in nature[44]. Consequently, the overall qualitative adhesion force trend is the same, but the force is larger for the high humidity case.

Fig. 5.4(B) illustrates that the ABT 089 adhesion to steel is similar to that of the lactose. The trends for both the RH ranges qualitatively follow the same upwards curve as the particle size decreases, and the normalized Γ'_{132} values are higher in the 30-40% RH range than in the low range. The qualitative similarity between the two trend lines implies the same property effects are being described through the normalized Γ'_{132} distributions, and the same adhesion behavior is controlling. As with the lactose, the ABT 089 is likely absorbing the condensed water in the higher humidity range causing deformation, increased contact area and an overall increase in adhesion.

The Γ'_{132} describing the HPMC behavior varied from those for both the lactose and the ABT 089 in that the Γ'_{132} values are larger for all particle sizes in the lower humidity range. The difference in behavior is attributed to the dramatically different shapes of the HPMC particles compared to the ABT 089 and lactose in Fig. 5.5. The HPMC particles seen in Fig. 5.5(B) have more variability in shape and size compared to the generally spherical lactose particles. The HPMC particles include needle-like, rectangular and spherical shapes. The way these irregular and larger particles interact with the surface may explain why the adhesion dropped when the humidity increased for the HPMC powder. When water condenses on a surface, it does not immediately create a uniform layer of water, but instead creates pockets of water in tight crevices on the surface[110]. The larger, irregular HPMC particles may be suspended over these indentations and may not contact the water. The water in these crevices does not cause swelling of the HPMC and does not form capillaries against it, but does screen the vdW interactions, lowering the overall adhesion[49,118]. At the lower RH, there is less water on the steel screening the vdW interactions, leading to higher adhesion forces. This behavior was likely not observed for the lactose and the ABT 089 because the particle sizes are smaller and more regular in shape (spherical), and therefore may more readily access the adsorbed moisture. Additionally, the ABT 089 and lactose may be

more hygroscopic in nature compared to the HPMC, allowing them to uptake more water and causing greater deformation and contact with the surface. Or alternatively, the lactose and ABT 089 may uptake the same quantity of water as HPMC, but based on their material properties they become more deformable under this condition which causes the increase in contact. A separate investigation beyond this work is needed to determine the water absorption and subsequent deformation for each powder to further distinguish which phenomenon discussed above is the cause for the adhesion behavior observed.

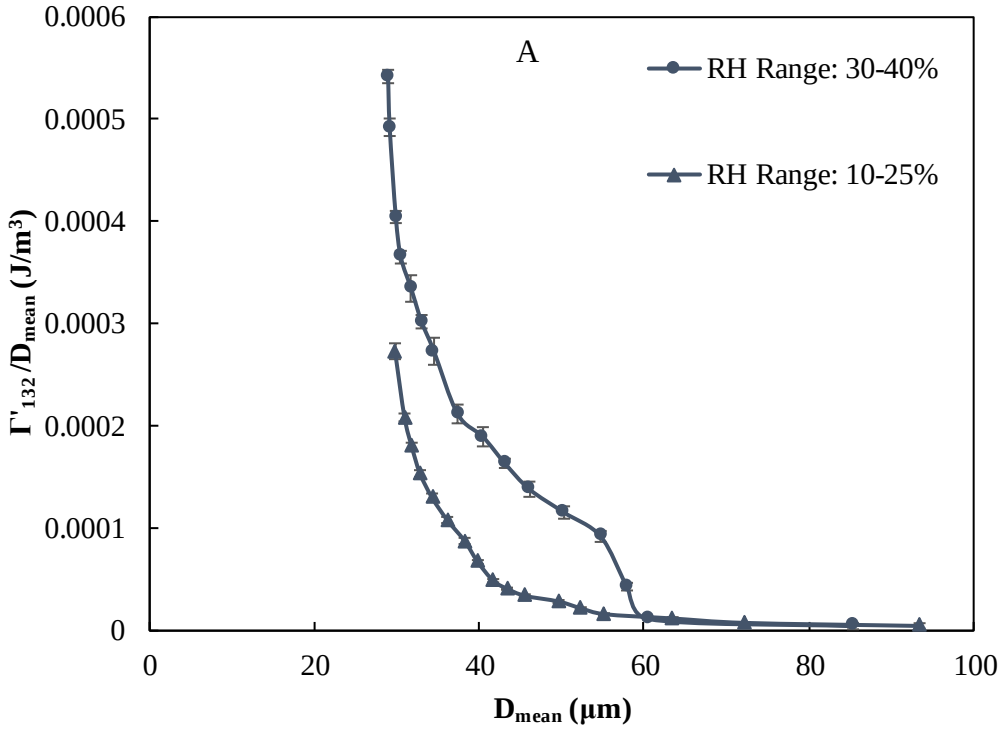

Figure 5.4 (A) lactose, (B) ABT 089, and (C) HPMC adhesion to stainless steel in two RH ranges: 10-25% (triangle) and 30-40% (circle) represented through the normalized Γ'_{132} distributions as a function of particle size. The error bars represent the standard deviation around the mean normalized Γ'_{132} for each bin.

Figure 5.4 Continued

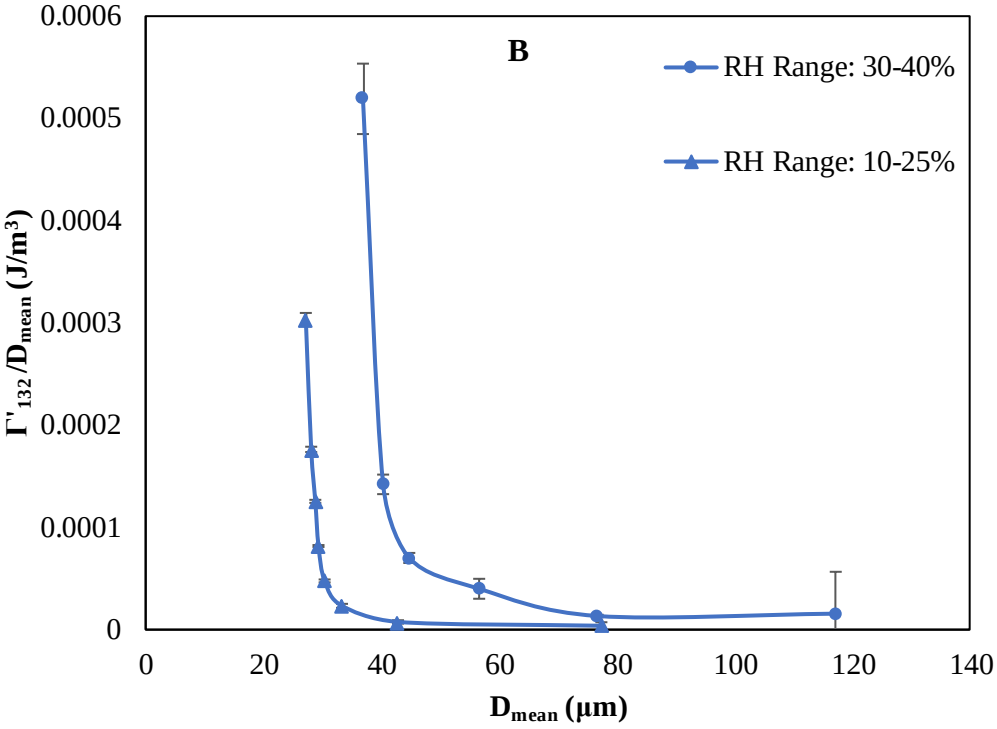

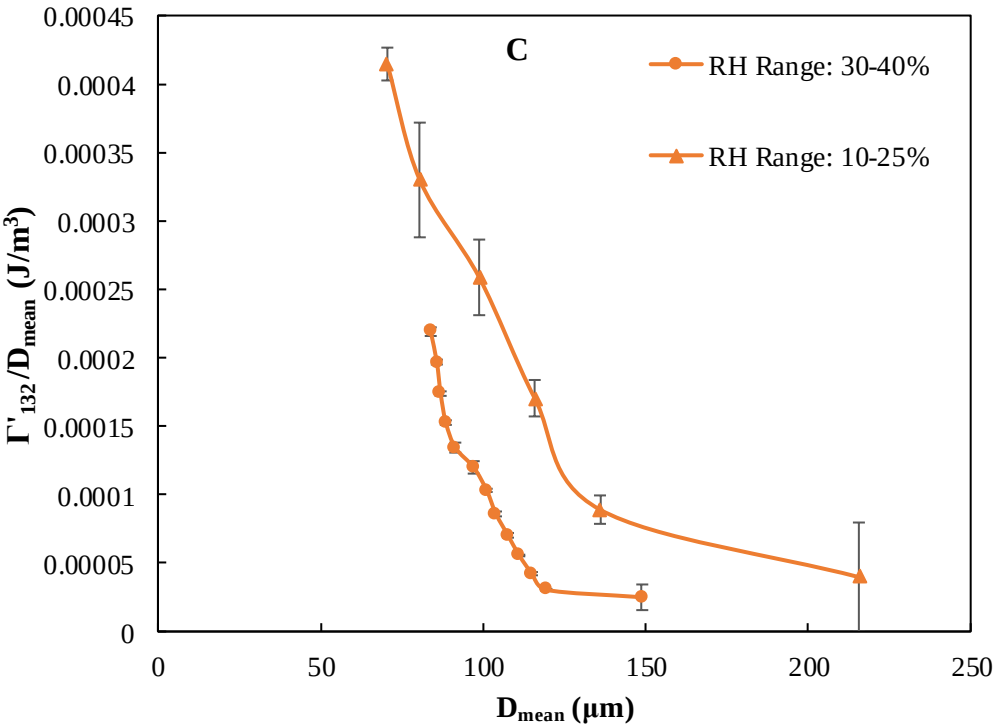

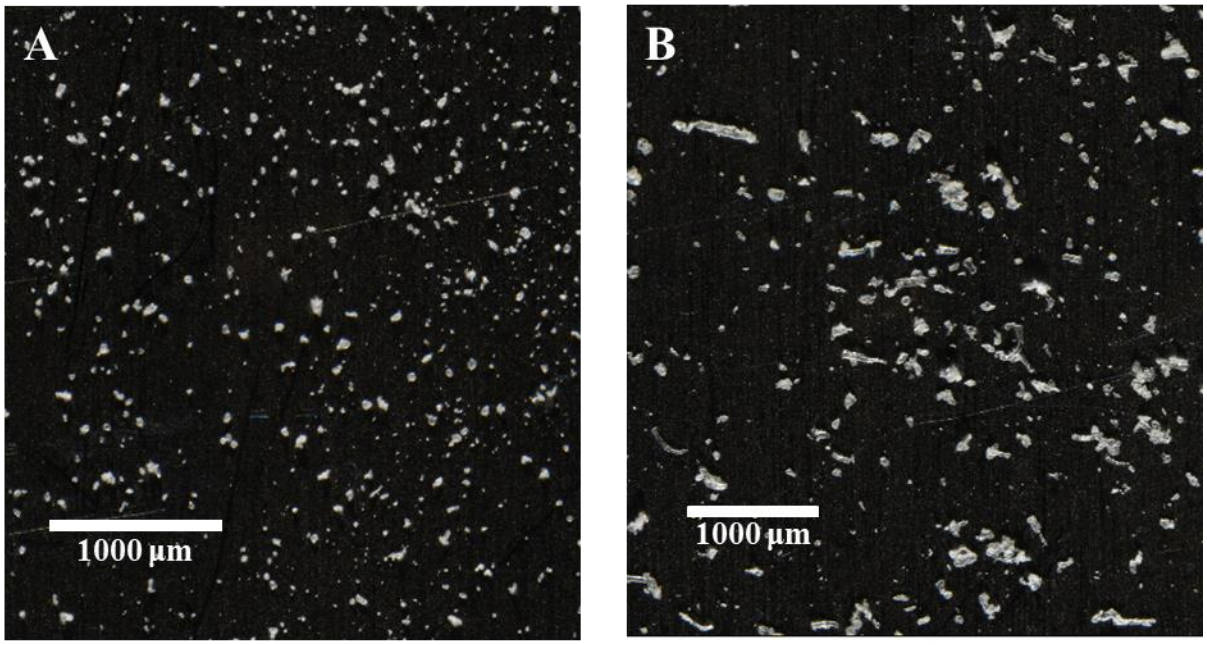

Figure 5.5 Optical microscopy images of (A) lactose adhered to stainless steel and (B) HPMC adhered to stainless steel.

5.3.2 Powder adhesion to stainless steel with varying surface topography

To investigate how the changing surface properties impact pharmaceutical powder adhesion, a secondary study was performed to characterize the work of adhesion against stainless steel with systematically varied surface topography. A first generation study validated this approach by using the ECM to study the adhesion of a polystyrene particles (spherical in shape) to silica with systematically varied surface topography[116]. Here, the ECM is adapted to the JKR adhesion model as the pharmaceutical powders studied are considered to be more deformable in nature compared to the rigid polystyrene particles.

The adhesion of the lactose, ABT 089 and the HPMC was measured against stainless steel polished in 3 different manners, as described in the methods section. The resulting topography on each surface was captured by AFM. The root mean square (RMS) roughness, R_q, of the surface topography scans was calculated according to

$$R_q = \sqrt{\frac{1}{n}\sum_{i=1}^{n} y_i^2} \qquad 5.5$$

where n is the number of points tracked along a surface and y_i is the difference between the height value of each point and the mean height value of the data set (the trace)[54]. An average RMS roughness was calculated by taking the average of the RMS values determined from the 25 scans taken across 4 plates polished at each condition. The results are shown in Table 5.1. The previous study[116] performed found that RMS roughness is not a complete descriptor for how the roughness will affect the adhesion. The adhesion is instead affected by the scale of the specific surface topography features (*i.e.* distance between roughness peaks in addition to peak height) to the scale of the particle properties. The relation between the surface and particle scale properties controls how the particles contact the surface. The 'effective' adhesion parameters outputted by the ECM capture the relationship between the surface and particle properties across an entire powder and all locations on the surface.

Table 5.1 RMS roughness characteristics of the three stainless steel polish cases.

Polish Case	Average RMS Roughness (nm)	Standard Deviation (nm)
'No Polish'	19	3
'Smooth'	4	2
'Rough'	21	17

The adhesion of the three powders was measured to each stainless steel surface through the centrifuge method described in the methods section. Fig. 5.6 displays the particles remaining as a function of the rotational speed of the centrifuge for each powder adhered to each stainless steel surface. In Fig. 5.6(A), the lactose behavior against the 'no polish' steel is most similar to the 'smooth' polish case, and both cases show stronger adhesion than the 'rough' polish case. However, Fig. 5.7(A) illustrates that once the ECM is executed to determine the Γ'_{132} distributions, normalized by particle size, the work of adhesion is comparable across all three surface finishes for most particle sizes. For particle sizes < 40 μm and > 60 μm the normalized 'effective' work of adhesion is very similar for all polished surfaces, while for particle sizes between 40 μm and 60

μm the normalized Γ'_{132} are higher against the 'no polish' and 'smooth' polished surfaces, although their form varies slightly. Although the normalized Γ'_{132} are similar quantitatively, the actual properties affecting the normalized Γ'_{132} differ in each case which can be explained by the particles interacting in different manners on each of the surface topography cases. Likely, the number of roughness peaks the particles interact with yields similar separation between the surface of the particles and the steel in the 'smooth' and 'rough' cases than in the 'no polish' case.

The normalized Γ'_{132} displayed in Fig. 5.7(B) illustrate the ABT 089 adhesion behavior is very similar to the lactose behavior excluding particle sizes above 50 μm. In contrast to the lactose, for particle sizes above 50 μm, the normalized Γ'_{132} representing the ABT 089 adhered to the 'rough' polish surface are higher than the 'smooth' polish surface. The ABT 089 particles in this larger size region are hypothesized to be more complementary to the features on the 'rough' polish surface than the features on the 'no polish' surface.

The normalized Γ'_{132} trends describing the work of adhesion of the HPMC to the steel showed the same general behavior as the other powders. For particle sizes above 125 μm, the trendlines for each polish type collapse on top of each other. This behavior illustrates that the particle properties are the key contributors to the normalized Γ'_{132} values in that the particles are so much larger compared to the surface features they are the controlling effect on the work of adhesion for all surface finishes. The normalized Γ'_{132} for particle sizes between ~60 and 125 μm show varying behavior for the different finishes because the different scales of the surface topography interact differently with the particles at each size. Below ~60 μm the 'no polish' and the 'smooth' steel behavior again is very similar, indicating that the particles have similar interactions with the features on these surfaces.

The normalized Γ'_{132} distributions describing the work of adhesion of the lactose, ABT 089 and the HPMC against the different steel surfaces that are illustrated in Fig. 5.7 provide a method to determine how specific surface and particle properties affect the work adhesion. These distributions further illuminate how altering one of those properties (in this case surface topography) changes the work of adhesion across an entire powder.

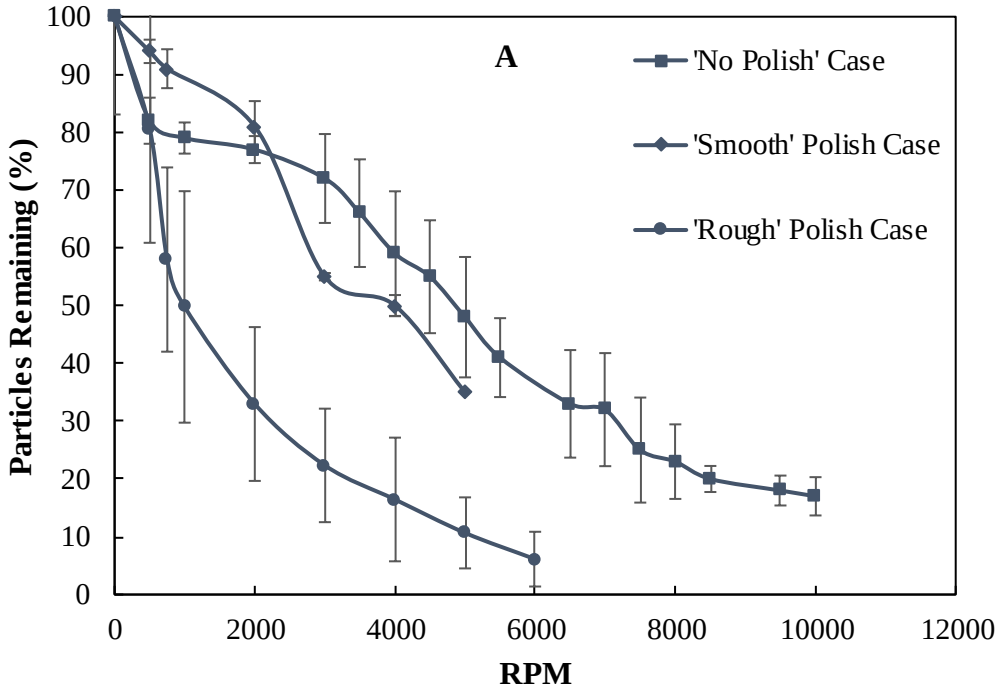

Figure 5.6. Average percent of particles remaining at varying inertial forces (RPM) for (A) lactose, (B) ABT 089, and (C) HPMC adhering to three different stainless steel surfaces with varying surface topography: 'no polish' (square), 'smooth' (diamond) and 'rough' (circle). The error bars represent the standard deviation in particles remaining across 4 replicates.

Figure 5.6 Continued

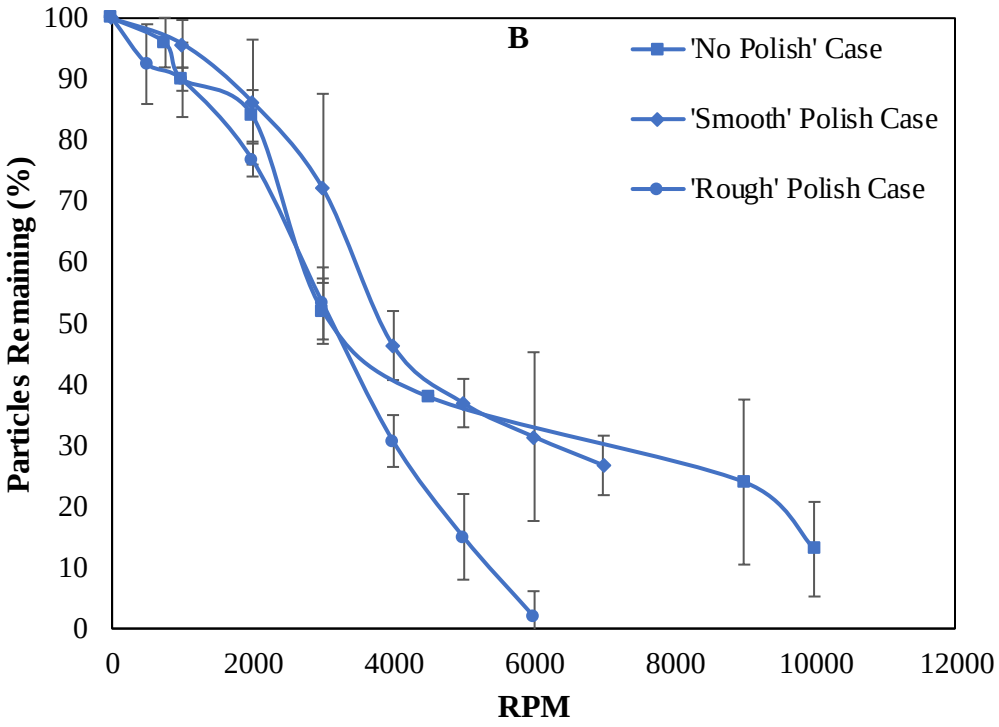

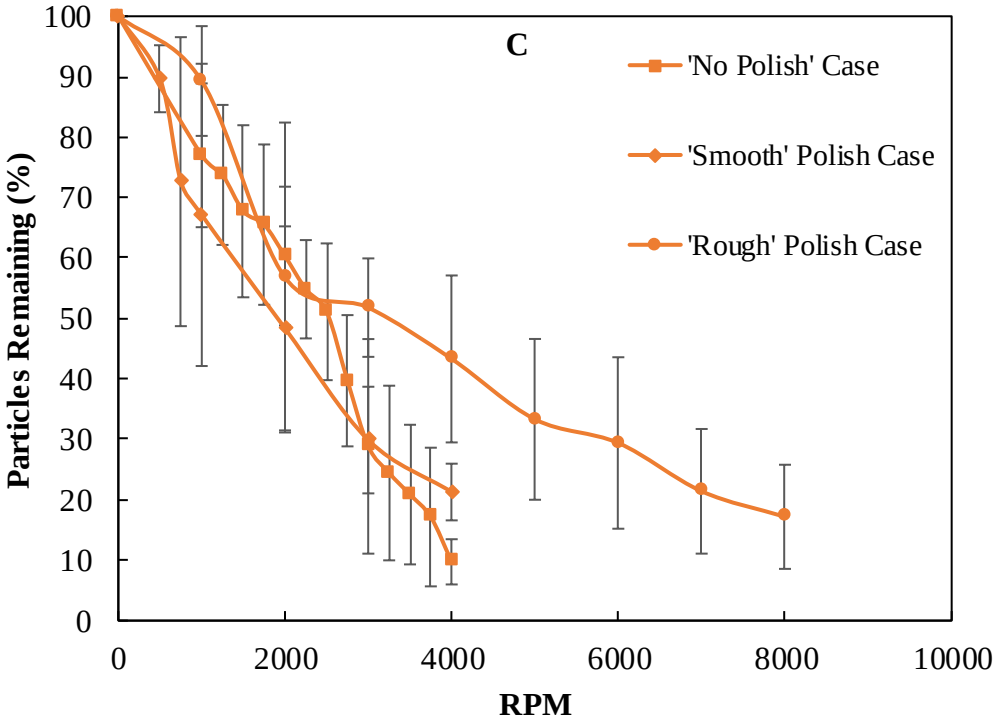

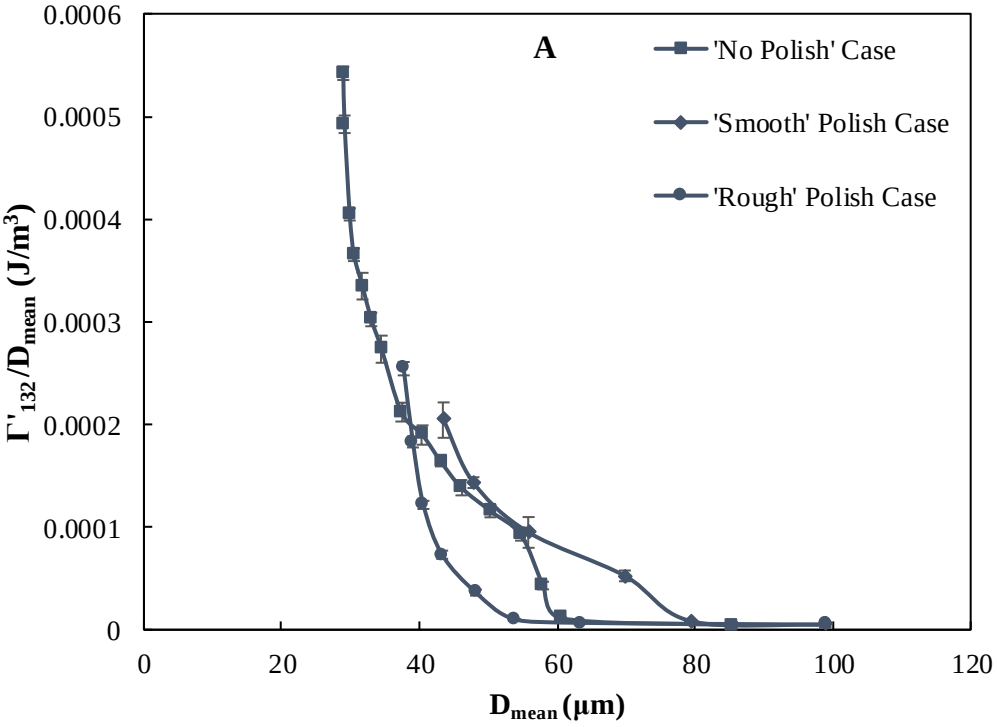

Figure 5.7 Normalized Γ'_{132} distributions for **(**A) lactose, (B) ABT 089, and (C) HPMC adhering to stainless steel with three different surface finishes as a function of particle size: 'no polish' (square), 'smooth' (diamond), and 'rough' (circle) The error bars represent the standard deviation around the mean Γ'_{132} for each bin.

Figure 5.7 continued

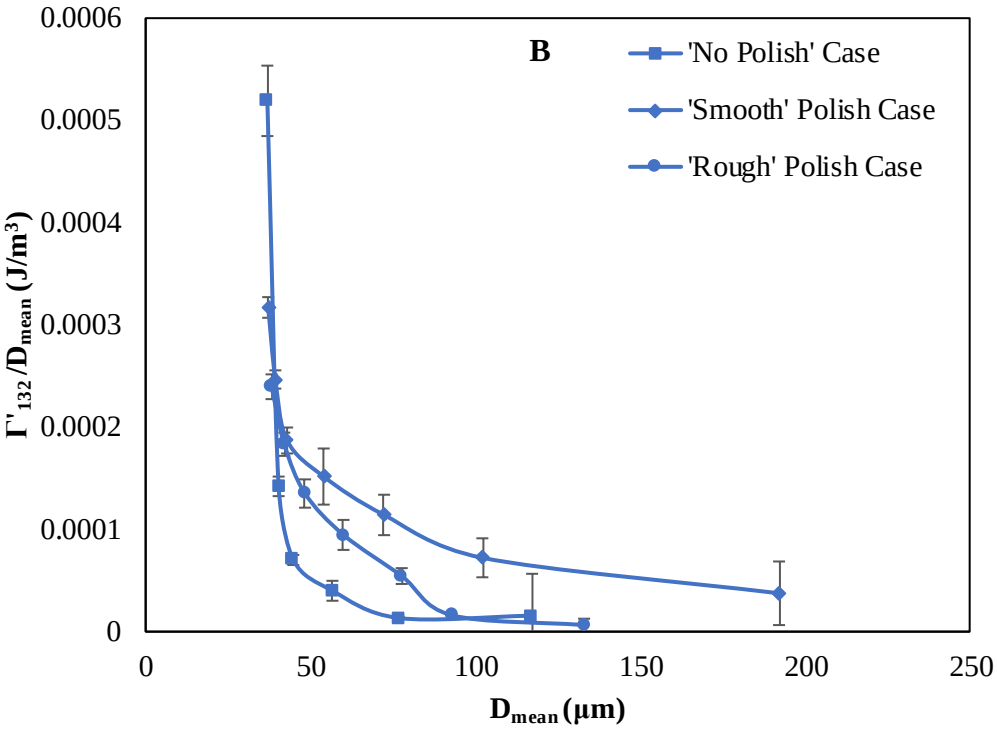

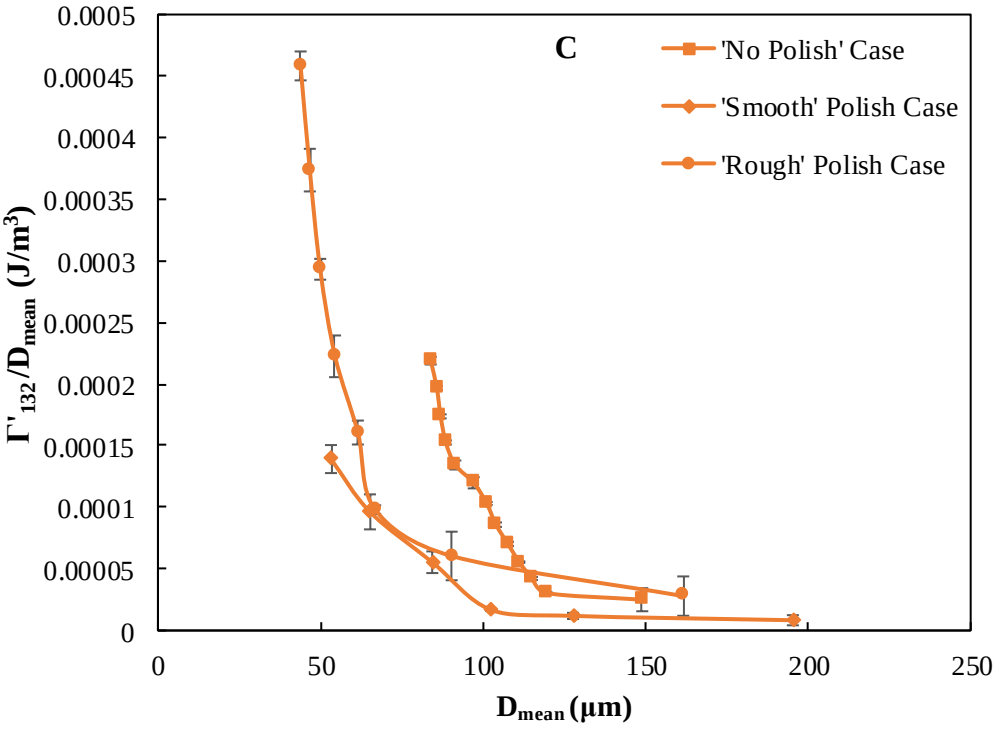

5.4 Conclusions

The adhesion between stainless steel and lactose, ABT 089 and HPMC was measured across RH increments of 15-25 and 30-40%. The ECM was used to further characterize the effect of the humidity on the work of adhesion between the particles and surfaces. The normalized Γ'_{132} for the lactose and the ABT 089 showed an increase in humidity produced an increased work of adhesion over all particle sizes. In contrast, the normalized Γ'_{132} for the HPMC illustrated the increase in humidity caused a decreased work of adhesion. For the ABT 089 and lactose adhesion cases, the properties of these powders, such as shape and hygroscopicity, likely encouraged the particles to uptake water and deform in this higher RH range which resulted in the higher normalized Γ'_{132}, while the non-uniformity of the HPMC particle shapes and sizes resulted in less water uptake and subsequent deformation. In the HPMC case, the water acted to screen and reduce the vdW adhesion force instead of encouraging it through deformation.

A secondary study was performed in this work which characterized the powders' work of adhesion against steel of varying surface roughness. In this study, the ECM was used to characterize the effect of the surface and particle properties on the adhesion through normalized Γ'_{132} distributions. These distributions illustrated the lactose and ABT 089 adhered similarly to all the steel surfaces for sufficiently small and sufficiently large particles. However, for particle diameters between ~50 and 60 µm the normalized Γ'_{132} representing the lactose adhered to the 'no polish' surface were higher compared to the 'rough' polish case while the normalized Γ'_{132} representing the ABT 089 adhered to the 'no polish' case were lower compared to the 'rough' polish case. For the lactose adhesion, the 'no polish' surface topography features encouraged contact with these particles, while the same surface topography features discouraged contact with the ABT 089 particles. Instead, the 'rough' steel surface topography features encouraged more contact with the ABT 089 particles. In contrast to the lactose and ABT 089, the HPMC particles in this size region interacted very similarly with the surface topography features on both the 'rough' and 'no polish' case as illustrated by the Γ'_{132} distributions collapsing against each other.

Across both studies, the value of the ECM was illustrated through the normalized Γ'_{132} distributions providing a quick and quantitative measure of how the RH, the particle properties and surface topography impact the powder's adhesion.

5.5 Acknowledgements

Andrew Vogt, Maxx Capece and William Ketterhagen are employees of AbbVie and may own AbbVie stock. AbbVie and Purdue contributed to the design; participated in the collection, analysis and interpretation of data, and in writing, reviewing and approval of the final presentation.

6. INCORPORATING THE EFFECT OF HUMIDITY ON SURFACE AND PARTICLE INTERACTIONS THROUGH THE ENHANCED CENTRIFUGE METHOD

6.1 Introduction

Solids processing is relevant in a wide variety of industries– some example industries being pharmaceutical, food and defense[3,79,119]. To best understand how a powder behaves under a process, it is critical to first determine how the powder coheres to itself and adheres to other dissimilar surfaces[16,120,121]. The van der Waals force, the electrostatic force and the capillary force all affect adhesion[17,122,123]. The environment in which a powder process is performed dictates which of the three forces controls the adhesion.

One environmental condition that is present in industrial processing and affects powder adhesion is humidity[49,124–128]. Depending on the humidity conditions, moisture may condense on the surfaces of interest leading to the formation of capillary bridges between the particles and the surfaces[36]. The particle properties, such as size and shape, and the surface roughness play a role towards particle adhesion and determine how a liquid meniscus forms between surfaces[51,129,130]. The contact area of the liquid bridge with the particle and the surface is impacted by the surface topography and particle shape[51,58,129]. Studies so far have focused on understanding the influence of particle properties across humidity environments at the single particle scale. To describe these properties across an entire powder, Thomas *et al.* created a framework called the enhanced centrifuge method to quantify the effect of the surface and particle properties on the capillary adhesion through an empirically-tuned parameter called the 'effective' contact angle[131]. This method involves tuning the contact angle within the simple model describing the capillary adhesion between a sphere and a flat plate as a function of particle size shown here:

$$F_{cp} = 2\pi\gamma R_P(cos\theta_1 + cos\,\theta_2) \tag{6.1}$$

where F_{cp} is the capillary adhesion force, γ is the surface tension of the water, R_P is the particle radius and θ_1 and θ_2 being the contact angles of (1) the liquid with the particle and (2) with the surface. The contact angle ordinarily describes the angle tangent to the liquid bridge's surface at the point of contact with the solid surface. When one or the other of these contact angles are tuned

as a function of particle size to capture the effects of particle shape, particle topography, and surface roughness on the resulting adhesion, it is expressed as a distributions of 'effective' contact angles [131].

The purpose of this study was to extend this simulation-based work further and use the enhanced centrifuge method to characterize the effect of silica particle properties and surface topography on the adhesion between silica spheres and nominally flat silica plates as a function of relative humidity (RH). Silica was selected as the material for this study as it is a material commonly used to examine particle adhesion – usually in single particle studies using atomic force microscopy[20,52,129]. Additionally, it is often used to make products such as the glass for solar panels or the wafers used in microelectronics[123,128]. The current work sheds light into how an entire silica powder's adhesion is affected by the changing interaction between the particle and surface due to the RH and subsequent water formation on the surface.

6.2 Materials and methods

6.2.1 Materials

A powder comprised of green-fluorescent silica particles (DiagNano™, $d_{50} \sim 20\mu m$) was chosen because the fluorescent labelling allowed the particles to be visible under the in-house Nikon SMZ18 Stereoscope. The surface of choice was ground polished fused quartz (silica) (Technical Glass Products) that was cut to 0.5 x 0.5 x 0.2 cm pieces and glued to stainless steel backings (1 x 1 x 0.07cm) in order to fit into specially-designed centrifuge tubes used in the enhanced centrifuge method, as described below. The centrifuge tubes are 11 cm in length and have a diameter of 2.5 cm. The tubes are solid except for a 2 cm x 2 cm opening on the side that contains a holder for the plates. The holder allows the silica glued to the stainless steel backing to be oriented such that the silica is parallel to the center of rotation of the centrifuge. A schematic of a specially designed centrifuge tube is presented in Fig. 6.1.

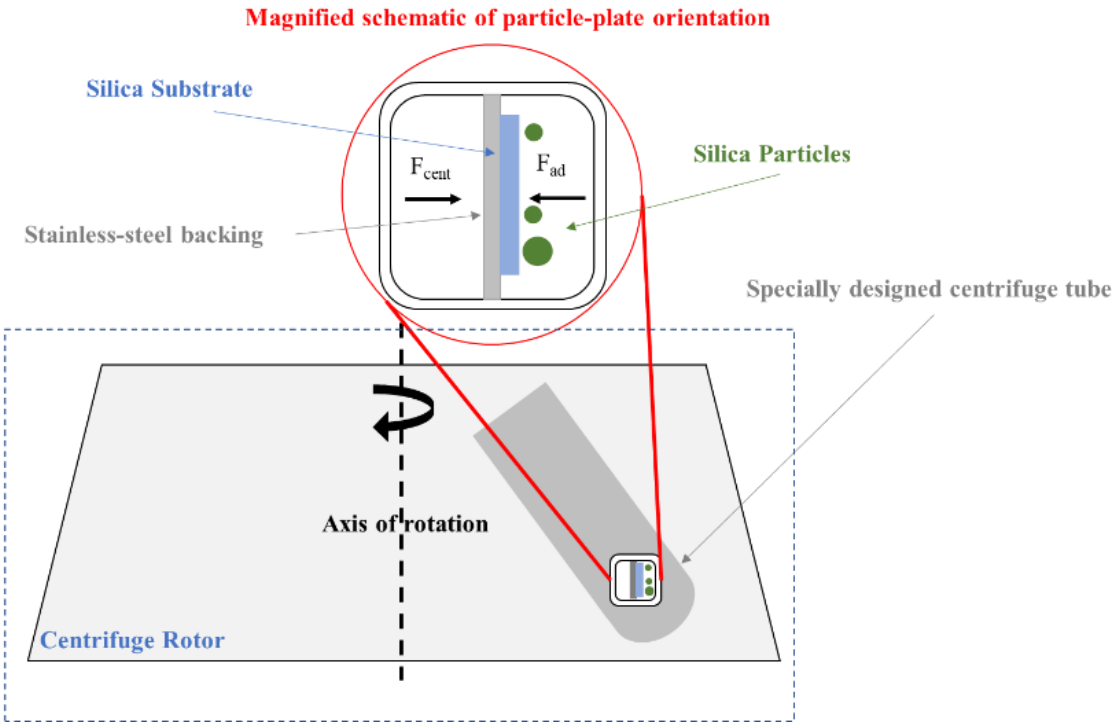

Figure 6.1 Illustration of a powder-laden silica surface mounted in a specially designed centrifuge tube. The powdered surface is oriented parallel to the axis of rotation of the centrifuge with the particles facing radially outward. When a particle detaches from the surface, the inertial force, F_{cent} imparted by the centrifuge has overcome the adhesion force, F_{ad}.

6.2.2 Experimental methods

Atomic force microscopy surface topography and phase diagram measurements

A Multi-Mode 8 atomic force microscope (AFM) and RTESPA-300 etched silica probe (Bruker) were used in tapping mode to measure the surface topography of the silica. Five topographical scans of the silica surface were measured. Each topographical scan area was 5 μm x 5 μm.

The same AFM system was used to capture phase diagrams of the silica surface under the presence of controlled RH. The AFM is equipped with an atmospheric hood which allows the ability to control the ambient atmosphere around the experiment. The atmospheric hood is attached to dry nitrogen (99.5%) and humid gas via a two-stage bubbler humidifier. The dry and humid gases were mixed in order to obtain the desired humidity level. The humidity inside the atmospheric hood was measured via a Vaisala HPMC233 humidity meter. The system was allowed

to equilibrate for 30 minutes within each humidity range studied before taking a representative phase scan.

Centrifuge method

Many methods exist to measure adhesion forces, which include: the centrifuge technique, the aerodynamic technique, the hydrodynamic technique, the impact-separation method, the ultrasonic vibration method, the electrical field detachment technique, force microscopy, the drop test, acoustic base excitation, and the mechanical surface energy tester [40,41,81,90,91]. The classical centrifuge technique is a practical method that measures particle adhesion, is simple to perform, and describes the adhesion behavior of an ensemble of particles in terms of the average adhesion force for the ensemble. To perform the centrifuge method, the following steps were executed. First, a #3 paint brush was dipped into the silica powder of interest and tapped just above the silica so that the particles fell on the silica without agglomerating. The particles were deposited in the presence of a STATICMASTER Ionizer (500 µCi) chip which ionized the air to neutralize the charge on all surfaces to reduce electrostatic forces and prevent agglomeration.

A Nikon SMZ18 Stereoscope was used to capture optical images of the silica particles adhering to the silica. The images were taken at 5X magnification to easily differentiate the particles from any defects on the silica surface. The plates were imaged in the presence of the STATICMASTER Ionizer (500 µCi) chip to reduce electrostatic forces. To perform the particle removal, each powder coated surface was mounted in a specially designed centrifuge tube described above and illustrated by Fig. 6.1. Based upon the orientation of the surface and particles in the tube, it can be inferred that when a particle detaches from the surface, the inertial force of the centrifuge has overcome the adhesion force. The inertial force, F_{cent} (N) is described in Eq. 6.2, where R (m) is the radius of the particle, ρ_p (kg/m^3) is the particle density, ω (s^{-1}) is the angular velocity of the rotor and r_c (m) is the distance of the particle-laden surface from the center of rotation:

$$F_{cent} = \frac{4}{3}\pi R^3 \rho_p \omega^2 r_c \tag{6.2}$$

A Sorval Lynx 6000 centrifuge was operated at 500, 750, 1000, 2000, 3000, 4000, 5000, 6000, 7000, 8000, 9000, and 10000 RPM for two-minute intervals to perform the particle removal. Each

study began at the lowest rotational speed. After a powdered surface was evaluated following rotation in the centrifuge, the surface was returned to the centrifuge and the work was repeated at a higher rotational speed.

After rotation at each speed, the Nikon SMZ18 Stereoscope was used to take optical images of the particles remaining on the surfaces. ImageJ (NIH) was used to process these images to determine the number of particles remaining as a function of the rotational speed. The entire surface and the initial size distribution of the deposited silica particles were captured by analysis of an image taken before the plates were placed in the centrifuge at the start of an experiment (*i.e.*, when 100% of the particles were on the surface).

To ensure humidity did not vary across experiments, a humidity control zone was constructed around the experimental workspace. This humidity control zone was constructed by creating a 2 x 4 x 3 m enclosure made out of plastic tarp and PVC pipe. The humidity within this enclosure was controlled to the desired relative humidity range within +/-5% with the combined use of humidifiers and dehumidifiers.

6.2.3 Simulation methods

Determination of 'effective' adhesion distribution

After performing the centrifuge method, the ECM was executed. The ECM was developed to determine the adhesion force of all the particles of a powder against a surface as a function of their size [32]. The ECM is an engineering approach that allows powders comprised of real particles, which are challenging to model, to be described as if they are comprised of perfect, smooth spheres, which are comparatively easy to model. Previous studies have validated that the complexity associated with the actual particles and their interactions with a complex surface is captured by the empirical force parameter outputted by the ECM approach [32,116]. Specifically, the ECM approach was applied to a system which isolated van der Waals (vdW) adhesion forces, and a purely simulation-based capillary adhesion study [32,116,131,132]. The empirical 'effective' force parameter in the determined by vdW adhesion case described by Eq. 6.3 is defined to be an 'effective' Hamaker constant, A'_{132}.

$$F_{vdW}(D) = \frac{AR}{6D^2} \tag{6.3}$$

In Eq. 6.3, *A* is the Hamaker constant, *R* is the sphere's radius, and *D* is the separation between the sphere and the flat plate

The parameter tuned in the capillary adhesion case describe by Eq. 6.1 is defined to be an 'effective' contact angle, θ_{eff}[32,116,131,132]. An in-depth description of the ECM used to determine these specific 'effective' force parameters is published previously[32,116,131,132].

Here, the silica adhesion was measured across increasing RH levels. Due to the changing humidity conditions, the adhesion system could not be strictly characterized as either a vdW or capillary adhesion. Consequently, the complexity associated with the silica particles and the surface topography of the silica substrate is captured in a general 'effective' force parameter described by the following symbol: F'_{ad}. In brief, the procedure for determining these F'_{ad} used to capture the effect of surface roughness and particle shape and topographical properties on the adhesion through the ECM is described through the following steps:

1. The size distribution of the silica powder as deposited on a plate at the start of an experiment is measured via ImageJ.
2. A simulated powder comprised of 1000 spherical particles is generated *in silico* such that the size distribution matches that of the experimental powder. This distribution is referred to as the *ideal particle size distribution*.
3. If the adhesion system (vdW or capillary) is clearly defined, the adhesion force is computed between the ideal spheres from step 2 and a flat surface based on either the Derjaguin approximation[116] for the vdW force case or the simple approximation for the capillary adhesion[51,125].
4. The expression for the inertial force in Eq. 6.2 is rearranged to isolate the angular velocity observed when spherical particles are dislodged from the smooth surface

$$\omega = \sqrt{\frac{3F_{cent}}{4\pi R^3 \rho_P r_c}} \tag{6.4}$$

and the angular velocity is converted into the rotational speed observed at the point of particle removal, $RPM_{removal}$, through Eq. 6.5:

$$RPM_{removal} = \frac{60\omega}{2\pi} \quad 6.5$$

5. The 'experimental powder adhesion curve' is created by plotting the observed percent of silica powder remaining adhered to the silica as a function of the rotational speed of the centrifuge when using the centrifuge method discussed in section 6.2.2 (inertial force from the centrifuge causes particles to detach from the surface, and optical and image analysis is used to track the number of particles of each size that remain as a function of inertial force).
6. The 'ideal powder adhesion curve' is created using Eqs. 6.2,6.4 and 6.5 with the ideal particle size distribution and an assumed value for the 'effective' Hamaker constant or 'effective' contact angle, and then plotting the percent of particles remaining adhered after each rotational speed increment of the centrifuge. The 'ideal' and 'experimental' adhesion curves will not match because the ideal adhesion case has not been tuned to account for the particles' surface roughness and shape variation, nor for the roughness on the silica.
7. To map the ideal powder behavior to the experimental powder adhesion, the ideal particle size distribution is sorted from largest to smallest and the particles are placed in bins by size, such that the percent of particles in each bin matches the percent of particles observed to be removed at each RPM increment implemented experimentally. For example, if 30% of the experimental powder was removed between 0 and 2000 RPM, bin 1 would contain the largest 30% of the ideal size distribution. An assumption/limitation of this method is that the particles fall off from largest to smallest as the inertial force increases.
8. The average particle size for each bin, also called the mean bin particle diameter (D_{mean}), of the discretized ideal size distribution is determined and the F'_{ad} is adjusted for each bin such that a particle with the mean bin particle diameter is removed at the observed experimental rotational speed. In this way, the adhesion of the ideal D_{mean} is adjusted by tuning the F'_{ad} parameter so that the adhesion of the ideal powder matches that of the experimental powder.

As the ambient humidity condition was altered across this study, neither the capillary nor the vdW adhesion model was directly applied to the ECM. Consequently, to compare results across humidity increments, the 'effective' force parameter was left as a generalized F'_{ad} description and not described through either a A'_{132} distribution or a θ_{eff} distribution.

6.3 Results and discussion

The purpose of this work is to characterize the effect of the silica particle properties and silica surface topography on the adhesion across increasing humidity increments. To begin to do this, the surface topography on the silica substrate was measured via AFM as described in section 6.2.2 and the surface had a root mean square (RMS) roughness of approximately 9 nm. This RMS roughness was determined to validate that the surface topography on average was similar across replicates.

Silica powder adhesion was measured against the silica substrate in five different humidity ranges: 10-25%, 30-40%, 40-50%, and 60-70%. The direct result of each of the centrifuge method experiments is displayed as the percent of particles that remained as a function of RPM, as shown in Fig. 6.2.

At the lowest rotational speeds (0 – 5000 RPM), Fig. 6.2 shows that the percent of particles that remained adhering at humidity ranges of 30-40% and 40-50% are overall lower compared to the other three humidity ranges studied, except at the lowest rotational speeds for the 40-50% case. In addition, the percent of particles that remained in the upper two humidity ranges of 50-60% and 60-70% are virtually identical over all rotational speeds studied. At these humidity ranges, moisture likely adsorbs to fill crevices on the two surfaces with bulk water[49,118,133,134]. This bulk water screens vdW forces, but also has the potential to bridge adjacent locations on the particle and surface. In this case, the capillary forces between the nanoscale contacts will increase the adhesion, leading to large quantities of particles adhering at all rotational speeds. Also consistent with existing studies [110,118,133], at the lowest RH (10 – 25%) adsorbed molecular water likely fills the smallest crevices on the two interacting surfaces, shielding vdW interactions but doing little else to influence the adhesion. In this case, the adhesion is most likely resulting from lightly screened vdW forces. To further investigate the effects of the specific particle properties, such as size, and the silica substrate topography towards the adhesion across various RH levels, the ECM was performed.

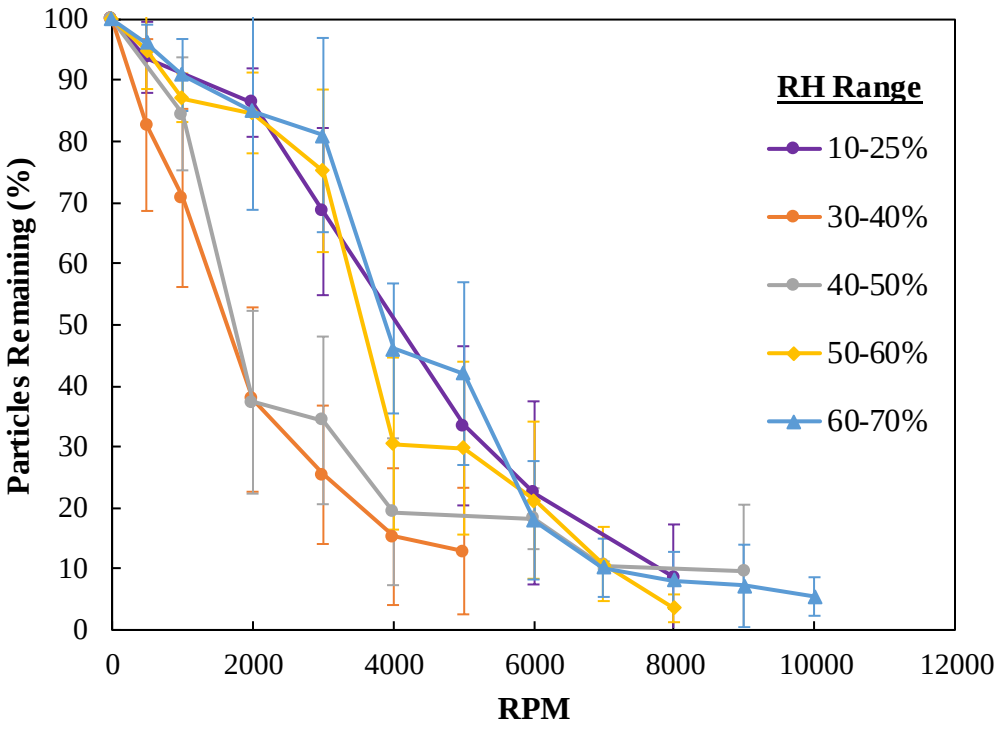

Figure 6.2 Measured percent of silica particles remaining on ground polished silica after rotation in centrifuge at various rotational speeds at varying RH. Error bars represent the standard deviation of the percent adhering to the ground polished silica in each humidity range across 4 replicates.

In order to determine the 'effective' adhesion force distributions that further describe the effect of the silica properties on the adhesion, the size distribution of the silica was first measured through ImageJ particle analysis of the particles deposited on the silica in each experiment in each humidity range. These size distributions are provided in Fig. 6.3. It is important to note that the size distributions of the silica particles deposited on the silica substrates were similar across experiments.

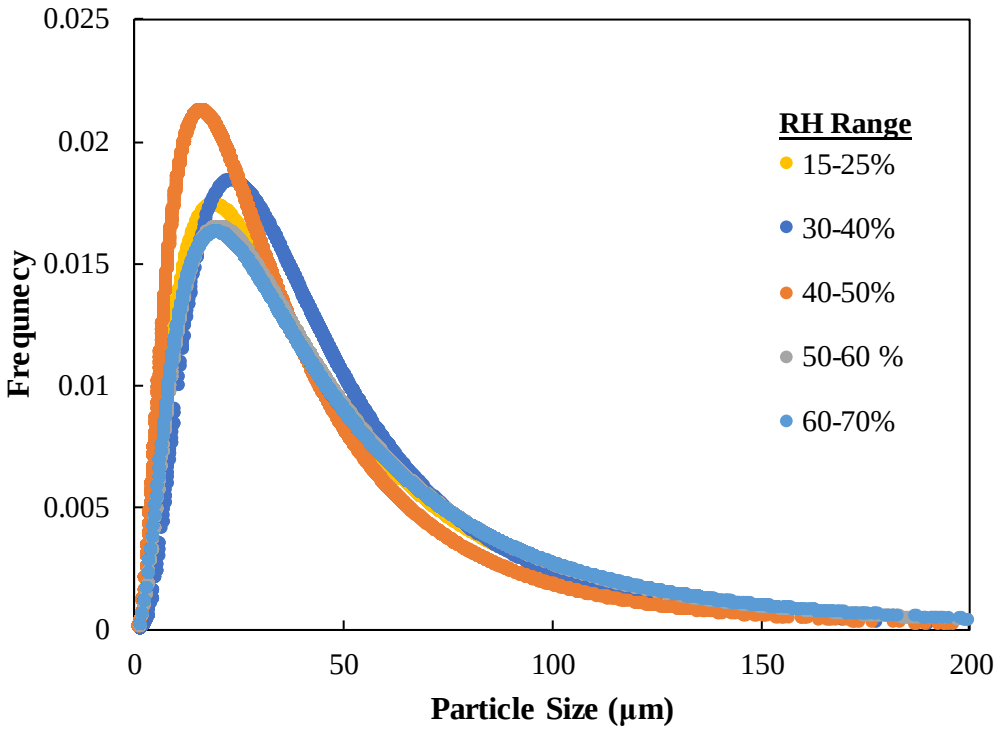

Figure 6.3 Number-based particle diameter frequency distribution determined from the size distributions, compiled across replicates in each humidity range, of the silica particles measured via the Particle Analysis function in ImageJ.

The percent of particles observed to remain as a function of the RPM and size distributions in each humidity range were inputted into the ECM to build the normalized 'effective' force of adhesion plots (F'_{ad} as a function of particle size) presented in Fig. 6.4. To further distinguish and compare the adhesion trends across relative humidity ranges, the y-axis representing the normalized 'effective' adhesion force was plotted on a lognormal scale in Fig. 6.5.

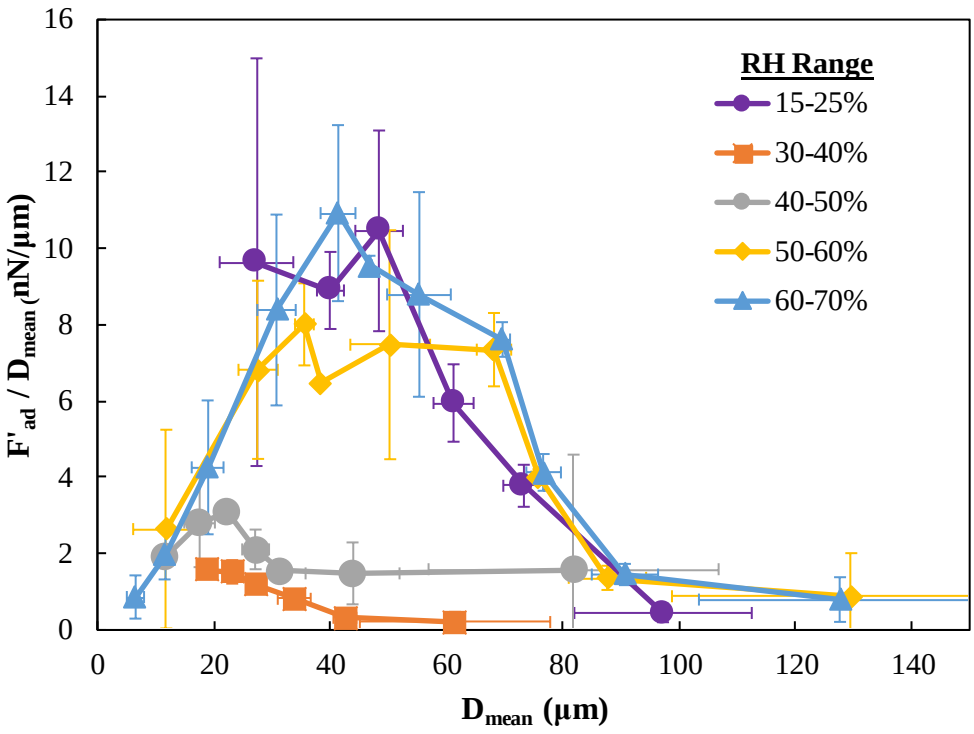

Figure 6.4 Normalized 'effective' adhesion force curves across humidity ranges of 15-25%, 30-40%, 40-50%, 50-60% and 60-70%. The horizontal error bars represent the standard deviation around the D_{mean} for each bin. The vertical error bars represent the standard deviation around the mean F'_{ad} for each bin.

Two regions of adhesion are observed in Fig. 6.5. The first regime illustrates the adhesion in the relative humidity ranges of 30-40% and then 40-50%. The adhesion behavior for these two humidity ranges overall follows the same qualitative trend with the adhesion quantitatively being higher for the 40-50% case. The adhesion is lowest in the 30-40% RH range, likely due to the initial formation of adsorbed water that fills partially, but not completely, the surface roughness features such that instead of creating a bridge between the particles and surface, and inducing capillary adhesion, the water acts to instead reduce the vdW interaction between the particle and surface [49,51,118]. The spike in adhesion seen above an RH of 40% is likely due to the transition of the water completely layering across the surface roughness features such that many nano-scale capillary bridges now exist between the particle and surface[49,118,130]. The similarity in the 'effective' adhesion force values for the lowest and highest RH ranges has also between observed in other studies[51,110,129]. One study proposed this may be occurring due to the formation of icelike structures in the water causing lower than expected adhesion in the upper humidity range.

A separate study found the similarity between the two ranges was due to the surface roughness impeding the water's ability to bridge with the particles[51]. These sample studies illustrate the adhesion in the upper and lower humidity can look similar to each other even when the controlling adhesion force is different in each range.

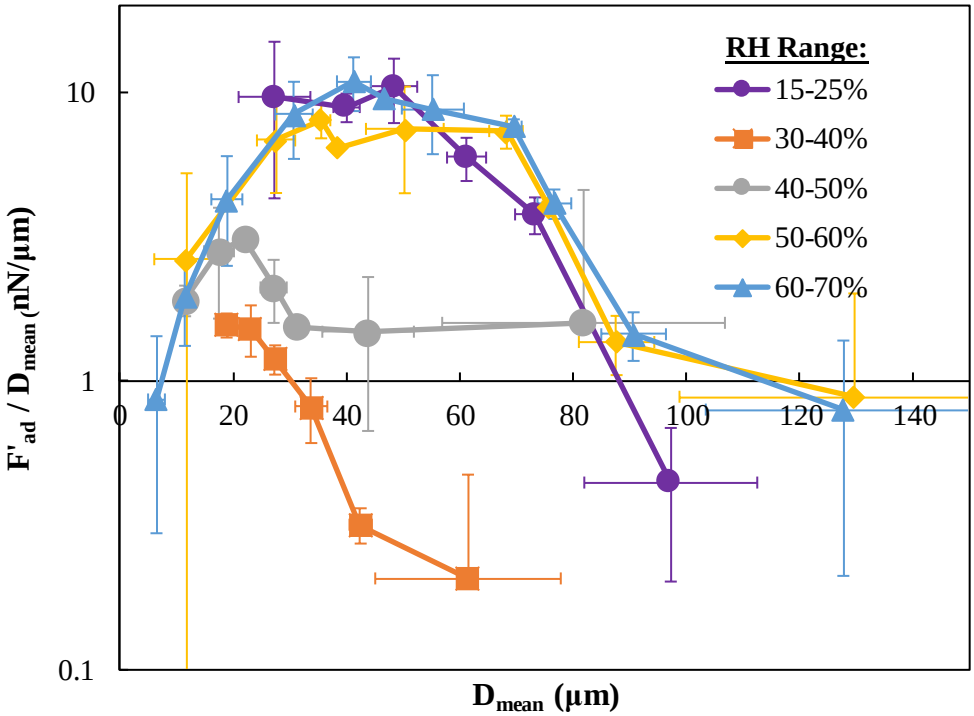

Figure 6.5 Normalized 'effective' adhesion force curves across humidity ranges of 15-25%, 30-40%, 40-50%, 50-60% and 60-70% The horizontal error bars represent the standard deviation around the D_{mean} for each bin on a log scale. The vertical error bars represent the standard deviation around the mean F'_{ad} for each bin on a log scale.

To further validate the adhesion behavior seen in each RH range, phase diagrams determined via atomic force microscopy were measured across increasing RH levels as described in section 6.2.2. The phase diagrams representing the adsorbed moisture at RH levels of 15%, 45% and 52% illustrated through Fig.6.6 A, Fig.6.6 C, and Fig. 6.6 D are qualitatively comparable to each other in terms of phase color contrast. The phase diagram representing the RH level of 35% (Fig. 6.6B) shows variation from the other increments as it contains pockets of the lighter colored regions. Thus implying that although water layering has begun, it has not completely layered across all the surface topography features. To further validate this, the average phase shift values were calculated

from each phase diagram shown in Fig. 6.6 and plotted as a function of humidity in Fig. 6.7. The average phase shift values become more negative in value as a function of increasing humidity demonstrating water continues to increase in amount on the surface as a function of increasing humidity.

The silica adhesion in the 30-40% RH range was lower compared to all other humidity ranges because although water is forming on the surface, it is just beginning to fill the surface topography crevices such that liquid bridging does not occur yet and instead the water acts to screen the vdW adhesion. As the presence of water increases as a function of RH, the water continues to fill the surface topography features reaching a point where liquid does span the space between the surface and particles, leading to the increases in adhesion with increasing RH above 40%.

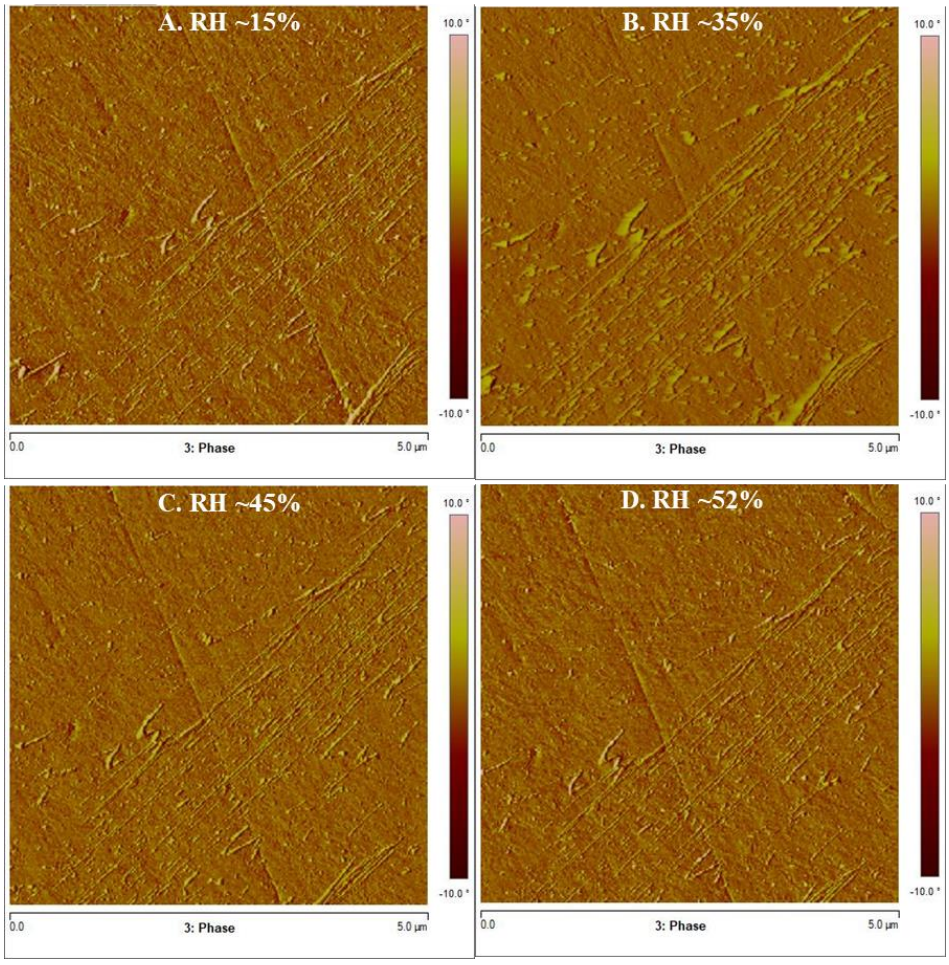

Figure 6.6 AFM phase diagrams of the ground polished silica surface under relative humidity conditions of A) ~15%, B) ~35%, C) ~45%, and D) ~52%.

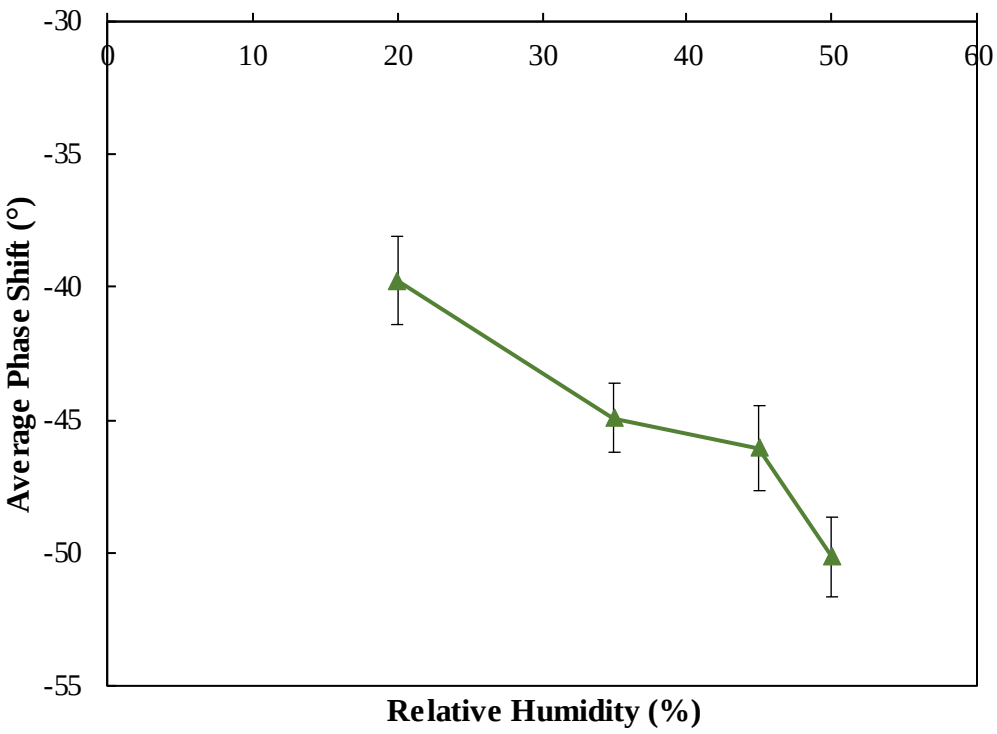

Figure 6.7 Average phase shift values corresponding to phase diagrams shown in Fig. 6.6 at each of the following humidity conditions: A) ~15%, B) ~35%, C) ~45%, and D) ~52%. The error bars describe the standard deviation around taking the mean phase shift value.

6.4 Conclusions

The ECM was utilized to study silica powder adhesion to a silica surface across increasing RH levels to characterize the effect of humidity had on the adhesion between silica particles and surfaces. This study and the 'effective' force distributions revealed that the RH level dictates how the liquid exists between the surfaces, and in turn how the particles contact and adhere to the surface. In the RH regime of 30-40% where liquid is likely just beginning to form in bulk on the surface, the particle adhesion is low as the particles do not contact a continuous layer of liquid, but instead the water fills the features on the silica surface and screens the vdW interactions. As the RH transitioned to the 40-50% range, the slightly higher 'effective' force of adhesion distribution revealed the build-up of water allowed liquid bridges to form between the particles and surface. The 'effective' force distributions further illuminated that above a RH value of 50%, the water has likely uniformly layered as the particles are adhering similarly with this layer for all humidity increments above 50%. Furthermore, these distributions illustrated that the particles interact

similarly with the water/surface layer in the highest RH range as they would with the surface in the lowest RH range. The 'effective' adhesion force distributions provide a guide for how the specific RH range is affecting the water formation and layering, and ultimately altering how the particles are interacting with the surface topography.

6.5 Acknowledgements

This work was funded in part by the Laboratory Directed Research & Development (LDRD) program. Sandia National Laboratories is a multi-mission laboratory managed and operated by National Technology and Engineering Solutions of Sandia, LLC., a wholly owned subsidiary of Honeywell International, Inc., for the U.S. Department of Energy's National Nuclear Security Administration under contract DE-NA0003525. This paper describes objective technical results and analysis. Any subjective views or opinions that might be expressed in the paper do not necessarily represent the views of the U.S. Department of Energy or the United States Government.

7. CONCLUSIONS & RECOMMENDED FUTURE WORK

7.1 Conclusions

This research focused on further developing an experimental and modeling framework, called the Enhanced Centrifuge Method (ECM), that maps particle-scale and surface properties onto experimentally-validated 'effective' adhesion distributions that describe the adhesion of the particles that comprise a powder. These distributions represent an engineering approach that allows powders comprised of particles of complex shape and roughness, which are challenging to model, to be described as if they were perfect, smooth spheres, which are comparatively simple to model. The complexity associated with the shape and size distributions of the individual particles is captured by the 'effective' adhesion parameter distributions.

The foundational study of this work involved measuring the vdW adhesion of a polystyrene powder comprised of nominally spherical particles against four silica surfaces with well-defined levels of RMS roughness. The resultant A'_{132} distributions illustrated two regions of adhesion. The first described particles that were significantly larger than the scale of any features on the surface to which they adhered. In this case, the A'_{132} distributions across all surfaces asymptotically approached a limiting reflective of the large particles interacting with the largest features on the surface. In the second region, the particles were sufficiently small that they experienced different adhesion interactions depending on the local topography on the surface and how that topography interacted with the particles' surfaces. The resulting A'_{132} distributions reflected this interplay between each particle and the surface's specific surface features. This study illustrated that the RMS roughness of the surface is an inadequate descriptor of how the surface topography impacts the adhesion. Instead, the scale of the surface topography features to the particle properties must be considered.

The same observations were made in a simulation-based investigation of the adhesion of substrates with hemispherical indentations, 40 μm in diameter, on their surfaces with a simulated ideal powder (comprised of smooth, spherical particles) and a simulated realistic powder (comprised of spherical particles with sinusoidal roughness applied to their surfaces). In this study, two regimes in the adhesion became apparent. In the first regime, the ideal and realistic particles showed the same adhesion force towards the indented surface. This occurred when the diameters

of the particles in either distribution were larger than the diameter of the indentation. In this case, the adhesion reflected large particles interacting with only the rim of the indentation, and the topography on the surface of the particles was irrelevant. The second region described the adhesion of the particles with diameters smaller than the diameter of the indentation. These were able to 'nest' within the indentations. In this case, the adhesion was directly influenced by the topography of the particle, whether smooth or sinusoidally rough. For this second case where the rough particles adhered differently than the smooth ones, the ECM was executed and the A'_{132} distributions required for the rough particles to be described as ideal spheres was noted. These distributions were affected by both the size and topography of the rough spheres.

The ECM was then utilized to investigate the effect of varying surface topography of stainless steel towards the adhesion of three different pharmaceutical powders: lactose monohydrate, ABT 089 and HPMC to the stainless steel. As a first approximation to describe the adhesion of the deformable particles, the force model used in the ECM was the JKR adhesion model. This model describes the adhesion between elastic spheres and a flat plate. The outputted parameter of the ECM for the JKR adhesion system is an 'effective' work of adhesion parameter instead of an 'effective' Hamaker constant. These size-dependent 'effective' work of adhesion parameters provide a quantifiable measure of the change in the adhesion that reflects the size, shape, and topographical features on the powder and the surface with which it interacts. This study also revealed two regions of adhesion. In the first, the particle sizes were sufficiently larger compared to the surface topography features that 'effective' work of adhesion distributions asymptotically approached a limiting value. In the second region, the particles were sufficiently small that they adhered to the surface depending on the local surface topography and how it related to the topography of the particles, and the resulting 'effective' work of adhesion distributions revealed this interplay.

In many powder processes, ambient conditions such as humidity may not be adequately controlled. Consequently, the effect of humidity on the work of adhesion of the pharmaceutical powders to the stainless steel was investigated via the ECM. The 'effective' work of adhesion distributions outputted revealed the same properties were controlling the adhesion in each humidity range, but to a greater extent in the upper humidity range for the ABT 089 and lactose monohydrate and to a lesser extent for the HPMC.

To further investigate the effect of the relative humidity on powder adhesion, a powder comprised of silica particles was measured against silica in increasing relative humidity environments. In this work, the ECM was modified to output a generalized 'effective' adhesion force parameter distribution to capture the particle and surface effects on the adhesion across humidity increments. A generalized 'effective' force parameter was used because the controlling adhesion force changes as a function of humidity in this system. Specifically, vdW forces dominate at low RH levels while capillary forces dominate at larger RH. The 'effective' adhesion force distributions reflected how the water from the air accumulated on the silica surface and how the topography on the particles interacted with this water. The 'effective' adhesion distributions quantified the silica adhesion decreased in the 30-40% RH range due to the water not completing filling the surface topography features such that liquid bridging did not occur and instead the water acted to reduce the vdW adhesion interaction. As the relative humidity increased beyond 40%, the water continued to build up on the surface such that the surface topography features were now completely filled with water allowing liquid bridging between the particles and the silica surface.

Each of the studies performed within this work demonstrated how the ECM and the 'effective' force parameters outputted by this tool capture the effect of the particle and surface properties on a powder's adhesion. A direct benefit of the ECM is that only a small amount of powder is needed to characterize the effect of the particle and surface properties on the powder's adhesion. Moreover, the 'effective' adhesion distributions outputted by the ECM further define the specific relationships between the particle and surface properties based on their scales and how these relationships impact the adhesion. Ultimately, the 'effective' force of adhesion distributions developed through the ECM provide the ability to quickly determine quantitatively how environmental and process conditions alter particle and surface properties, and overall powder behavior.

7.2 Future work

An objective of this work was to provide the community with a quantitative parameter which quickly and effectively captures the effects of the particle and surface properties on the adhesion. The studies demonstrated that the 'effective' adhesion force distributions quantify the effect of the particle and surface properties on the overall powder adhesion. A natural next step would be to isolate the effects of the particle properties from those of the surface properties through the

‘effective’ adhesion force distributions. This would require a study of the adhesion between real (rough, non-uniform) powders and extremely smooth surfaces. Effectively, the adhesion would be most impacted by the particle properties which would mean the ‘effective’ Hamaker constant distributions quantify solely the effect of the particle properties on the adhesion. A secondary course of action may include compacting a uniform powder layer on a specially designed centrifuge plate and dusting the powder on top of this uniform layer to measure the powder’s adhesion to itself. Challenges with this proposed method may include creating a uniform powder layer that will stay intact under the inertial forces introduced by the centrifuge, and ensuring the adhesive used to bond the layer to the plate does not cover the top of the bound layer to interact with the deposited powder.

Another expansion of this work is to adapt the ECM such that the ‘effective’ adhesion force parameters can be utilized in DEM simulations. Currently DEM simulations use methods such as the glued sphere approach to capture the effect of the particle properties on the adhesion. However, this approach can lead to inadequately describing the particle contact mechanics as many particles don’t behave as an agglomerate of smooth spheres. The value to the ‘effective’ work of adhesion force distributions is they directly quantify the particle and surface effects on the powder’s adhesion. In its existing state, the ‘effective’ work of adhesion distributions provide predictive ranges as to where to start tuning the work of adhesion parameter in the DEM model. However, the current ‘effective’ work of adhesion parameters describe particles at the micron scale while DEM use parcels of particles on the scale of mm. To transform these ‘effective’ work of adhesion parameters into useful parameters for DEM simulations, it is proposed to create on single agglomerate-scale work of adhesion parameter by taking the parameter of each particle in the agglomerate and weighing its contribution to the agglomerate scale parameter by the mass or volume fraction of the agglomerate occupied by that particle. This approach is represented through the following equation:

$$\Gamma_{effective,agglomerate} = \sum_{i=1}^{k} x_i \Gamma_{effective,i} \tag{7.1}$$

where x_i represents the mass or volume fraction of the individual particle which make up the bulk of the agglomerate and $\Gamma_{effective,i}$ is the 'effective' work of adhesion of the specific particle size of that fraction.

To further validate this approach, the Particle Adhesion Simulator would be utilized to predict the adhesion of a distribution of particles across a number of topography cases. The distributions of 'effective' Hamaker constants outputted by the Particle Adhesion Simulator would then be translated into 'effective' work of adhesions to be applied to the volume or mass-based approach describe above.

REFERENCES

[1] J.J. Fitzpatrick, L. Ahrné, Food powder handling and processing: Industry problems, knowledge barriers and research opportunities, Chem. Eng. Process. Process Intensif. 44

[2] J. Azmir, Q. Hou, A. Yu, Discrete particle simulation of food grain drying in a fl uidised bed, Powder Technol. 323 (2018) 238–249.

[3] B.C. Hancock, The Wall Friction Properties of Pharmaceutical Powders, Blends, and Granulations, J. Pharm. Sci. 108 (2019) 457–463.

[4] V. Garg, S.S. Mallick, P. Garcia-Trinanes, R.J. Berry, An investigation into the flowability of fine powders used in pharmaceutical industries, Powder Technol. 336 (2018) 375–382.

[5] W.R. Ketterhagen, M.T.A.M. Ende, B.C. Hancock, Process Modeling in the Pharmaceutical Industry using the Discrete Element Method, J. Pharm. Sci. 98 (2009) 442–470.

[6] H.A. Yu, T. Becker, N. Nic Daeid, S.W. Lewis, Fundamental studies of the adhesion of explosives to textile and non-textile surfaces, Forensic Sci. Int. 273 (2017) 88–95.

[7] M.N. Chaffee-Cipich, B.D. Sturtevant, S.P. Beaudoin, Adhesion of explosives, Anal. Chem. 85 (2013) 5358–5366.

[8] N. Govender, D.N. Wilke, P. Pizette, N. Abriak, A study of shape non-uniformity and poly-dispersity in hopper discharge of spherical and polyhedral particle systems using the Blaze-DEM GPU code, Appl. Math. Comput. 319 (2018) 318–336.

[9] S. Haeri, Y. Wang, O. Ghita, J. Sun, Discrete element simulation and experimental study of powder spreading process in additive manufacturing, Powder Technol. 306 (2017) 45–54.

[10] H. Tangri, Y. Guo, J.S. Curtis, Packing of cylindrical particles : DEM simulations and experimental measurements, Powder Technol. 317 (2017) 72–82.

[11] L. Litster, Jim Ennis, Bryan Liu, The Science and Engineering of Granulation Processes, 2004.

[12] K. H., Particle adhesion theory and experiment, Adv. Colloid Interface Sci. 1 (1967) 111–239.

[13] G. Donsi', S. Moser, L. Massimilla, Solid-solid interaction between particles of a fluid bed catalyst, Chem. Eng. Sci. 30 (1975) 1533–1535.

[14] J. Visser, Particle Adhesion and Removal: a Review, Part. Sci. Technol. 13 (1995) 169–196.

[15] S. Swaminathan, B. Ramey, J. Hilden, C. Wassgren, Characterizing the powder punch-face adhesive interaction during the unloading phase of powder compaction, Powder Technol. 315 (2017) 410–421.

[16] E. Teunou, J.J. Fitzpatrick, E.C. Synnott, Characterization of food powder flowability, J. Food Eng. 39 (1999) 31–37.

[17] M. Hans-Jurgen Butt and Kappl, Surface and Interfacial Forces, n.d.

[18] F. Podczeck, The relationship between particulate properties of carrier materials and the adhesion force of drug particles in interactive powder mixtures, J. Adhes. Sci. Technol. 11 (1997) 1089–1104.

[19] F. Podczeck, J.M. Newton, M.B. James, Adhesion and friction between powders and polymer or aluminium surfaces determined by a centrifuge technique, Powder Technol. 83 (1995) 201–209.

[20] K. Cooper, N. Ohler, A. Gupta, S. Beaudoin, Analysis of contact interactions between a rough deformable colloid and a smooth substrate, J. Colloid Interface Sci. 222 (2000) 63–74.

[21] D.M. Schaefer, M. Carpenter, B. Gady, R. Reifenberger, L.P. Demejo, D.S. Rimai, Surface roughness and its influence on particle adhesion using atomic force techniques, J. Adhes. Sci. Technol. 9 (1995) 1049–1062.

[22] Q. Li, V. Rudolph, W. Peukert, London-van der Waals adhesiveness of rough particles, Powder Technol. 161 (2006) 248–255.

[23] K.N.G. Fuller, D. Tabor, The Effect of Surface Roughness on the Adhesion of Elastic Solids, Proc. R. Soc. A Math. Phys. Eng. Sci. 345 (1975) 327–342.

[24] K. Cooper, A. Gupta, S. Beaudoin, Substrate morphology and particle adhesion in reacting systems, J. Colloid Interface Sci. 228 (2000) 213–219.

[25] K. Cooper, A. Gupta, S. Beaudoin, Simulation of the Adhesion of Particles to Surfaces, J. Colloid Interface Sci. 234 (2001) 284–292.

[26] S. Eichenlaub, A. Gelb, S. Beaudoin, Roughness Models for Particle Adhesion, J. Colloid Interface Sci. 280 (2004) 289–298.

[27] L. Suresh, J.Y. Walz, Effect of surface roughness on the interaction energy between a colloidal sphere and a flat plate, J. Colloid Interface Sci. 183 (1996) 199–213.

[28] J. Yang, Y. Guo, K.E. Buettner, J.S. Curtis, DEM investigation of shear flows of binary mixtures of non-spherical particles, Chem. Eng. Sci. (2019).

[29] R.P. Jaiswal, G. Kumar, C.M. Kilroy, S.P. Beaudoin, Modeling and Validation of the van der Waals Force During the Adhesion of Nanoscale Objects to Rough Surfaces: A Detailed Description, Langmuir. 25 (2009) 10612–10623.

[30] N. Govender, R. Rajamani, D.N. Wilke, C.Y. Wu, J. Khinast, B.J. Glasser, Effect of particle shape in grinding mills using a GPU based DEM code, Miner. Eng. 129 (2018) 71–84.

[31] H. Bagherzadeh, Z. Mansourpour, B. Dabir, A coupled DEM-CFD analysis of asphaltene particles agglomeration and fragmentation, J. Pet. Sci. Eng. 173 (2019) 402–414.

[32] M.C. Thomas, S.P. Beaudoin, An enhanced centrifuge-based approach to powder characterization: Experimental and theoretical determination of a size-dependent effective Hamaker constant distribution, Powder Technol. 306 (2017) 96–102.

[33] S. Peillon, A. Autricque, M. Redolfi, C. Stancu, F. Gensdarmes, C. Grisolia, O. Pluchery, Adhesion of tungsten particles on rough tungsten surfaces using Atomic Force Microscopy, J. Aerosol Sci. 137 (2019) 105431.

[34] J.P.B. van Dam, S.T. Abrahami, A. Yilmaz, Y. Gonzalez-Garcia, H. Terryn, J.M.C. Mol, Effect of surface roughness and chemistry on the adhesion and durability of a steel-epoxy adhesive interface, Int. J. Adhes. Adhes. 96 (2020) 102450.

[35] L.R. Hilbert, D. Bagge-Ravn, J. Kold, L. Gram, Influence of surface roughness of stainless steel on microbial adhesion and corrosion resistance, Int. Biodeterior. Biodegradation. 52 (2003) 175–185.

[36] J.N. Israelachvili, Intermolecular and Surface Forces, 2nd ed., San Diego, CA, 1985.

[37] D. Sedin, K. Rowlen, Adhesion forces measured by atomic force microscopy in humid air, Anal. Chem. 72 (2000) 2183–9.

[38] A.D. Zimon, Adhesion of Dust and Powder, 2004.

[39] H. Mizes, M. Ott, E. Eklund, D. Hays, Small particle adhesion: Measurement and control, Colloids Surfaces A Physicochem. Eng. Asp. 165 (2000) 11–23.

[40] G. Boehme, H. Krupp, H. Rabenhorst, G. Sandstede, Adhesion measurements involving small particles, Trans. Inst. Chem. Eng. 40 (1962) 252–259.

[41] T. Deng, V. Garg, M.S.A. Bradley, A study of particle adhesion for cohesive powders using a novel mechanical surface energy tester, Powder Technol. 391 (2021) 46–56.

[42] E.M. Lifshitz, The Theory of Molecular Attractive Forces between Solids, Sov. Phys. 2 (1956) 73–83.

[43] J.N. Israelachvili, G.E. Adams, Measurement of forces between two mica surfaces in aqueous electrolyte solutions in the range 0–100 nm, J. Chem. Soc. Faraday Trans. 1 Phys. Chem. Condens. Phases. 74 (1978) 975.

[44] A.D.R. K.L. Johsnon, K. Kendall, Surface energy and the contact of elastic solids, Proc. R. Soc. London. A. Math. Phys. Sci. 324 (1971) 301–313.

[45] B. V Derjaguin, V.M. Muller, Y.U.P. Toporov, Effect of contact deformation on the adhesion of particles., J. Colloid Interface Sci. 52 (1975) 105–108.

[46] D. Maugis, H.M. Pollock, Surface forces, deformation and adherence at metal microcontacts, Acta Metall. 32 (1984) 1323–1334.

[47] D. Maugis, Adhesion of spheres: The JKR-DMT transition using a dugdale model, J. Colloid Interface Sci. 150 (1992) 243–269.

[48] S. Hindi, Microcrystalline Cellulose: The Inexhaustible Treasure for Pharmaceutical Industry, Nanosci. Nanotechnol. Res. Vol. 4, 2017, Pages 17-24. 4 (2017) 17–24.

[49] N. V. Zarate, A.J. Harrison, J.D. Litster, S.P. Beaudoin, Effect of relative humidity on onset of capillary forces for rough surfaces, J. Colloid Interface Sci. (2013).

[50] R. Jones, H.M. Pollock, J.A.S. Cleaver, C.S. Hodges, Adhesion forces between glass and silicon surfaces in air studied by AFM: effects of relative humidity, particle size, roughness, and surface treatment, Langmuir. 18 (2002) 8045–8055.

[51] A. Ata, Y.I. Rabinovich, R.K. Singh, Role of surface roughness in capillary adhesion, J. Adhes. Sci. Technol. 16 (2002) 337–346.

[52] T.V. Vorburger, J.A. Dagata, G. Wilkening, K. lizuka, Characterization of Surface Topography, Proc. 16th Int. Conf. Soil Mech. Geotech. Eng. Geotechnol. Harmon. with Glob. Environ. 2 (2005) 465–468.

[53] T. Vorburger, Methods for characterizing surface topography, Tutorials Opt. (1992) 137–151.

[54] E.S. Gadelmawla, M.M. Koura, T.M.A. Maksoud, I.M. Elewa, H.H. Soliman, Roughness parameters, J. Mater. Process. Technol. 123 (2002) 133–145.

[55] Y.I. Rabinovich, J.J. Adler, A. Ata, R.K. Singh, B.M. Moudgil, Adhesion between nanoscale rough surfaces. I. Role of asperity geometry, J. Colloid Interface Sci. 232 (2000) 10–16.

[56] S. Perni, P. Prokopovich, Multi-asperity elliptical JKR model for adhesion of a surface with non-axially symmetric asperities, Tribol. Int. 88 (2015) 107–114.

[57] P. Prokopovich, S. Perni, Comparison of JKR- and DMT-based multi-asperity adhesion model: Theory and experiment, Colloids Surfaces A Physicochem. Eng. Asp. 383 (2011) 95–101.

[58] Y.I. Rabinovich, J.J. Adler, M.S. Esayanur, A. Ata, R.K. Singh, B.M.M. U, Capillary forces between surfaces with nanoscale roughness, (2002) 213–230.

[59] N. Govender, D.N. Wilke, C. Wu, J. Khinast, P. Pizette, W. Xu, Hopper flow of irregularly shaped particles (non-convex polyhedra): GPU-based DEM simulation and experimental validation, Chem. Eng. Sci. 188 (2018) 34–51.

[60] M. Molenda, Parameters and contact models for DEM simulations of agricultural granular

materials : A review, 7 (2016).

[61] R. Wilson, D. Dini, B. Van Wachem, The influence of surface roughness and adhesion on particle rolling, Powder Technol. 312 (2017) 321–333.

[62] D. Queteschiner, T. Lichtenegger, S. Pirker, S. Schneiderbauer, Multi-level coarse-grain model of the DEM, Powder Technol. 338 (2018) 614–624.

[63] A. Kumar, T. Staedler, X. Jiang, Role of relative size of asperities and adhering particles on the adhesion force, J. Colloid Interface Sci. 409 (2013) 211–218.

[64] J. Katainen, M. Paajanen, E. Ahtola, V. Pore, J. Lahtinen, Adhesion as an interplay between particle size and surface roughness, J. Colloid Interface Sci. 304 (2006) 524–529.

[65] C.Q. LaMarche, S. Leadley, P. Liu, K.M. Kellogg, C.M. Hrenya, Method of quantifying surface roughness for accurate adhesive force predictions, Chem. Eng. Sci. 158 (2017) 140–153.

[66] E.R. Beach, G.W. Tormoen, J. Drelich, R. Han, Pull-off force measurements between rough surfaces by atomic force microscopy, J. Colloid Interface Sci. 247 (2002) 84–99.

[67] S.P. Beaudoin, R.P. Jaiswal, C.M. Kilroy, D. Balachandran, Particle Adhesion, (2014).

[68] K. Cooper, A. Gupta, S. Beaudoin, Simulation of Particle Adhesion: Implications in Chemical Mechanical Polishing and Post Chemical Mechanical Polishing Cleaning, J. Electrochem. Soc. 148 (2001) G662.

[69] Y.I. Rabinovich, J.J. Adler, A. Ata, R.K. Singh, B.M. Moudgil, Adhesion between Nanoscale Rough Surfaces II . Measurement and Comparison with Theory, 24 (2000) 17–24.

[70] Y. Chen, M.A.S. Quintanilla, J. Yang, J.M. Valverde, R.N. Dave, Pull-off force of coated fine powders under small consolidation, (2009) 1–14.

[71] H. Rumpf, Particle Technology, Part. Technol. Ser. (1975).

[72] O. Laitinen, K. Bauer, J. Niinimäki, U.A. Peuker, Validity of the Rumpf and the Rabinovich adhesion force models for alumina substrates with nanoscale roughness, Powder Technol. 246 (2013) 545–552.

[73] S. You, M.P. Wan, Modeling and experiments of the adhesion force distribution between particles and a surface, Langmuir. 30 (2014) 6808–6818.

[74] M. Landin, P. York, M.J. Cliff, R.C. Rowe, A.J. Wigmore, Scale-up of a pharmaceutical granulation in fixed bowl mixer-granulators, Int. J. Pharm. 133 (1996) 127–131.

[75] N. Harnby, An engineering view of pharmaceutical powder mixing, Pharm. Sci. Technol. Today. 3 (2000) 303–309.

[76] J. Prescott, R. Barnum, On powder flowability, Pharm. Technol. 24 (2000) 60–84.

[77] F.J. Muzzio, T. Shinbrot, B.J. Glasser, Powder technology in the pharmaceutical industry: The need to catch up fast, Powder Technol. 124 (2002) 1–7.

[78] T. Freeman, The importance of powder characterisation, Pharm. Technol. Eur. 22 (2010) 21–26.

[79] J. Fitzpatrick, L. Ahrne, Food powder handling and processing: Industry problems, knowledge barriers and research opportunities, Chem. Eng. Process. 44 (2005) 209–214.

[80] J. Litster, B. Ennis, The Science and Engineering of Granulation Processes, 2004.

[81] F. Podczeck, Particle-particle Adhesion in Pharmaceutical Powder Handling, Imperial College Press, London, 1998.

[82] J.A. Greenwood, J.B.P. Williamson, Contact of Nominally Flat Surfaces, Proc. R. Soc. A Math. Phys. Eng. Sci. 295 (1966) 300–319.

[83] K. Cooper, A. Gupta, S. Beaudoin, Simulation of the Adhesion of Particles to Surfaces., J. Colloid Interface Sci. 234 (2001) 284–292.

[84] K. Cooper, S. Eichenlaub, A. Gupta, S. Beaudoin, Adhesion of Alumina Particles to Thin Films, J. Electrochem. Soc. 149 (2002) G239.

[85] L. Suresh, J. Walz, Effect of surface roughness on the interaction energy between a colloidal sphere and a flat plate, J. Colloid Interface Sci. 183 (1996) 199–213.

[86] J.F. Archard, Elastic Deformation and the Laws of Friction, Proc. R. Soc. A Math. Phys. Eng. Sci. 243 (1957) 190–205.

[87] A. Majumdar, B. Bhushan, Role of Fractal Geometry in Roughness Characterization and Contact Mechanics of Surfaces, J. Tribol. 112 (1990) 205.

[88] K. Komvopoulos, W. Yan, A Fractal Analysis of Stiction in Microelectromechanical Systems, J. Tribol. 119 (1997) 391.

[89] R.L. Jackson, A model for the adhesion of multiscale rough surfaces in MEMS, Proc. Annu. Southeast. Symp. Syst. Theory. (2011) 257–262.

[90] U. Zafar, C. Hare, A. Hassanpour, M. Ghadiri, Drop test: A new method to measure the particle adhesion force, Powder Technol. 264 (2014) 236–241.

[91] M.D.M. Peri, C. Cetinkaya, Non-contact microsphere-surface adhesion measurement via acoustic base excitations, J. Colloid Interface Sci. 288 (2005) 432–443.

[92] M.C. Thomas, S.P. Beaudoin, An enhanced centrifuge-based approach to powder characterization: Particle size and Hamaker constant determination, Powder Technol. 306 (2017) 96–102.

[93] H. Mizes, Small particle adhesion: measurement and control, Colloids Surfaces A Physicochem. Eng. Asp. 165 (2000) 11–23.

[94] G.R. Salazar-Banda, M.A. Felicetti, J.A.S. Gonçalves, J.R. Coury, M.L. Aguiar, Determination of the adhesion force between particles and a flat surface, using the centrifuge technique, Powder Technol. 173 (2007) 107–117.

[95] K.K. Lam, J.M. Newton, Investigation of applied compression on the adhesion of powders to a substrate surface, Powder Technol. 65 (1991) 167–175.

[96] S. Bhattacharjee, C.-H. Ko, M. Elimelech, DLVO Interaction between Rough Surfaces, Langmuir. 14 (1998) 3365–3375.

[97] M.C. Thomas, S.P. Beaudoin, An Enhanced Centrifuge-Based Approach to Powder Characterization: Particle Size and Hamaker Constant Determination, Powder Technol. 286 (2015) 412–419.

[98] M. Badal Tejedor, N. Nordgren, M. Schuleit, M.W. Rutland, A. Millqvist-Fureby, Tablet mechanics depend on nano and micro scale adhesion, lubrication and structure, Int. J. Pharm. 486 (2015) 315–323.

[99] F. Podczeck, "Particle–Particle Adhesion in Pharmaceutical Powder Handling," Eur. J. Pharm. Biopharm. 54 (2002) 101–102.

[100] D.T. Tran, R. Bittner, P. Zámostný, Adhesion force measurement by centrifuge technique as tool for predicting interactive mixture stability, Chem. Eng. Res. Des. 165 (2021) 467–476.

[101] G.A. Willing, T.R. Burk, F.M. Etzler, R.D. Neuman, Adhesion of pharmaceutical particles to gelatin capsules having variable surface physicochemical properties: Evaluation using a combination of scanning probe microscopy techniques, Colloids Surfaces A Physicochem. Eng. Asp. 193 (2001) 117–127.

[102] R. Roopwani, I.S. Buckner, Understanding deformation mechanisms during powder compaction using principal component analysis of compression data, Int. J. Pharm. 418 (2011) 227–234.

[103] P. Narayan, B.C. Hancock, The relationship between the particle properties, mechanical behavior, and surface roughness of some pharmaceutical excipient compacts, Mater. Sci. Eng. A. 355 (2003) 24–36.

[104] M. Capece, The Role of Particle Surface Area and Adhesion Force in the Sticking Behavior of Pharmaceutical Powders, J. Pharm. Sci. (2019) 1–11.

[105] T. Deng, V. Garg, H. Salehi, M.S.A. Bradley, Correlations between segregation intensity and material properties such as particle sizes and adhesions and novel methods for assessment, Powder Technol. 387 (2021) 215–226.

[106] W. Nan, M. Pasha, T. Bonakdar, A. Lopez, U. Zafar, S. Nadimi, M. Ghadiri, Jamming during particle spreading in additive manufacturing, Powder Technol. 338 (2018) 253–262.

[107] S. Paul, L.J. Taylor, B. Murphy, J.F. Krzyzaniak, N. Dawson, M.P. Mullarney, P. Meenan, C.C. Sun, Powder properties and compaction parameters that influence punch sticking propensity of pharmaceuticals, Int. J. Pharm. 521 (2017) 374–383.

[108] C. Bosquillon, C. Lombry, V. Preat, R. Vanbever, Comparison of particle sizing techniques in the case of inhalation dry powders, J. Pharm. Sci. 90 (2001) 2032–2041.

[109] A. Dandekar, Z.A. Roberts, S. Paulson, W. Chen, S.F. Son, M. Koslowski, The effect of the particle surface and binder properties on the response of polymer bonded explosives at low impact velocities, Comput. Mater. Sci. 166 (2019) 170–178.

[110] N. V. Zarate, A.J. Harrison, J.D. Litster, S.P. Beaudoin, Effect of relative humidity on onset of capillary forces for rough surfaces, J. Colloid Interface Sci. 411 (2013) 265–272.

[111] A.A. Feiler, P. Jenkins, M.W. Rutland, Effect of relative humidity on adhesion and frictional properties of micro- And nano-scopic contacts, J. Adhes. Sci. Technol. 19 (2005) 165–179.

[112] Y. Listiohadi, J.A. Hourigan, R.W. Sleigh, R.J. Steele, Moisture sorption, compressibility and caking of lactose polymorphs, Int. J. Pharm. 359 (2008) 123–134.

[113] W. Cheng, P.F. Dunn, R.M. Brach, SURFACE ROUGHNESS EFFECTS ON MICROPARTICLE ADHESION Modeling of Adhesion for Smooth Surfaces, (2002) 929–965.

[114] A.W. Bush, R.D. Gibson, T.R. Thomas, The elastic contact of a rough surface, Wear. 35 (1975) 87–111.

[115] P.G.C. Petean, M.L. Aguiar, Determining the adhesion force between particles and rough surfaces, Powder Technol. 274 (2015) 67–76.

[116] C.A. Stevenson, J.E. Monroe, C.G. Norris, A.R. Roginski, S.P. Beaudoin, The effects of surface and particle properties on van der Waals (vdW) adhesion quanti fi ed by the enhanced centrifuge method, Powder Technol. 392 (2021) 514–523.

[117] G. Violano, L. Afferrante, On DMT methods to calculate adhesion in rough contacts, Tribol. Int. 130 (2019) 36–42.

[118] A.J. Harrison, S.P. Beaudoin, D.S. Corti, Wang-Landau Monte Carlo simulation of capillary forces at low relative humidity in atomic force microscopy, J. Adhes. Sci. Technol. 30 (n.d.) 1165–1177.

[119] H. Lees, F. Zapata, M. Vaher, C. García-Ruiz, Study of the adhesion of explosive residues to the finger and transfer to clothing and luggage, Sci. Justice. 58 (2018) 415–424.

[120] P. Begat, D.A.V. Morton, J.N. Staniforth, R. Price, The cohesive-adhesive balances in dry

powder inhaler formulations I: Direct quantification by atomic force microscopy, Pharm. Res. 21 (2004) 1591–1597.

[121] C.G. Jange, R.P.K. Ambrose, Effect of surface compositional difference on powder flow properties, Powder Technol. 344 (2019) 363–372.

[122] F. Podczeck, J.M. Newton, Development of an ultracentrifuge technique to determine the adhesion and friction properties between particles and surfaces, J. Pharm. Sci. 84 (1995) 1067–1071.

[123] M.B. Ranade, Adhesion and removal of fine particles on surfaces, Aerosol Sci. Technol. 7 (1987) 161–176.

[124] E.Y.T. Chen, L. Ma, Y. Yue, B. Guo, H. Liang, Measurement of dust sweeping force for cleaning solar panels, Sol. Energy Mater. Sol. Cells. 179 (2018) 247–253.

[125] M. Thomas, E. Krenek, S. Beaudoin, Capillary Forces Described by Effective Contact Angle Distributions via Simulations of the Centrifuge Technique, MRS Adv. 1 (2016) 2237–2245.

[126] R. Jones, H.M. Pollock, J.A.S. Cleaver, C.S. Hodges, Adhesion forces between glass and silicon surfaces in air studied by AFM: Effects of relative humidity, particle size, roughness, and surface treatment, Langmuir. 18 (2002) 8045–8055.

[127] R. Price, P.M. Young, S. Edge, J.N. Staniforth, The influence of relative humidity on particulate interactions in carrier-based dry powder inhaler formulations, Int. J. Pharm. 246 (2002) 47–59.

[128] H.R. Moutinho, C.S. Jiang, B. To, C. Perkins, M. Muller, M.M. Al-Jassim, L. Simpson, Adhesion mechanisms on solar glass: Effects of relative humidity, surface roughness, and particle shape and size, Sol. Energy Mater. Sol. Cells. 172 (2017) 145–153.

[129] M. Paajanen, J. Katainen, O.H. Pakarinen, A.S. Foster, J. Lahtinen, Experimental humidity dependency of small particle adhesion on silica and titania, J. Colloid Interface Sci. 304 (2006) 518–523.

[130] M.D. Butler, D. Vella, Journal of Colloid and Interface Science Liquid bridge splitting enhances normal capillary adhesion and resistance to shear on rough surfaces, J. Colloid Interface Sci. 607 (2022) 514–529.

[131] M. Thomas, E. Krenek, S. Beaudoin, Capillary Forces Described by Effective Contact Angle Distributions via Simulations of the Centrifuge Technique, MRS Adv. 1 (2016) 2237–2245.

[132] C.A. Stevenson, M.C. Thomas, S.P. Beaudoin, An enhanced centrifuge-based approach to powder characterization: The interaction between particle roughness and particle-scale surface topography described by a size-dependent ‘effective’ Hamaker constant, Powder Technol. 391 (2021) 198–205.

[133] D.B. Asay, S.H. Kim, Effects of adsorbed water layer structure on adhesion force of silicon oxide nanoasperity contact in humid ambient, J. Chem. Phys. 124 (2006) 174712.

[134] H. Kim, B. Smit, J. Jang, Monte carlo study on the water meniscus condensation and capillary force in atomic force microscopy, J. Phys. Chem. C. 116 (2012) 21923–21931.

VITA

Caralyn Stevenson was raised in Aurora, Colorado and graduated from Denver School of Science and Technology (DSST) Montview high school in 2013. Upon graduating high school, Caralyn enrolled in the chemical engineering program at New Mexico Institute of Mining and Technology (NMT). She graduated with her Bachelor of Science in chemical engineering from NMT in 2017 with high honors and the distinguishment of the Cramer Award. In the Fall of 2017, Caralyn started her Ph.D. studies in the Davidson School of Chemical Engineering at Purdue University.

PUBLICATIONS

Please note I previously published under the name Coultas-Mckenney.

1. **Stevenson, C.A**., Thomas, M.C., Beaudoin, S.P. An Enhanced Centrifuge-Based Approach to Powder Characterization: Particle Scale Roughness Effects Described by a Size-Dependent Effective Hamaker Constant. *Powder Technology*. **2021**, *391*.

2. **Stevenson, C.A.,** *et.al.* The effect of the variation of surface and particle properties quantified through van der Waals adhesion and the Enhanced Centrifuge Method. *Powder Technology*. **2021**, *392*.

3. Novosselov, I., **Coultas-McKenney, C.A.**, *et. al.* Trace Explosives Sampling for Security Applications Study: Creation of Procedures and Methodology to Measure Sampling Efficiency. *Talanta*. **2021**, 234.

4. Mier, F. A.; Morales, R.; **Coultas-McKenney, C. A.**; Hargather, M. J.; Ostanek, J. Overcharge and Thermal Destructive Testing of Lithium Metal Oxide and Lithium Metal Phosphate Batteries Incorporating Optical Diagnostics. *J. Energy Storage.* **2017**, *13.*

5. **Stevenson, C.A.,** Rimza, J., Beaudoin S.P. Incorporating the effect of humidity on surface and particle interactions through the Enhanced Centrifuge Method. *Journal of Colloid and Interface Science*. 2021, In Preparation.

6. **Stevenson, C.A**., *et. al.* The effect of the variation of stainless steel surface and pharmaceutical particle properties on powder adhesion quantified through the Enhanced Centrifuge Method. 2021, In Preparation.

7. Monroe, J.M., **Stevenson, C.A.**, Beaudoin, S.P. The effect of surface properties and particle properties on RDX powder adhesion quantified through the Enhanced Centrifuge Method. In Preparation.